ESCUELA TÉCNICA SUPERIOR DE INGENIEROS INDUSTRIALES Y DE TELECOMUNICACIÓN

Titulación :

INGENIERO DE TELECOMUNICACIÓN

Título del proyecto:

TUNABLE ANTENNA DESIGN BY METAMATERIAL STRUCTURES OPERATING AT S BAND

Cristina Juliá Yepes

Tutor: Ramón Gonzalo García

Pamplona, 27 de Abril de 2015

ESCUELA TÉCNICA SUPERIOR DE INGENIEROS INDUSTRIALES Y DE TELECOMUNICACIÓN

Titulación :

INGENIERO DE TELECOMUNICACIÓN

Título del proyecto:

TUNABLE ANTENNA DESIGN BY METAMATERIAL STRUCTURES OPERATING AT S BAND

Cristina Juliá Yepes

Tutor: Ramón Gonzalo García

Pamplona, 27 de Abril de 2015

”Be you, cause
life is too short to
be anybody else”

AGRADECIMIENTOS / ACKNOWLEDGMENTS

Nunca se me ha dado bien eso de decir en alto lo que siento o pienso pero… hoy tengo que hacer una excepción por todos vosotros, los que habéis formado parte de mi vida desde el principio y a los que he encontrado en mitad del camino. Y si en las siguientes líneas no encontráis vuestro nombre, no penséis que me he olvidado de vosotros, simplemente es que no puedo nombraros a todos o que no he tenido el valor para hacerlo.

En primer lugar, como no, quiero dar las gracias a la persona que ha hecho posible que hoy esté aquí, Ramón, muchas gracias por estar siempre ahí, por ayudarme y por enseñarme algo nuevo cada día. Ha sido un placer tenerte como tutor del proyecto y espero, espero, espero que esto no sea un punto final sino que sólo sea un punto y coma. Nunca me cansaré de aprender y mucho menos me cansaré de aprender de ti.

La siguiente persona a la que tengo que agradecer su tiempo es a Juan Carlos Iriarte (a.k.a. JC), gracias por solucionarme todos los problemas que me ha dado el "maldito" software, por tus conocimientos y por tu disponibilidad a todas horas. Si no llega a ser por ti, habría desesperado a Ramón y a Ismael a la semana de empezar.

A ti Ismael, gracias por ser mi amigo y compañero en estos últimos años, por esas tardes de billar o esas noches de cine en las que me dejabas soltarlo todo para que me quedase a gusto. Gracias por ser mi diccionario ambulante cuando sólo me sale la definición de la palabra, por aguantarme cada vez que he estado insoportable y por reírte conmigo (o más bien de mi) cada vez que tengo el día tonto, que suelen ser muchos. Deberías estar incluido en la sección de amigos pero has formado parte de mí proyecto casi tanto como las personas de ahí arriba.

Son muchos los amigos (incluida mi archienemiga) que hoy nombraría aquí que estos agradecimientos se extenderían más que el propio proyecto y por eso hoy voy a quedarme con dos. Sergio, mi amigo desde la infancia, al que teniéndolo tan cerca lo veo tan poco, y aún así nada cambia. Gracias por todo estos año y los que vendrán, se que no ha sido fácil… Y mi queridísima Andrea, ¿¿qué habría hecho yo sin ti??, ¿¿qué sería yo sin ti?? Gracias An por tu sinceridad, por tu apoyo, por esos benditos viernes, por no

olvidarte nunca de mi y por estar ahí en los buenos y en los malos momentos. No me olvidaré nunca de todo lo que me has aportado.

Para el final he dejado a mi familia, que aunque sea pequeñita no quiere decir que tenga menos importancia. A mi madre Ana, gracias por no rendirte y por luchar cuando no te quedaban fuerzas, porque no lo solo lo has conseguido, sino que nos lo has enseñado, nos has enseñado a luchar por todo. A mis dos hermanas, ¿qué puedo deciros? Somos tan diferentes y hemos pasado por tantas cosas que solo puedo daros las gracias por estar ahí siempre. 'Blasi', espero que el 10 del 10 sea un día increíble para ti y para Marcos, y que a partir de entonces los días sean inimaginables. 'Susi', más amigas que hermanas, somos únicas, ya lo sabes.

Y si a alguien quería darle las gracias es a la única persona con la que no podré compartir este día, mi padre Enrique. Gracias por cambiar mi vida, por darme dos hermanastras a las que adoro, por darme a esos tres diablillos de sobrinos que tengo, por enseñarme lo que es tener un padre, por darme una familia increíble, por darme Galicia… Te fuiste muy pronto… Te echo de menos…

Y aunque no lo diga mucho no hay duda de que os quiero a todos y a cada uno de vosotros, tanto los que han sido nombrados como los que no. No cambies nunca, seguid así, y gracias por hacerme llegar hasta aquí. No sabéis cuanto significa para mi.

ABSTRACT

A "metamaterial" by its widely accepted definition is an artificially engineered structure that gains its material properties from its structure as opposed to its intrinsic material composition. The field of metamaterials has gained much attention within the scientific community over the past decade. With continuing advances and discoveries leading the way to practical applications, metamaterials have earned the attention of technology-based corporations and defense agencies interested in their use for next generation devices. Frequency Selective Surfaces (FSS) are a potent variety of metamaterials that, depending on the surface geometry, can be used to engineer specific radiation properties such as directional emission, linear and circular polarized emission, and spectral selectivity. The elements of the FSS can either be patches or apertures, and in traditional designs, the FSS usually operates around the half-wavelength resonance of the elements.

In this project a Frequency Selective Surface (FSS) is used in order to realize tunable metamaterials –a broad class of controllable artificially engineered metamaterials, and develop a tunable antenna operating at 2.4 GHz. The FSS consist of an array of square patches loaded with varactors and tunable ferroelectric thin film capacitors (BST) for external tuning of the effective medium parameters. Therefore a BST varactor is designed and located between the patches of the FSS. The effect of the Frequency Selective Surface is studied in two different antennas –an End-Loaded Planar Open-Sleeve Dipole (ELPOSD) and a Square Patch.

An End-Loaded Planar Open-Sleeve Dipole consist of a conventional planar dipole with two closely spaced parasitic elements, or sleeves, and loaded stubs at the end of the dipole. The main benefits of this type of antennas is that in addition to retaining similar performance to that of conventional planar open-sleeve dipole, end-loaded planar open-sleeve dipole (ELPOSD) antennas can be miniaturized. The Square Patch antenna used in this work is a conventional planar square patch feed with a microstrip line.

Barium Strontium Titanate (BST) is a well-known ferroelectric material and up to now. A BST thin film is used to design the varactors, along with the Interdigital Capacitors (IDCs) geometry used in the metal layer.

The overall antenna consists of a multilayer substrate with tunable FSS layer and dipole or patch antenna. The capacitance of the whole FSS changes introducing the BST ferroelectric material into the varactor. As can be seen in the results, by varying the BST permittivity from 200 to 300, a variation in frequency is achieved from 1.98 GHz to 1.717 GHz with a distance around 100 MHz between resonance frequencies, which equals a variation of the frequency about 8% in the adjacent permittivity values.

upna Universidad Pública de Navarra Nafarroako Unibertsitate Publikoa

RESUMEN

Un "metamaterial" por su definición ampliamente aceptada es una estructura construida artificialmente que obtiene sus propiedades materiales de su estructura en lugar de la composición de su material intrínseco. El ámbito de los materiales ha ganado mucha atención dentro de la comunidad científica en la última década. Con los continuos avances y descubrimientos conducen al camino de las aplicaciones prácticas; los metamateriales han ganado la atención de las empresas de base tecnológica y los organismos de defensa interesados en el uso de dispositivos de próxima generación. Las superficies selectivas en frecuencia (FSS) son una variedad potente de metamateriales que, dependiendo de la geometría de la superficie, se pueden utilizar para diseñar propiedades de radiación específicas tales como la emisión direccional, emisión polarizada circular y lineal, y la selectividad espectral. Los elementos de la FSS pueden ser tanto elementos metálicos sólidos como elementos metálicos con aberturas, y en los diseños tradicionales, la superficie selectiva en frecuencia (FSS) normalmente opera en torno a la resonancia de media longitud de onda de los elementos.

En este proyecto se va a utilizar una superficie selectiva de frecuencia (FSS) con el fin de realizar metamateriales sintonizables -una amplia clase de metamateriales controlables diseñados artificialmente, y desarrollar una antena sintonizable que trabaje a 2.4 GHz. La FSS consiste en una serie de elementos rectángulos cargados con varactores y capacitores con una película delgada de material ferroeléctrico sintonizable (BST) para el ajuste externo de los parámetros de medio efectivo. Por lo tanto se diseñan unos varactores BST que son colocados entre los elementos metálicos que conforman la FSS. El efecto de la superficie selectiva en frecuencia es estudiado en dos antenas diferentes – antena ELPOSD (End-Loaded Planar Open-Sleeve Dipole) y una antena de parche microstrip.

La antena ELPOSD consiste en un dipolo plano convencional con dos elementos parásitos muy juntos, y una carga en cada extremo del dipolo. Los beneficios principales de este tipo de antenas es que, además del rendimiento similar de la antena POSD (Planar Open-Sleeve Dipole) convencional, las antenas ELPOSD pueden ser miniaturizadas. La

antena parche utilizada en este trabajo es un elemento metálico cuadrado plano alimentado a través de una línea microstrip.

El material ferroeléctrico Barium Strontium Titanate (BST) es un material muy bien conocido hasta el momento. Para diseñar los varactores se utiliza una película delgada de BST, junto con los capacitores interdigitales (IDCs) que se utilizan en la capa del metal.

La antena general consiste en un sustrato de múltiples capas donde en una capa se encuentra la Superficie selectiva en frecuencia (FSS) sintonizable y en otra la antena dipolo o antena de parche. La capacidad de la FSS completa varía introduciendo el material ferroeléctrico BST en el varactor. Como puede verse en los resultados, variando la permitividad del material BST de 200 a 300 se consigue una variación en frecuencia de 4.15 GHz a 3.5 GHz con una distancia alrededor de 100 MHz entre frecuencias resonantes. Esto equivale a una variación de la frecuencia alrededor del 8% entre los valores de permitividad adyacentes.

CONTENTS

Abstract..... i
Resumen..... iii

1 Introduction.....1

1.1 State of art.....1

1.2 Goals of the Project.....20

1.3 Descrition of the project.....20

2 Background Theory.....22

2.1 Microstrip 22

2.2 Metamaterial.....23

2.3 Frequency Selective Surface (FSS).....25

2.4 Barium Strontium Titanate (BST).....27

2.5 Interdigital Capacitors 29

2.6 End-Loaded Planar Open Sleeve Dipole Antenna 30

2.7 Microstrip Patch Antenna 34

3 Design of the antenna's elements and results 39

3.1 Dipole antenna design.....39

3.2 Square Patch antenna design.....47

3.3 BST Varactor design.....51

3.4 Frequency Selective Surface Design.....59

4 Final Antenna Design 64

4.1 Design and results of the ELPOSD and Square patch antenna together with the FSS structure….....64

4.2 Design and results of both antennas with the FSS replacing the BST varactors by lumped capacitors.....70

4.3 Design and results of the main antennas with the FSS with BST varactors.....77

5 Conclusions and guidelines for future research 87

References 88

upna Universidad Pública de Navarra Nafarroako Unibertsitate Publikoa

CHAPTER 1. INTRODUCTION

1.1. STATE OF ART

Since the first radio link was built by Hertz in 1886, antennas have become a critical technology which allows people to stay connected and informed. Several advances have been made in the field of antenna theory and technology in the past hundred twenty years.

To the best of our knowledge, the first attempt to explore the concept of "artificial" materials appears to trace back to the late part of the nineteenth century when in 1898 Jagadis Chunder Bose conducted the first microwave experiment on twisted structures-geometries that were essentially artificial chiral elements by today's terminology. In 1914, Lidman worked on "artificial" chiral media by embedding many randomly oriented small wire lenses by arranging conducting spheres, disks, and strips periodically and effectively tailoring the effective refractive index of the artificial media. Since then, artificial complex materials have been the subject of research for many investigators worldwide. In recent years new concepts in synthesis and novel fabrication techniques have allowed the construction of structures and composite materials that mimic known material responses or that qualitatively have new, physically realizable response functions that do not occur or may not be readily available in nature. These metamaterials can in principle be synthesized by embedding various constituents/inclusions with novel geometric shapes and forms in some host media (Figure 1-1). Various types of electromagnetic composite media, such as double-negative (DNG) materials, chiral materials, omega media, wire media, bianisotropic media, linear and nonlinear media, and local and nonlocal media, to name a few, have been studied by various groups worldwide.

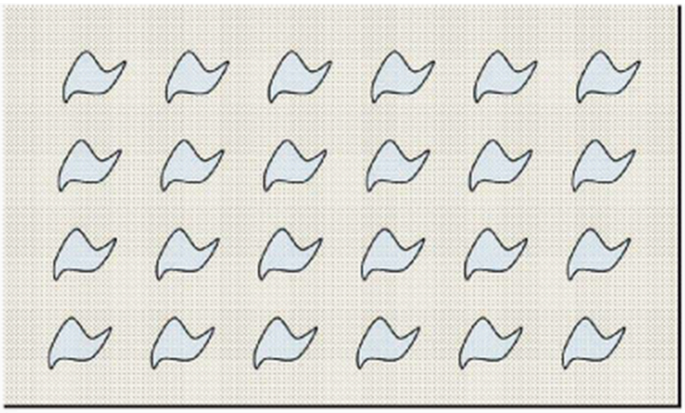

Figure 1-1. Generic sketch of a volumetric metamaterial synthesized by embedding various inclusions in a host medium.

As is well known, in particulate composite media, electromagnetic waves interact with the inclusions, inducing electric and magnetic moments, which in turn affect the macroscopic effective permittivity and permeability of the bulk composite "medium". Since metamaterials can be synthesized by embedding artificially fabricated inclusions in a specified host medium or on a host surface, this provides the designer with a large collection of independent parameters (or degrees of freedom) –such as the properties of the host materials; the size, shape, and composition of the inclusions; and the density, arrangement, and alignment of these inclusions–to work with in order to engineer a metamaterial with specific electromagnetic response functions not found in each of the individual constituents. All of these design parameters; the geometry (or shape) of the inclusions is one that can provide a variety of new possibilities for metamaterials processing.

Recently, the idea of complex materials in which both the permittivity and the permeability possess negative real values at certain frequencies has received considerable attention. In 1968, Veselago theorically investigated plane-wave propagation in a material whose permittivity and permeability were assumed to be simultaneously negative [Ves98]. His theoretical study showed that for a monochromatic uniform plane wave in such a medium the direction of the phase velocity, contrary to the case of plane-wave propagation in conventional simple media. Veselago termed this material such media left-handed (LH) due to the LH triad formed by the electric field vector, the magnetic field vector, and the phase propagation vector. However, since no such naturally occurring materials were known, Veselago's work laid dormant for nearly 30 years. Recently though, a composite material, also known as a metamaterial, consisting of a periodic array of either radiating or non-radiation elements or slots has been shown to exhibit left-handed properties. Therefore a frequency selective surface is a periodic array of either radiating or non-radiating elements or lots, which effectively act as band stop or band pass filter respectively to electromagnetic waves.

Metamaterials are being applied to the development and construction of many new devices throughout the electromagnetic spectrum. Limitations posed by the metamaterial operational bandwidth and losses can be effectively mitigated through the incorporation of tunable elements into the metamaterial devices. There are a wide range of approaches that have been advanced in the literature for adding reconfiguration to metamaterial

devices all the way from the RF through the optical regimes, but some techniques are useful only for certain wavelength bands. A range of tuning techniques span from active circuit elements introduced into the resonant conductive metamaterial geometries to constituents materials that change electromagnetic properties under specific environmental stimuli. This state of art presents a survey of the development of reconfigurable and tunable metamaterial technology as well as of the applications where such capabilities are valuable.

1.1.1. OVERVIEW OF EFFORTS AND TECHNIQUES

1.1.1.1. Metamaterials and Metamaterial-inspired devices

Many antenna, microstrip/transmission line and frequency-selective surface (FSS) applications use the term "metamaterial-inspired" to describe their use of resonant structures as loading or filter elements within the design, especially when the resonator in question has been repurposed from a metamaterial structure. The design and measurement procedure and goals may be viewed as a loose discriminator between a "metamaterial-enabled" and a "metamaterial-inspired" device. Metamaterial-enabled devices make use of the effective bulk or scattering properties of a metamaterial and will typically employ these desired effective properties in simulations during the design process. A metamaterial-inspired device, however, will rely on the exact behavior of individual resonators and will generally not utilize the metamaterial unit cells so as to obtain effective bulk behavior.

Although these structures are not true metamaterials, the fabrication approaches and design decisions share many similarities with metamaterial design, especially in the case of reconfigurable devices. Many of the examples in the literature of tunable metamaterials are more properly metamaterial-inspired devices which use individual resonators (most commonly a split-ring resonator (SRR)), often strongly coupled to transmission lines or antennas, as the proof of concept or even the final application for the design. The challenges towards implementation are shared for both approaches and a reconfigurable metamaterial-inspired transmission line or antenna may be viewed as the first step in the development of bulk tunable metamaterial-enabled devices.

1.1.1.2. Tuning method vs. Frequency

A variety of tuning methods have been examined in the literature to generate dynamic changes in a metamaterial's performance. These include direct changes to the unit cell's circuit model by varying capacitance or conductance, using electrically, chemically, thermally, or optically sensitive materials to change the constituent material properties of a structure and therefore change its electrical response and altering the geometry of the unit cell through stretching, shifting, or deforming all or part of the structure.

Some of these techniques (such as varactor diodes) have been applied for operation at particular wavelengths, while others (such as phase-change materials) have been applied across the electromagnetic spectrum. Each of these tuning methods is described in more detail in the next section.

1.1.1.3. Common unit cell designs

The base unit cell on which a reconfigurable metamaterial device is designed determines the fundamental behavior of the structure. In most cases, the starting point for the reconfigurable device is a static design, which is then augmented with the tunable component, material, or structure. The physical geometry of the unit cell determines the electromagnetic coupling into the metamaterial, provides (potentially desirable or undesirable) frequency selectivity, and can allow for cancellation of electric (in the case of the SRR) or magnetic (for the electric LC resonator) excitations as well as for strongly coupling the electric and magnetic responses. Especially at optical wavelengths, many unit cells do not explicitly couple to the electric or magnetic fields but are tuned to resonate simultaneously in the same geometry.

Unit cells with well-defined resonant and EM-coupling properties are commonly used to implement metamaterials with desired material properties, while designs for scattering control or antenna enhancements may be less sensitive to cross-polarization or E-H field (magneto-electric) coupling. Most tunable metamaterials are based on common elemental building blocks or particles, such as the widely used split-ring resonator (SRR), the complementary split-ring resonator (CSRR), and their electric-field coupled cousin the electric LC resonator (ELC). Often, the structure is modified to a greater or lesser degree to accommodate the constraints of the tuning mechanism. Tunable impedance surfaces are generally constructed from grounded square patches (mushroom-type artificial magnetic conductor (AMC) structures). In [Sie02] a beam steering microwave reflector

based on electrically tunable impedance surface is studied. A periodic resonant texture can transform a conductive sheet into a high-impedance surface. By adjusting the resonance frequency using varactor diodes, the surface impedance and the reflection phase are tuned. The reflection phase can be varied across the surface, to create an electronically tunable phase gradient, which can steer a reflected beam in two dimensions. Figure 1-2 shows the tunable surface, and is typically constructed as a printed circuit board, with a lattice of metal plates of the front side, connected to a solid ground plane on the back by metal plated vias.

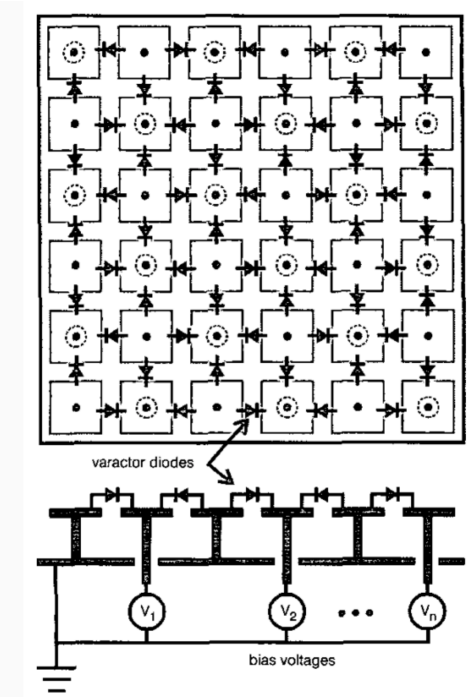

Figure 1-2. Electrically tunable impedance surface.

The pattern for three different phase gradients are shown in Figure 1-3, corresponding to beam positions of 0°, 20°, and 40°. The frequency of the plots is 4.2 GHz.

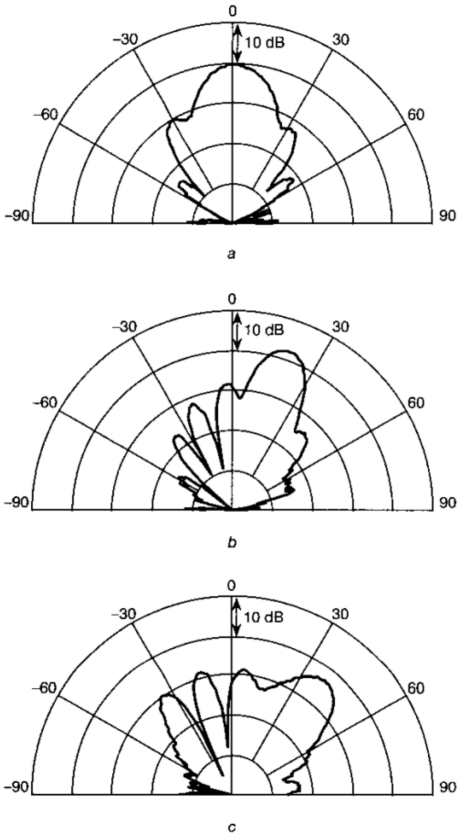

Figure 1-3. Radiation patterns at 4.2 GHz for three different phase gradients, corresponding to (a) 0°, (b) 20°, and (c) 40°.

Although basing a design on an existing resonator can be useful, many studies have developed new structures subject to limitations or to specifically leverage the capabilities of a given tuning mechanism; this includes the use of reorientable or variable distributions of colloidal nanoparticles, interconnected grid structures, and optimized binary FSS patterns. Transmission-line metamaterials may not use such a recognizable geometric unit cell pattern as an SRR or spiral but achieve periodic behavior instead based on their equivalent circuit model.

1.1.2. TUNING MECHANISMS

The various tuning mechanisms that have been demonstrated in the literature may be divided into three general categories. Circuit tuning involves the targeted insertion or modification of individual impedances into the unit cell circuit model; this includes the use of variable capacitors and switches within and between unit cells. We classify geometric tuning as those methods that physically perturb the structure of the unit cell in such a way that many or multiple changes occur in the equivalent circuit model. This would include moving subsets of the unit cell relative to a fixed point or using MEMS

devices to change orientation or location of a significant fraction of the unit cell. Finally, material tuning leverages changes in material parameters of a substrate, patterned layer, or small region of the unit cell to modify the response and properties. Phase change materials and liquid crystal devices are examples of this technique. The remainder of this section is devoted to describing the use of these methods as reported in the literature.

1.1.2.1. Circuit tuning

Since most metamaterial/metasurfaces are based on resonant particles, they can, in general, be modelled by LC circuits. The equivalent circuit depends on its geometrical parameters. However, if a variable lumped element is connected to the circuit their response can be tuned. Different approaches can be found in the literature:

- Varactor diodes

  Varactors are generally used to augment the capacitance in the metamaterial unit cells. Regarding frequency, ferroelectric varactors, such as those built with barium-strontium-titanate (BST) thick-film ceramic, have been used in Ka band in a transmit array design.

  Using varactors to reconfigure planar metamaterials (such as HIS or AMC) alleviates the bias distribution issue by allowing bias signals to be delivered through the bias and traces behind the ground plane, isolated from the incident RF signals. Applying varactors to transmission-line metamaterials also simplifies the bias distribution. Figure 1-4 shows an example of tunable AMC structure with integrated bias lines.

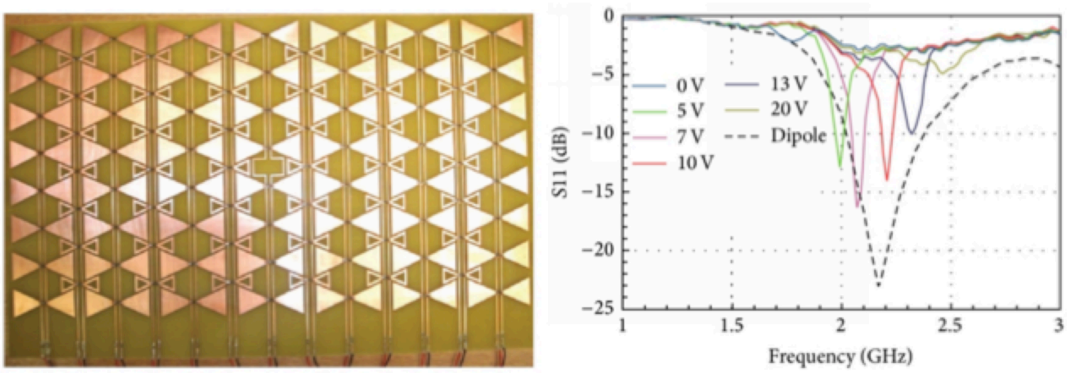

Figure 1-4. (a) Bow-tie AMC structure with bias lines to varactor diodes running throughout the structure. (b) When placed beneath a dipole antenna, tuning the varactors in the AMC controls the resonant frequency of the dipole.

upna Universidad Pública de Navarra Nafarroako Unibertsitate Publikoa

- Microelectomechanical Systems (MEMS)

  By using MEMS both the magnitude and the phase response of a metasurface can be controlled. MEMS have been used in antenna applications, in particular in reconfigurable reflectarrays for frequencies up to the W band. Their main advantages are the very loss losses and power consumption, linearity and possibility of monolithic integration. The main disadvantage is that analog control is not reliable enough and therefore they are used for digital control.

  Applying multiple switches per unit cell or group of unit cells allows multiple responses to be generated, as illustrated in Figure 1-5.

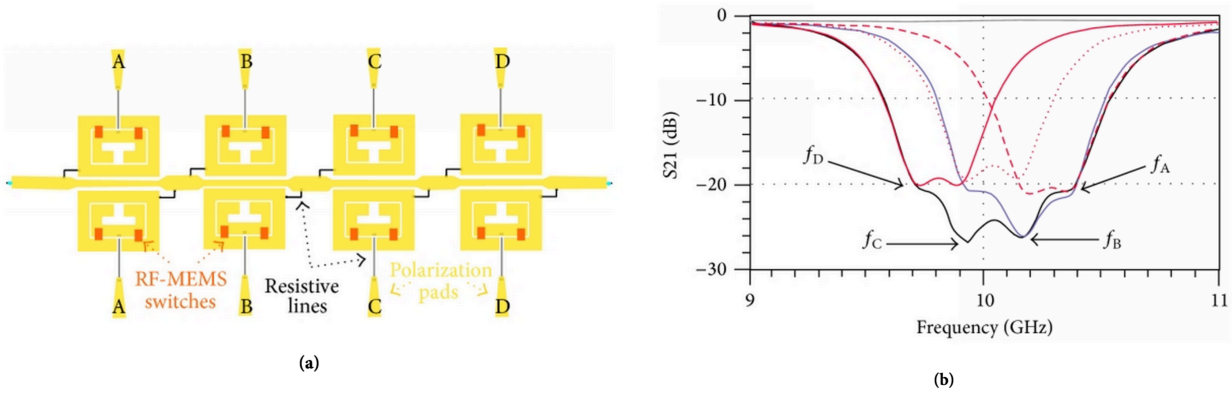

Figure 1-5. (a) The SRR-loaded microstrip line with RF-MEMS switches controlling the resonances acts as a bandstop filter. (b) The stopband frequency can be altered by changing the combination of switch states.

- P-i-n diodes

  A similar approach for unit cell reconfigurability can be obtained by means of P-i-n diodes. Recently a transmit array scanning antenna with 400 elements has been proposed and built working in the X-band, reaching 40º scanning.

- Ferrolectric varactors

  These types of varactors have several advantages such as design versatility, relative low cost and fast tuning speed. They have been used both in transmit array and metamaterial substrate based scanning antennas.

1.1.2.2. Geometrical tuning

Many metamaterials rely on conducting elements that can couple with impinging electromagnetic waves in order to achieve a desired electric or magnetic resonance or other effective behavior. Because the metamaterial properties typically depend on the

shape, size, orientation, and proximity of the conducting elements, techniques that alter the geometry of the conducting elements can provide an excellent means for tuning or switching the metamaterial response.

For instance piezoelectric actuators were used to modify the response of an AMC. Another example of this type of tuning is done with the displacement between two textured substrates that changes the dispersion properties and therefore the pointing angle of a leaky antenna.

In addition to reorienting entire elements, metamaterial can be geometrically tuned by moving conducting elements in relation to each other. MEMS are frequently employed to perform the mechanical movement of conducting elements for THz metamaterials. Several tunable HIS (High Impedance Surfaces) have been demonstrated that operate by mechanically shifting an upper plate of elements along the surface or vertically in order to adjust the phase of the reflected wave, illustrated in Figure 1-6. Tuning the phase of a HIS is effective for steering a radiated beam from an antenna system. Several tunable HIS have also been demonstrated that employ MEMS to raise or lower capacitive conducting plates in the unit cell. This technique effectively changes the capacitance in a part of element and operates similar to the circuit tuning techniques described in Section 1.1.2.1.

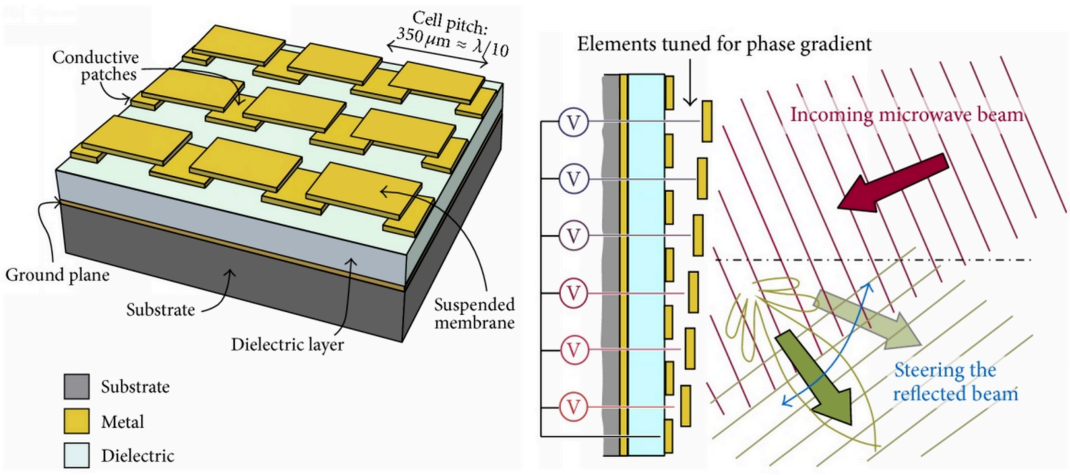

Figure 1-6. (a) Vertical motion of a suspended conductive membrane changes the resonant frequency of the high-impedance surface. (b) Varying the MEMs actuation voltage across the surface allows the metamaterial to act as a reflectarray.

1.1.2.3. Material tuning

Since most metamaterials and metasurfaces are built on dielectric substrates, by modifying their properties, it is possible to reconfigure the response of the device. Different candidates have been proposed, such as ferroelectric films or liquid crystals.

upna Universidad Pública de Navarra Nafarroako Unibertsitate Publikoa

1.1.3. APPLICATIONS AND TUNING GOALS

The inherent nature of tunable and reconfigurable metamaterials affords them the ability to be used in a wide variety of applications. The distinctions between these end goals are largely a matter of perspective. Shifting the frequency of a pass band is functionally identical to changing from a transmissive to reflective surface at a fixed frequency. Interpretation of an identical change in response can be made in terms of scattering parameters, effective material parameters, or the metamaterial's loading effect on an adjacent antenna or transmission line. We acknowledge the discretionary nature of categorizing tunable metamaterials into intended applications; however, in this literature survey, we define four broad common application areas. First, we discuss the design of tunable metamaterials as an enabling technology for tunable filters and antennas; this focuses on metamaterials that are primarily designed to shift the resonant frequency or alter the device's bandwidth. We then note metamaterials that are optimized to modulate the scattering (transmission, reflection, and absorption) of a material at a given resonant frequency. We classify designs meant to spatially vary the index of refraction with a focus on transformation electromagnetics. Finally, we recognize tunable structures that manipulate wave propagation characteristics including directivity, radiation pattern, polarization, and propagation mode.

1.1.3.1. Tunable filters and antennas

A major focus of tunable and reconfigurable metamaterials lies with designing tunable filters and frequency-reconfigurable antennas. One desirable feature of such devices is tunable frequency band selectivity. In wireless communications, using tunable metamaterials enables wider ranges of operating bands within a minimal geometry. Bossard et. al. have applied liquid crystal superstrates to shift the frequency of the transmission band in an infrared FSS device [Bos08], as illustrated in Figure 1-7 and Figure 1-8.

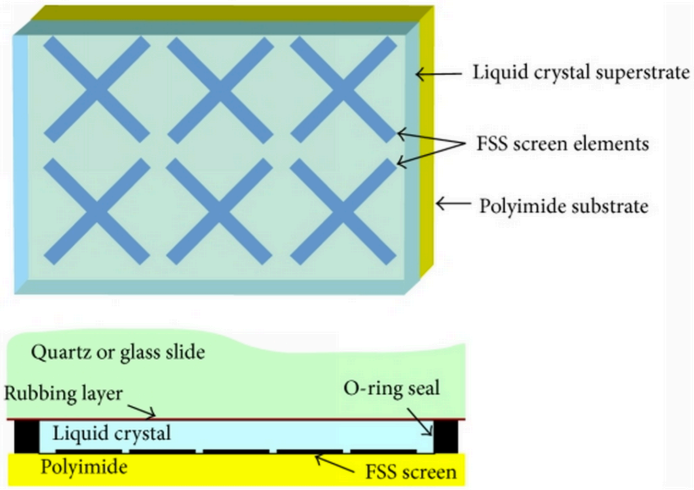

Figure 1-7. An illustration of a liquid-crystal-based tunable FSS unit cell.

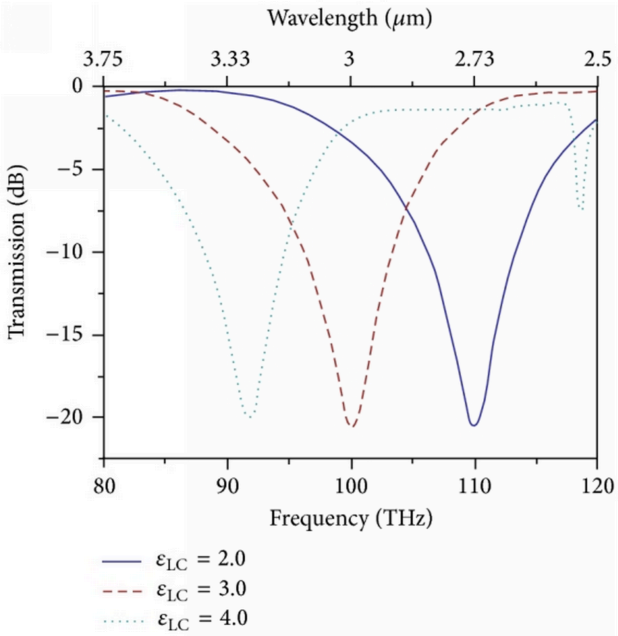

Figure 1-8. Changing the applied potential difference between the FSS and the quartz slide changes the liquid orientation and the scattering response of the FSS.

Reynet and Acher demonstrated tunable varactor-loaded metamaterials based on conducting coils [Rey04]. Later works introduced this concept into transmission lines and antennas, where tuning was achieved by varying capacitance, typically of SRRs and CSRRs [Lim08, Gil06, Mir11, Bou08]. Zhu et al. demonstrated an electrically small, tunable SRR antenna operating in the UHF frequency band [Zhu13]. As shown in Figure 1-9, this varactor-loaded dipole-like structure provides a tunable narrowband (notch filter) alternative to wideband antennas in RF communication systems. The antenna has the advantage of compact size, low cost, and easy fabrication as well as implementation.

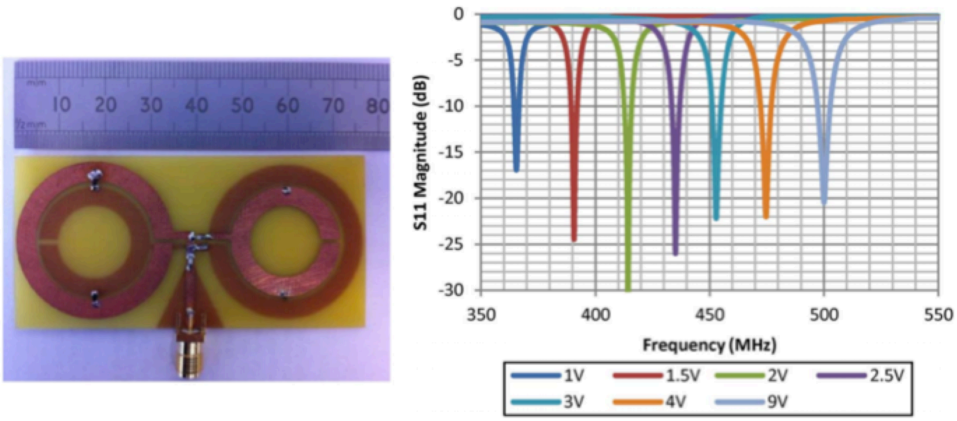

Figure 1-9. (a) This varactor-loaded dipole-like antenna has a (b) narrow-band but tunable notch-filter response, allowing operation over a wide range of frequencies while avoiding spurious signals.

Researchers have attained similar RF frequency tunability through a variety of other methods, such as through MEMS [Ekm09, Cho09, Gil07], tunable EBG surfaces [Lia09, San03, Fer10, Bra04], ferroelectric rods and films [Ozb07, Hou10, Gil09, Kan08], vanadium dioxide switches [Bou09, Bou10], and liquid crystals [Bos08, Zha07]. These proposed designs exhibited varied tunable RF filter types, such as band-stop, band-pass, and notch filters. Whereas the filters discussed above are actively voltage-controlled, designers have also demonstrated nonlinear varactor-loaded (or p-i-n-loaded) metamaterial filters that vary with incident power, making them ideal for nonlinear devices such as RF limiters [Kat11]. Frequency tunability is especially desirable for fabricating flexible devices in the terahertz and optical bands. Such devices could include sensitive platforms for measuring chemical or biological agents, temperature sensors, and intelligent detectors among other applications [Han08, Xia09, Jep10]. Furthermore, in contrast to scanning the center frequency of a desired response feature, another essential functionality is tunable bandwidth, or reconfigurable filtering type, that is, dynamically switching between band-pass, band-stop, notch, and so forth. Several authors have demonstrated metamaterial structures that exhibit reconfigurable filter types, as well as tunable center frequencies [Bay09, Wiw11]. Tunable filters, FSSs, and antennas have wide ranges of applications across the electromagnetic spectrum. Tunable metamaterials offer a cost-effective, compact, and flexible option for implementing tunable band selectivity and reconfigurable filter functionality in applications ranging from RF communication system design to optical sensors and detectors.

1.1.3.2. Scattering parameter tuning

Tuning the transmission, reflection, and absorption characteristics of a material at a particular frequency affords the designer the creation of devices such as switches, modulators, FSSs, absorbers, sensors, and more. Tunable metamaterials offer avenues for realizing these devices in low-profile mediums with ultrafast tuning capabilities. A fundamental goal for dynamically controlling the scattering from a material is amplitude modulation. Tunable metamaterials enable designers to create high-speed modulators that alter the transmission and/or reflection amplitude of an incident electromagnetic wave [Che06, Shr11, Kas09]. Practical devices emerge from this fundamental functionality, such as high-speed switches operating in the terahertz and near-infrared bands [Ou13, Pad06]. Ou et al. demonstrated a switchable metamaterial that operates in the optical band at three orders of magnitude faster than previously achieved [Ou13]. As shown in Figure 1-10, electrostatic forces were used to drive parallel strings at megahertz frequencies to modify the transmission and reflection spectra of the device. The characteristics of this device make it ideal for protective optical circuitry and reconfigurable optical networks. Tunable scattering characteristics are also vital to developing tunable cloaks and electromagnetically transparent materials.

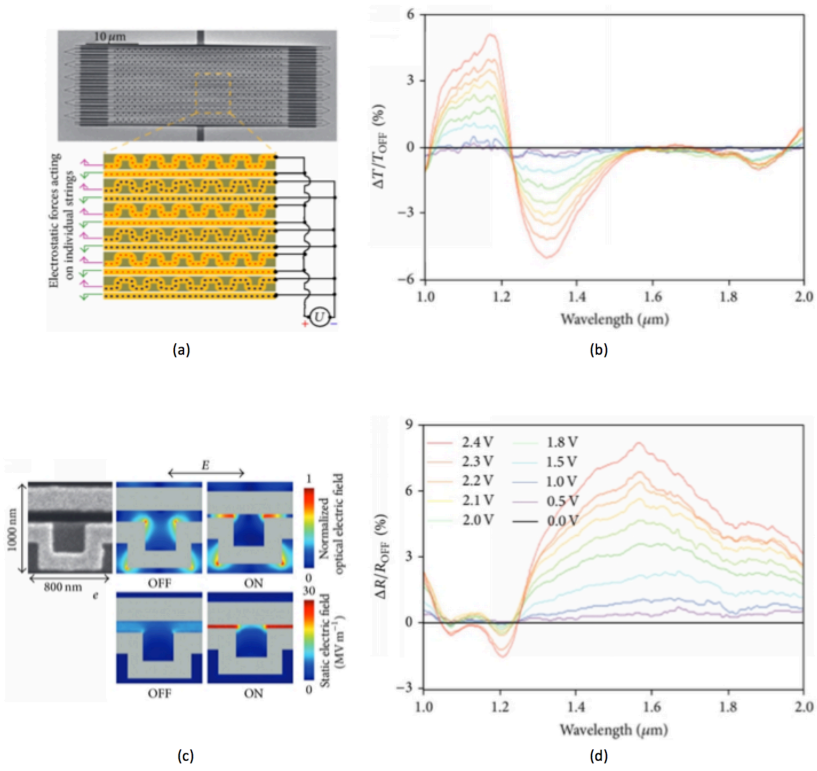

Figure 1-10. (a) Scanning electron microscope (SEM) image of photonic metamaterial device and schematic of driving circuit. (c) SEM image of single metamolecule and plasmonic field distribution for OFF and ON state. (b) Transmission and (d) reflection spectra of photonic metamaterial at varied induced static voltages.

In particular, by controlling the reflection and transmission, designers can create perfect absorbers, reduce radar cross-section, or achieve complete transmission and reflection from a surface [Mia07, Lia05, Tao11]. Tao et al. designed a MEMS-based structurally tunable metamaterial that can dynamically modify its transmission amplitude in the terahertz regime [Tao11]. As shown in Figure 1-11, rotating the unit cell plane with respect to the incident electric and magnetic fields alters the coupling efficiency. Structural reconfiguration time can be on the order of milliseconds, allowing this design to be used in applications ranging from reconfigurable filters, thermal cantilever-based detection, or tunable absorbers, cloaks, or concentrators.

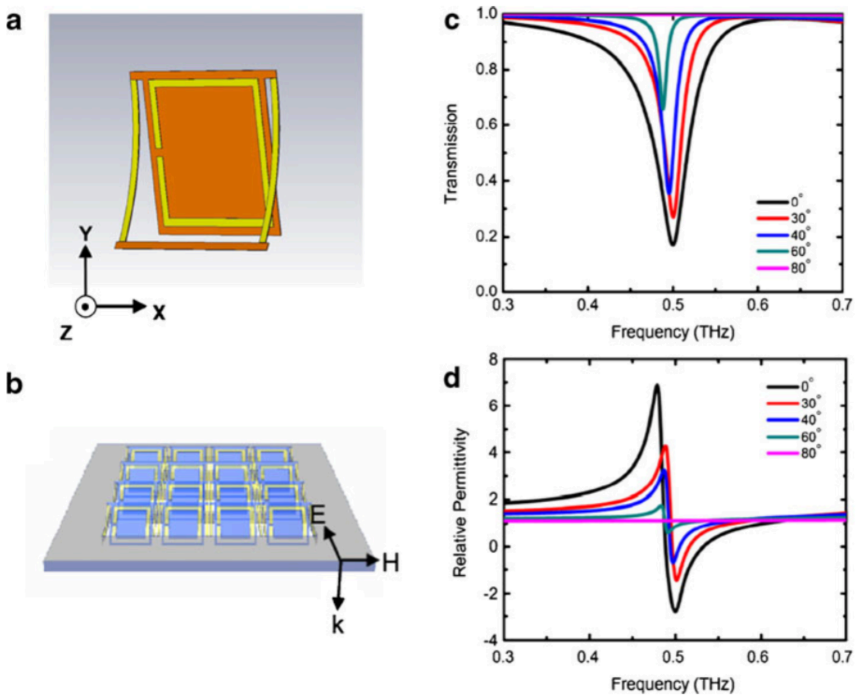

Figure 1-11. Simulation of pure tunable electrically resonant responses of the structurally tunable THz metamaterials: **a** schematic of the unit cell; **b** schematic of polarization of the incident radiation; **c** transmission spectrum as a function of frequency; **d** extracted effective permittivity (***ε***) as a function of frequency.

Controlling scattering also has several applications in the optical band; varying transmission and reflection enables the development of optical temperature sensors, switches, modulators, and other planar optical metamaterial-enabled devices [Liu10, Ou11]. One particular application is in compressive sensing. Werner et al. demonstrated a phase change material that could spatially modify its complex index of refraction to dynamically change the effective size and shape of an aperture [Wer11]. This beam-forming aperture, with its ultrafast response in the infrared band, could then be used for compressive sensing, a technique where few information rich measures are sampled to

construct high-resolution images. This technique is a step towards achieving the desired resolution while maintaining the area coverage and minimizing the cost, size, weight, and power of the sensor system. Controlling the scattering characteristics of a material enables designers to create a wide variety of common devices across the electromagnetic spectrum.

1.1.3.3. Spatial tuning for GRIN lenses

The recent explosion of research in transformation electromagnetics techniques [Kwo10] has increasingly put emphasis on spatially modifying the parameters of materials. In particular, these spatial gradients are primarily focused on altering index of refraction. Sheng and Varadan investigated the effect of substrate dielectric (relative permittivity) on a metamaterial structure [She06]. By varying the relative permittivity from 1 to 14, the structure's resonant frequency dropped from 16 GHz to 6 GHz [She07]. This discovery provided a foundation for designing voltage tunable dielectric substrates, which led to the development of microfabricated artificial dielectrics for microwave circuits [Chi11]. While this research addressed only modifying the overall index of refraction of a substrate, several authors developed methods for creating materials with spatially varying indices of refraction [Gol09, Han09]. Spatial gradients are the fundamental mechanisms in electromagnetic cloaking. Researchers have demonstrated spatially varying material parameters that are intended to guide electromagnetic waves around a desired region [Wan08, Hra10]. Wang et al. designed a reconfigurable cloak that could be tuned for multiple operating frequencies. Furthermore, this cloak could be switched from a visible to invisible status [Wan08]. The mechanism for attaining this cloak's spatial gradient index of refraction relaxes fabrication precision constraints because each unit cell can be tuned independently. These features make it ideal for cloaking in RF communication systems [Kwo08]. The structure, material parameters, and field distribution of this cloak are depicted in Figure 1-12. In addition to varying index value, researchers have also demonstrated metamaterials that vary in anisotropy [Zhu12]. Such features can be used in creating displays, beamsplitters, isolators, cloaks, and hyperlenses and in controlling luminescence.

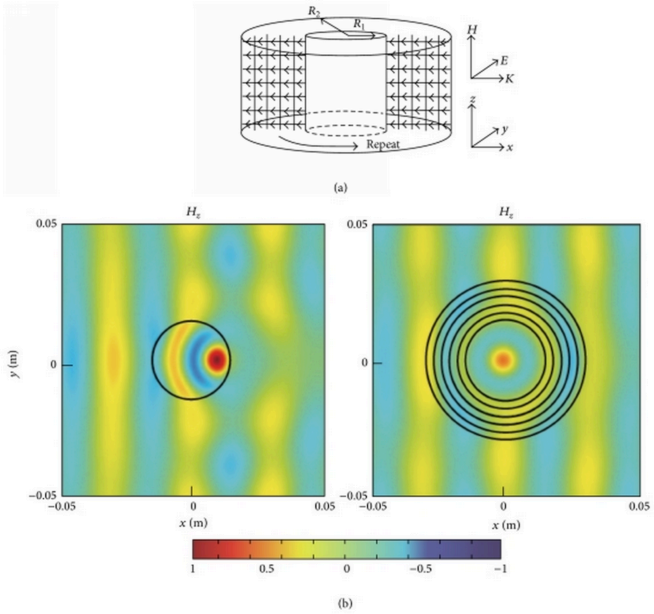

Figure 1-12. (a) Configuration of TM mode reconfigurable cloak; independent control over the effective material properties of each unit cell within the cylindrical region is achieved through independent biasing of each column of diodes. (b) Magnetic field distributions surrounding and within the dielectric cylinder with and without the cloak shell at 9,5 GHz. The material properties throughout the structure may be tuned to act as a cloak around the inner cylinder.

1.1.3.4. Antenna propagation tuning

Tunable metamaterials also provide the potential for increasing existing component functionality and enhancing propagation properties, such as scanning range, radiation pattern, and directivity, while simultaneously reducing costs. In particular, tunable metamaterials have found applications in fabricating reconfigurable directive antennas and beam steering devices, especially for radar and communication systems: radomes, radar absorbent materials, reflectors, electromagnetic interference shielding, and terrestrial and satellite communications. Many of the efforts towards achieving beam steering focus on developing electrically and mechanically tunable high-impedance or artificial magnetic surfaces [Sie01, Hig03, Cos08, Han07]. Artificial magnetic surfaces typically consist of planar periodic metallic elements backed by a PEC ground plane. Coupled with tuning elements, they are commonly utilized as tunable high impedance ground planes to achieve low-profile antenna configurations. Costa et al. employed this concept to create a steerable bow-tie antenna [Cos08]. Figure 1-13 displays the artificial magnetic surface, the reflection phase at varied capacitance values, and the resulting beam deflections.

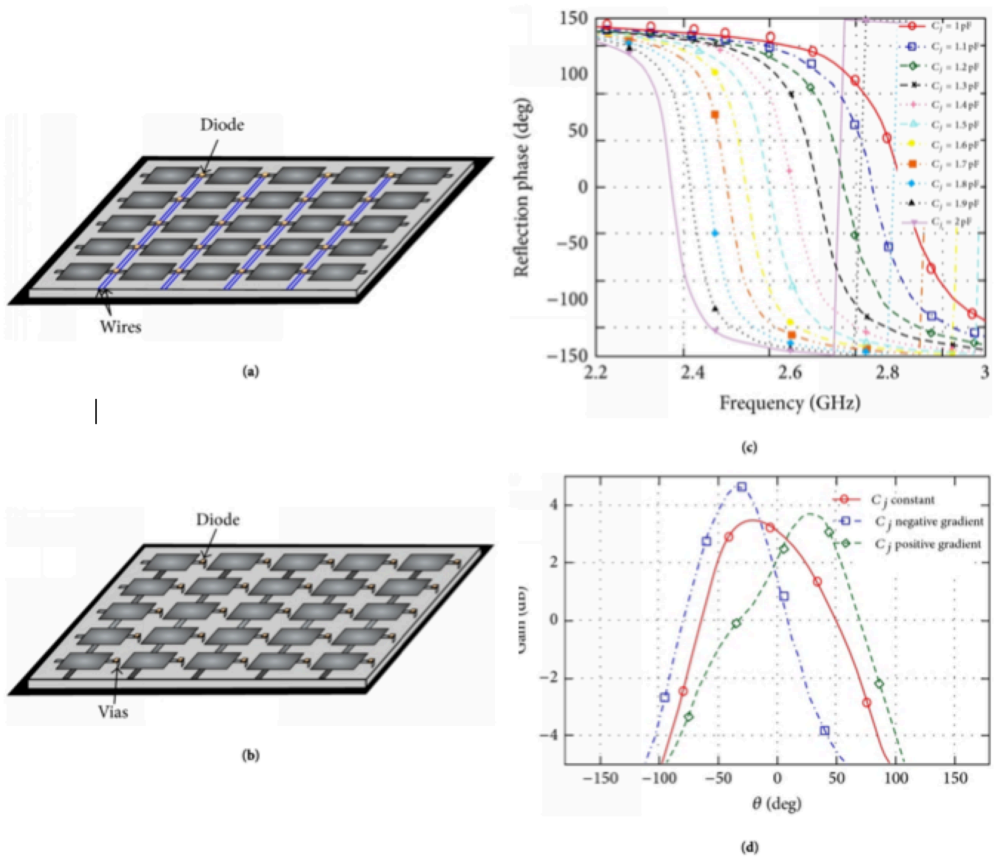

Figure 1-13. (a) – (b) Active AMC bow-tie surface showing varactor diode tuning between the bias lines and the bias to the ground plane. (c) Tuning the varactor state changes the frequency response of the AMC. (d) Applying a constant gradient to the AMC capacitances allows beamfroming by a bow-tie antenna placed above the surface.

Ratajczak et al. demonstrated a directive antenna using a planar electromagnetic band-gap reflector based on the same design principles [Rat07], which is shown in Figure 1-14. This proposed design offers advantages over traditional directive array antennas, which suffer from complex, expensive, and bulky feeding networks with high losses. This design is easier to fabricate and simple to use in large frequency bands, has low losses due to a waveguide feed structure, and has a tunable radiation pattern. With average tuning ranges of approximately ±45 degrees, these tunable impedance surfaces offer low-cost, low-profile, and light-weight alternatives to traditional scanning antennas and reflectors.

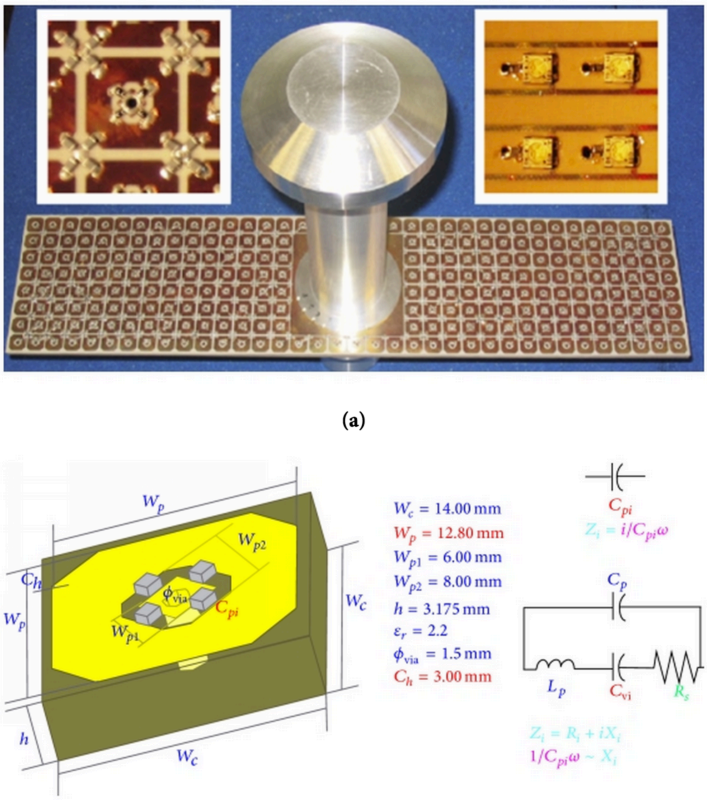

Figure 1-14. (a) Reconfigurable reflectarray that changes the reflection coefficient from the surface by varying the capacitance between the central via and the ground plane. (b) Reflectarray unit cell geometry and equivalent circuit model.

Similar functionality can be achieved with digitally addressable, anisotropic, and SRR-based metamaterials [Sie12, Sie13]. Several papers also document work towards creating partially reflective surfaces that alter the reflection and transmission phases for use in Fabry-Perot cavity systems to obtain directive emissions [Wei08]. Tunable metamaterials also offer increased functionality when incorporated into existing devices. Meng et al. demonstrated a reconfigurable magnetic metamaterial-loaded waveguide in which the propagation mode could be switched between left-handed and right-handed [Men11]. This increases the functionality of microwave waveguide systems by allowing designers to broaden the scanning range or control the radiation pattern of leaky wave antennas, which increases the link capacity for multi-input/output communication systems.

upna Universidad Pública de Navarra Nafarroako Unibertsitate Publikoa

1.1.3.3. Remaining challenges

Based on the existing capabilities described in the literature, several broad goals are seen for future developments. Extending tuning concepts that have been demonstrated at an individual or small number of unit cells to tile or fill large regions is necessary for the implementation of many metamaterial or transformation electromagnetics/optics devices, such as lenses. Very few studies have demonstrated spatial tuning of metamaterials for the creation of reconfigurable gradient-index lenses, for example. Expanding the reconfigurable unit cells to large regions of independently tunable elements requires the associated development of tuning and control signal distribution throughout the metamaterial. Finally, extending the tunable range and application flexibility of reconfigurable metamaterial devices will enhance the usefulness and applicability of this design strategy to solving real-world problems.

Another general area for future development is the expansion of available tunable materials. In particular, phase-change materials are under continued development to expand the range of material formulations and to refine the switching and tuning circuitry. While phase-change materials have already been commercialized for high speed memory applications in computer hardware, their suitability for incorporation into practical, high-speed switchable metamaterials is a topic of ongoing research. The development of smart materials that respond to environmental stimuli is also an area of future development. Multiple works were highlighted in the literature looking at conducting polymers that can change properties under stimulus by chemical analytes. Further work is required in both the material science and electromagnetic fields to identify candidate sensing materials and develop metamaterial platforms to bring other smart devices into practice.

Finally, extending the tunable range and application flexibility of reconfigurable metamaterial devices will enhance the usefulness and applicability of this design strategy to solving real-world problems. There is room for advances in material and switch development as well as identifying metamaterial geometries that are sensitive to the switching property in order to increase the device tuning range and functionality.

upna Universidad Pública de Navarra Nafarroako Unibertsitate Publikoa

1.2. GOALS OF THE PROJECT

This project has set the goal to design a planar dipole antenna and a Square Patch antenna that uses a frequency selective surface (FSS) that is tunable using BST varactors whose capacity can be altered by applying a voltage. The tunable unit cell is a square patch working at 2.4 GHz. These unit cells were located along the FSS at a certain distance from each other where BST varactors are accommodated. The varactors used are barium strontium titanate (BST) designed with interdigital capacitors, and they were placed only along one dimension of the FSS to avoid the use of bias and simplify the dc-bias network.

The overall design of both antennas is performed at a frequency of 2.4GHz. Once obtained the results, a comparison between both antennas will be done in order to decide which of the two main antennas are better for this performance. The return loss, the radiation pattern and the E field is studied for both antennas.

The software used for the modeling and design of the antennas is Ansys HFSS.

1.3. DESCRIPTION OF THE PROJECT

In the first chapter it has made a survey of the development of reconfigurable and tunable metamaterial technology as well as of applications where their capabilities are valuable.

In chapter 2, we discuss the theoretical bases on which we work throughout the project as frequency selective surface (FSS), BST material, interdigital capacitors, metamaterial, microstrip structure, end-loaded open sleeve planar dipole antenna and Square Patch antenna.

In chapter 3 the design and results of the antenna are presented. This section consists of four major parts. The first one is the design of one of the main antennas, the ELPOSD antenna. The second shows the design of the Square Patch antenna that is used to be the main antenna. The third part the design of BST varactors diode with three different combinations of interdigital capacitors, the advantages and disadvantages of using an interdigital capacitor of 3, 5 or 7 fingers are studied. Four parts illustrate the design of the square patches of the frequency selective surface (FSS). Once defined its dimensions is integrated as array of element in the FSS where their correct operation in

upna Universidad Pública de Navarra Nafarroako Unibertsitate Publikoa

the operational frequency is checked. Afterwards, the BST varactors diodes are inserted and the results are studied to verify their proper operation.

In the forth and last part of this chapter all devices are integrated into the final system in order to study their behavior as a whole.

In chapter 4 the devices designed previously are integrated into the final design in order to study their behavior as a whole. In addition, a comparison between ELPOSD antenna and Square Patch antenna is carried out to decided which antenna is better for the overall design.

Chapter 5 includes the conclusions of the results obtained with both antennas and possible future research based on the study in this project.

CHAPTER 2. BACKGROUND THEORY

2.1. MICROSTRIP

Microstrip transmission lines consist of a conductive strip of width "W" and thickness "t" and a wider ground plane, separated by a dielectric layer, also known as the "substrate", of thickness "h" as shown in Figure 2-1. Microstrip is by far the most popular microwave transmission line, especially for microwave integrated circuits and MMICs (Monolithic Microwave Integrated Circuits). The major advantage of microstrip over stripline is that all active components can be mounted on top of the board. The disadvantages are that when high isolation is required such as in a filter or switch, some external shielding may have to be considered. Given the chance, microstrip circuits can radiate, causing unintended circuit response. A minor issue with microstrip is that it is dispersive, meaning that signals of different frequencies travel at slightly different speeds.

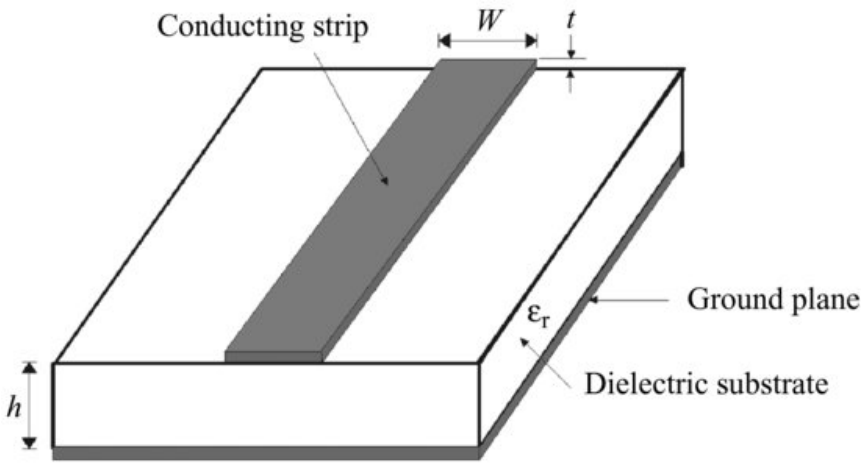

Figure 2-1. Microstrip

Part of the fields from the microstrip conductor exists in the air as shown in Figure 2-2. Because of this the two-media nature of microstrip causes its dominant mode to be hybrid (Quasi-TEM) not TEM, with the results that the phase velocity, characteristic impedance, and field variation in the guide cross-section all become mildly frequency dependent. Based on waves theory the velocity of propagation depends only on the material properties, namely, the magnetic permeability "μ" and the electric permittivity "ε_r ".

When the longitudinal components of the field for the dominant mode of a microstrip line are much smaller than the transverse components, the Quasi-TEM approximation is applicable to facilitate design.

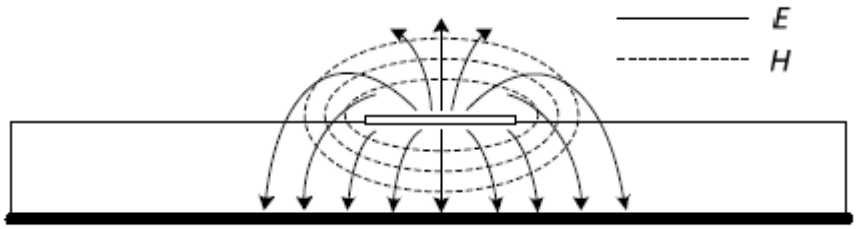

Figure 2-2. Microstrip electric an magnetic field lines

Since some of the electric energy that is stored in this conductor configuration is in the air, and some is in the dielectric, the effective dielectric constant for the waves on the transmission line will lie somewhere between that of the air and that of the dielectric. Typically, the effective dielectric constant will be 50-85% of the substrate dielectric constant, depending on the geometry of the microstrip. This effective dielectric constant determines the phase velocity of electromagnetic waves on the microstrip transmission line.

2.2. METAMATERIAL

Usually, the material properties are characterized by an electric permittivity (ε) and a magnetic permeability (μ). The thinnest material in nature is free space or air, whose permittivity is ε_0 and permeability is μ_0. The relative permittivity and permeability of a material are defined as $\varepsilon_r = \varepsilon/\varepsilon_0$ and $\mu_r = \mu/\mu_0$, respectively, which define another important material parameter, the refractive index, as $n = \sqrt{\varepsilon_r \mu_r}$. In nature, most materials have the permeability μ_0 and permittivity larger than ε_0. The metamaterial opens a door to realize all possible material properties by designing different cellular architectures and using different substrate materials. Figure 2-3 illustrates all possible properties of isotropic and lossless materials in the $\varepsilon - \mu$ domain. In Figure 2-3, the first quadrant ($\varepsilon > 0$ and $\mu > 0$) represents right-handed materials (RHM), which support the forward propagating waves. From the Maxwell's equations, the electric field **E**, the magnetic field **H**, and the wave vector **k** form a right-handed system. The second quadrant ($\varepsilon < 0$ and $\mu > 0$) denotes electric plasma, which support evanescent waves.

The third quadrant ($\varepsilon < 0$ and $\mu < 0$) is the well-known left-handed materials (LHM), which was proposed by Veselago in 1968 [Ves98], supporting the backward propagating waves. In LHM, the electric field **E**, the magnetic field **H**, and the wave vector **k** form a left-handed system. The fourth quadrant ($\varepsilon > 0$ and $\mu < 0$) represents magnetic plasma, which supports evanescent waves.

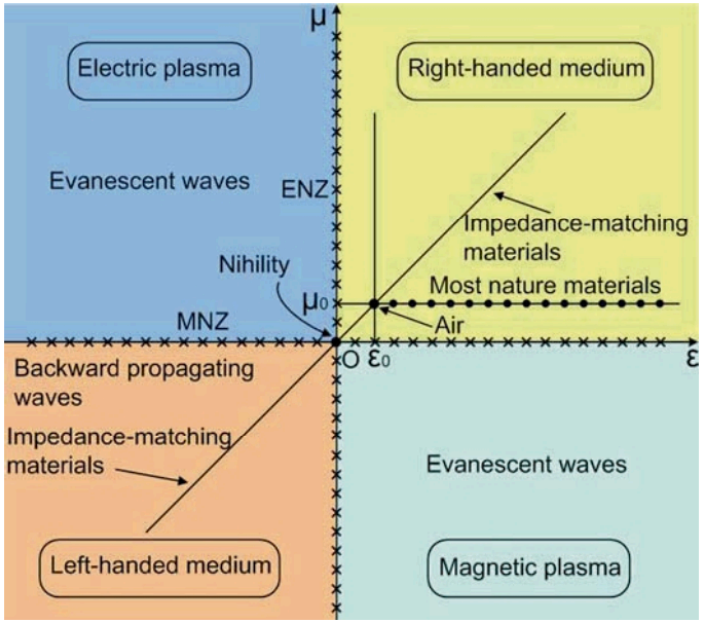

Figure 2-3. All possible properties of isotropic materials in the $\boldsymbol{\varepsilon - \mu}$ domain.

In recent years metamaterials have been used in the field of electromagnetics. The term is used to define materials with properties and characteristics that cannot be found in nature. In [Yan08], the materials are classified according to their properties as double negative (DNG), left-handed (LH), negative refractive index (NRI), artificial magnetic conductor (AMC), soft and hard surfaces, magneto materials, and high impedance surfaces (HIS). Some materials exhibit properties associated with more than one of the above classification.

In a long period, metamaterials, left-handed materials, negative-refractive index materials, double negative materials, and backward-wave materials have been regarded as the same terms. However, the actually represent different meanings. Metamaterials have much broader scope than LHM, as shown in Figure 2-3. In the $\varepsilon - \mu$ domain, there are several special lines and points indicating special material properties. For example, the point $\mu = -\mu_0$ and $\varepsilon = -\varepsilon_0$ represents an anti-air in the LHM region, which will produce a perfect lens; the point $\mu = 0$ and $\varepsilon = 0$ represents a nihility, which can yield a perfect tunneling effect; the line $\mu = \varepsilon$ in both RHM and LHM regions represents

impedance-matching materials, which have perfect impedance matching with air, resulting no reflections. Also, the vicinity of $\mu = 0$ is called as μ -near zero (MNZ) material, and the vicinity of $\varepsilon = 0$ is called as ε-near zero (ENZ) material, which has special properties.

Actually, metamaterials have much more features beyond those shown in Figure 2-3. Metamaterials can be design as weakly and highly anisotropic, depending on different requirements. The flexibility to design various material properties together with the optical transformation makes it possible to control electromagnetic waves at will using metamaterials.

2.3. FREQUENCY SELECTIVE SURFACE (FSS)

A frequency selective surface is a periodic array of either radiating or non-radiating elements or slots, which effectively act as band stop or band pass filter respectively to electromagnetic waves.

There are four different types of possible element-type FSS arrays: center connected, loop, plate and combination. Some examples are shown in Figure 2-4. Each group of elements is ordered from most narrow-banded on the left to most wide-banded on the right.

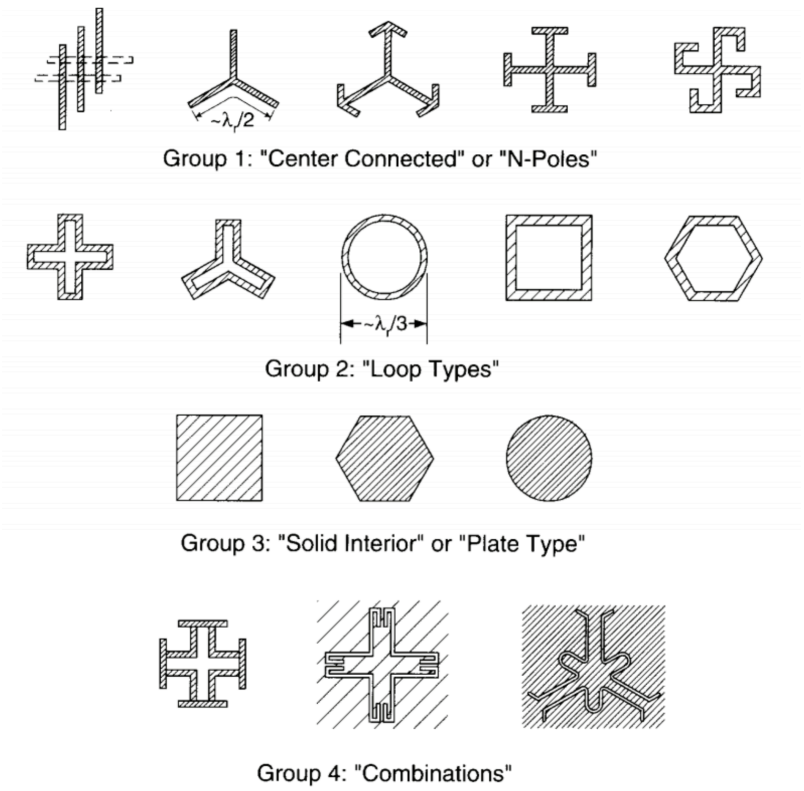

Figure 2-4. The four major groups of FSS elements. Elements are ordered from the most narrow-banded on the left to most wide-banded on the right.

The first group, the center connected elements, are a viable candidate for both radiating and non-radiating arrays. Perhaps the most recognizable from the center connected group is the dipole. This is by nature a narrow banded element, but when placed in a well designed array this element is capable of reaching a ratio of 4:1 without the addition of a dielectric matching section added in front of the array of a bandwidth or a decade or better with a dielectric matching section. This is mentioned to demonstrate that the bandwidth of an individual element does not necessarily determine the bandwidth of the array.

The loop elements are in general an excellent choice for non-radiating element FSS arrays. These elements are typically smaller in the x and y directions than the center connected elements with respect to a wavelength and thus can be spaced close to one another.

Plate elements in general do not have very desirable characteristics. First the element have x and y dimensions around a half of a wavelength, which limits how closely these elements can be placed next to one another. In addition plates are highly inductive elements with small capacitances between them, leading to issues with regard to achieving resonance. If the FSS never resonates, then it is impossible to achieve perfect reflection. This is due to the fact that at resonance, the FSS becomes a short circuit (assuming the materials are lossless) and thus acts as a perfect electric conductor (PEC) ground plane.

Finally combination elements are too diverse to generalize in any meaningful way. The possibilities in this group are as boundless as the imagination of the designer.

The chosen group for the purpose of this project is the plate elements, more specifically the square patch, due to the simple shapes that form this group. These types can be characterized as being made with solid interior. Figure 2-5 shows the S11 parameter versus frequency of an infinity FSS made with square patches working at 2.4 GHz varying the distance between the patches. The distances used in terms of lambda are 0.125 λ, 0.168 λ, 0.232 λ, 0.248 λ, 0.344 λ, and 0.368λ. As can be see, the closer they are, the more act as perfect electric conductor. Also, the distance that the patches are placed makes vary the resonance frequency around 2.4 GHz, but when the patches are very close the resonance frequency differs significantly from 2.4 GHz.

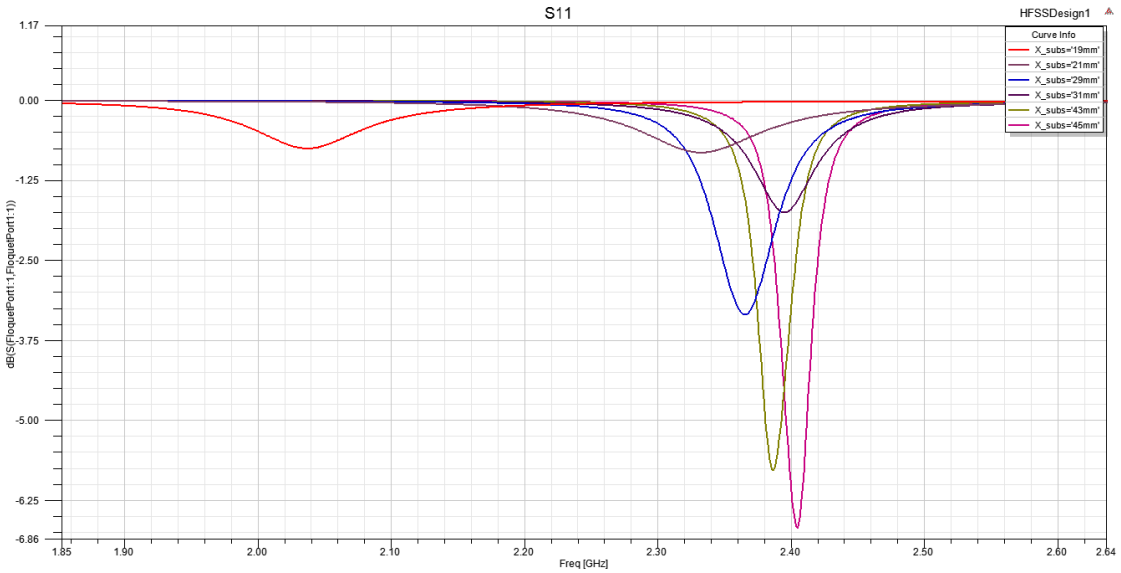

Figure 2-5. Comparison of S11 performances when the distance between patches is varied.

2.4. BARIUM STRONTIUM TITANATE (BST)

With the growth of wireless communication systems, there is a high demand for frequency-agile components. Ferroelectric thin films, particularly barium strontium titanate (BST) have been widely investigated for the applications of tunable filters, matching networks, phase shifters and other radio frequency (RF) and microwave (MW) devices.

BST is a popular ferroelectric material due to its high permittivity and low loss, which yield RF components with high tunability and quality factors, respectively. The tunable nature of BST is derived from its electric field-dependent permittivity.

Over the past several years the semiconductor industry has shown increasing interest in Barium Strontium Titanate due to its inherent high dielectric constant. BST is envisioned as an enabling material in several integrated circuit (IC) applications, including DRAM (Dynamic Random Access Memory), on-chip capacitors and integrated RF filters (Figure 2-6).

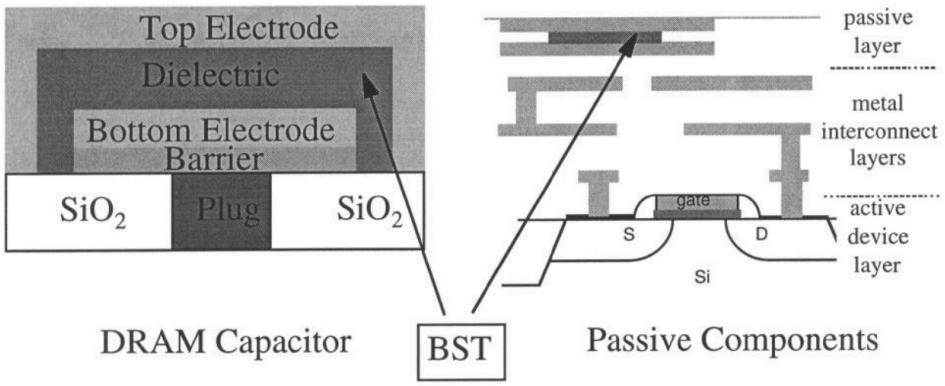

Figure 2-6. Schematic depictions of potential applications of BST in integrate circuits.

An attribute of BST is the dependence of its electrical behavior upon its physical and chemical properties, allowing the BST behavior to be tailored by the thin film deposition process. However this attribute requires a thorough knowledge of these relationships and the ability to measure and control the material properties. Among these relationships is the dependence of dielectric constant on both Sr/Ba ratio and A/B [(Ba+Sr)/Ti] site ratio; for example, a 10 % change in A/B site ratio has been shown to result in a 50% decrease in dielectric constant, as shown in Figure 2-7.

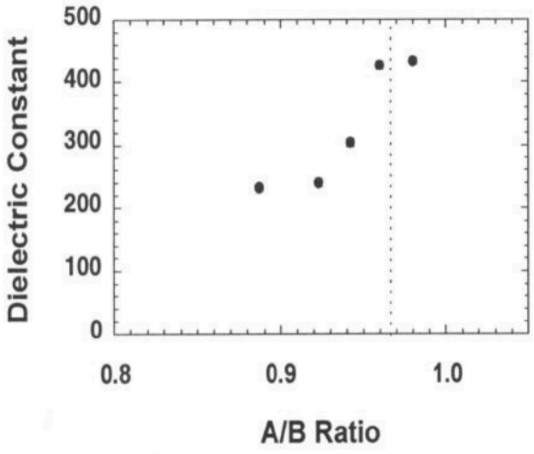

Figure 2-7. Variation in dielectric constant with A/B ratio.

2.5. INTERDIGITAL CAPACITOR

The interdigital (or interdigitated) capacitor is an element for producing a capacitor-like, high pass characteristic using microstrip lines. The shape of conductors is defined by the parameters shown in Figure 2-8. Notice that the long conductors or "fingers" provide coupling between the input and output ports across the gaps. Typically, the gaps (G) between fingers and at the end of the fingers (G_E) are the same. The length (L) and width (W) of the fingers are also specified. Since the conductors are mounted on a substrate, its characteristics will also affect performance. Of particular importance are the height of the substrate (h) and its dielectric constant (ε_r). In addition, the thickness of the conductor (t) and its resistivity (ρ) will also impact the electrical characteristics.

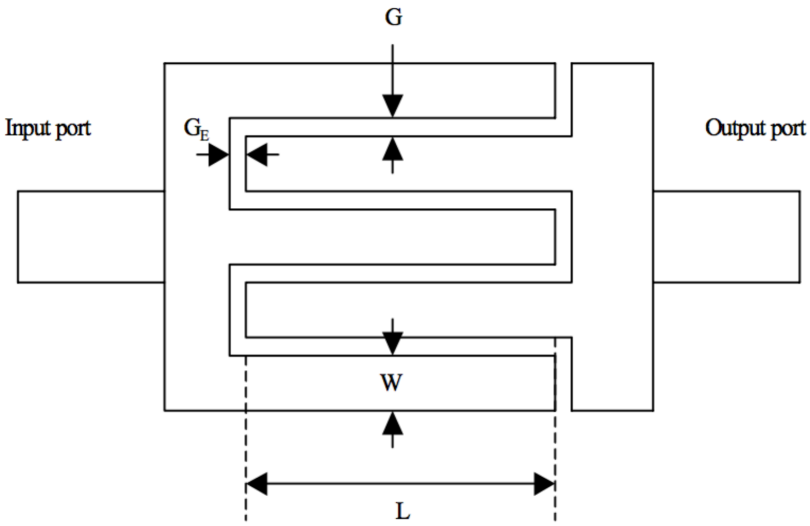

Figure 2-8. Interdigital capacitor geometry.

The design objectives are generally to provide the desired capacitance at the design frequency in a reasonable area. The dielectric constant is often given, since the printed circuit board may have other uses. The capacitance increases as the gaps are decreased. Manufacturing tolerances may dictate the smallest repeatable gap. Reducing the width of the fingers reduces the required area, but increases the characteristic impedance of the line, and in general lowers the effective capacitance.

2.6. END-LOADED PLANAR OPEN-SLEEVE DIPOLE ANTENNA

A simple variation of a conventional cylindrical dipole is the cylindrical sleeved dipole. In a sleeved dipole, the outer shield of the coaxial feed line is extended along the axis of the dipole in order to serve as a radiating element. This particular configuration is useful because it can be designed to exhibit a much larger bandwidth than conventional cylindrical dipole. The cylindrical open-sleeve dipole is a modification of the cylindrical sleeve dipole antenna. This antenna consists of a dipole with two closely spaced parasitic elements, or sleeves.

These antennas are attractive primarily because they have several design parameters that can be varied to achieve a wide range of VSWR performance and operating bandwidth. By properly adjusting the parameters, it is possible to create versions of these antennas that have either a broadband or dual-band response. In addition to the cylindrical open-sleeve dipole, planar forms have also been investigated, which are conformal and can be used to achieve a broadband or dual-band response. The basic geometry of a planar open-sleeve dipole (POSD) antenna is shown in Figure 2-9 (a).

In the design of POSD antennas, the length of the antenna is basically fixed by the desired operating frequency. Since the main radiating element is the planar dipole, this length is roughly fixes at $\lambda/2$. End loading is a well-known and very common technique that has been employed to reduce the resonant length of antennas. By extending the concept of end loading to planar open-sleeve dipole, it is possible to reduce the overall length of the antennas. The main benefit of this type of antenna is that in addition to retaining similar performance to that of conventional planar open-sleeve dipole, end-loaded planar open-sleeve dipole (ELPOSD) antennas can be miniaturized.

Thus they exhibit comparable VSWR performance while encompassing a smaller area than conventional POSD antennas. These antennas are ideal for design applications that require a conformal geometry, broad bandwidth, and compact size. The basic geometry of an ELPOSD antenna is shown in Figure 2-9 (b).

The ELPOSD antenna type selected for this work provides several design parameters that can be varied to achieve a wider range of voltage standing wave radio (VSWR) performance and operating bandwidth with negligible change in the radiation

patterns. A list of the parameters for the ELPOSD antenna is shown below and detailed in Figure 2-9:

- L and W = Length and Width of the Dipole
- W = length of the dipole feed
- Lp and Wp = Length and Width of the Parasitic element
- S = Space between the tapered feed and parasitic
- Ls and Ws = Length and width of end-load stub length
- Wf = width of the tapered dipole feed

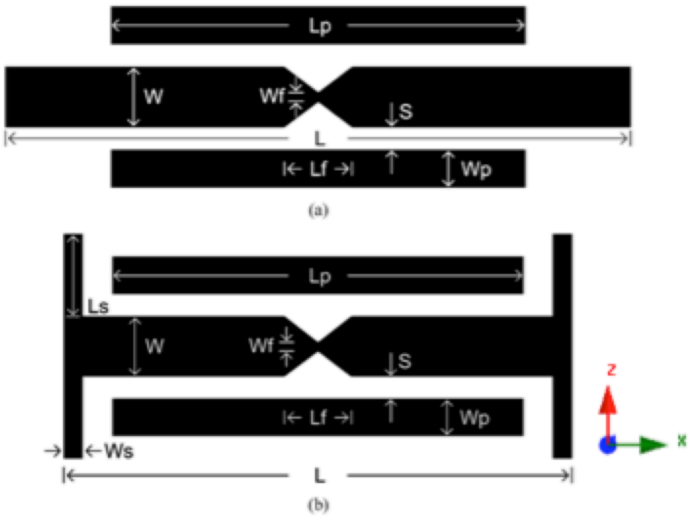

Figure 2-9. (a) Planar open-sleeve dipole (POSD) (b) and End-loaded planar open-sleeve dipole (ELPOSD).

While all of the parameters of the antenna play a role in its overall performance, the lengths of the dipole and parasitic elements have the largest impact on controlling the location of the upper and lower resonances in the VSWR response. An increase in the length of the dipole results in a decrease in the lower resonance frequency and vice versa. If the difference in length between the dipole and parasitic elements is minimal, the upper and lower resonances are closely spaced and the VSWR response of the antenna appears to have a single resonance. As the difference in length is increased, two resonances appear, and a wideband VSWR response results. Increasing it further allows for a dual-band response.

The spacing between the dipole and parasitic elements has a large impact on the VSWR response of the POSD and ELPOSD antennas. The element spacing determines the degree of coupling between the dipole and parasitic elements, which in turn accounts

for the formation of an upper resonance. For small spacings, coupling with the parasitic elements is strong and a wideband or dual-band response can exist. If the spacing is made very large the coupling is minimal and the response of the antenna approaches that of a stand-alone dipole.

The end-load stubs of the ELPOSD have the effect of increasing the electrical length of the driven element of the antenna. Thus they can be used to reduce the frequency of the lower resonance and adjust the degree of miniaturization of the ELPOSD antennas. Small end-load stub lengths allow for slight miniaturization, while larger stub lengths can result in further miniaturization. The width and length of the end-stubs also have a direct impact on the VSWR matching of the driven dipole.

In the following figures (Figure 2-10, Figure 2-11 and Figure 2-12), as a baseline for comparison of all of the designs, the VSWR versus frequency, broadside gain versus frequency and the E-plane and H-plane of the radiation patterns are shown for the three design antennas (elemental dipole, POSD and ELPOSD) working at 1 GHz taken from [Spe06]. Moreover, S11 versus frequency of the measured results of an ELPOSD antenna using two commercial electromagnetic analysis codes: FEKO and HFSS are shown in Figure 2-13. The design of this antenna was fabricated also in [Spe06].

For all of the results, the antennas are oriented such that they lie in the xy plane with the feed centered at the origin and the dipole positioned parallel to the x-axis.

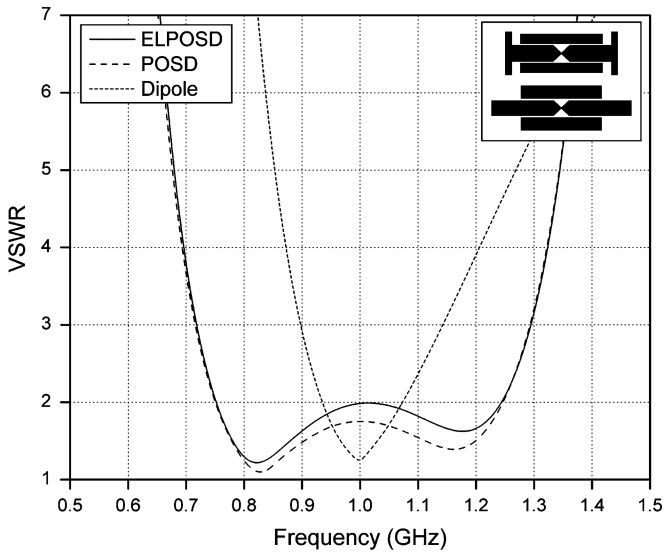

Figure 2-10. VSWR versus frequency for the narrowband dipole, broadband POSD, and the miniature broadband ELPOSD. Inset: Geometry of the broadband POSD and the miniature broadband ELPOSD (shown to scale).

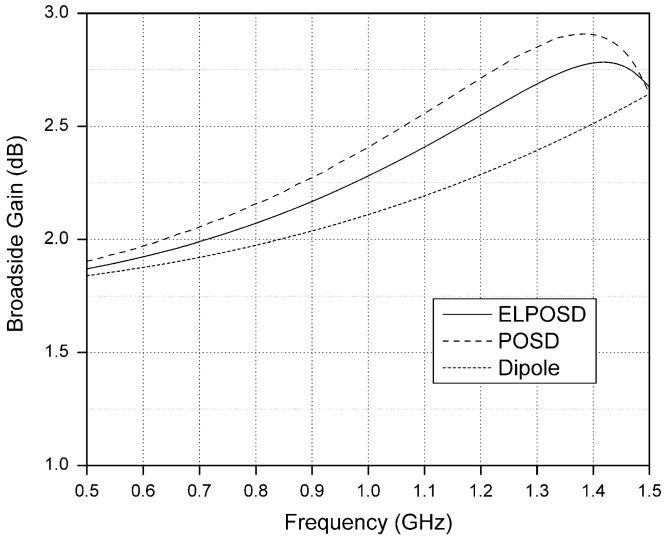

Figure 2-11. Broadside gain versus frequency for the narrowband dipole, broadband POSD, and the miniature broadband ELPOSD.

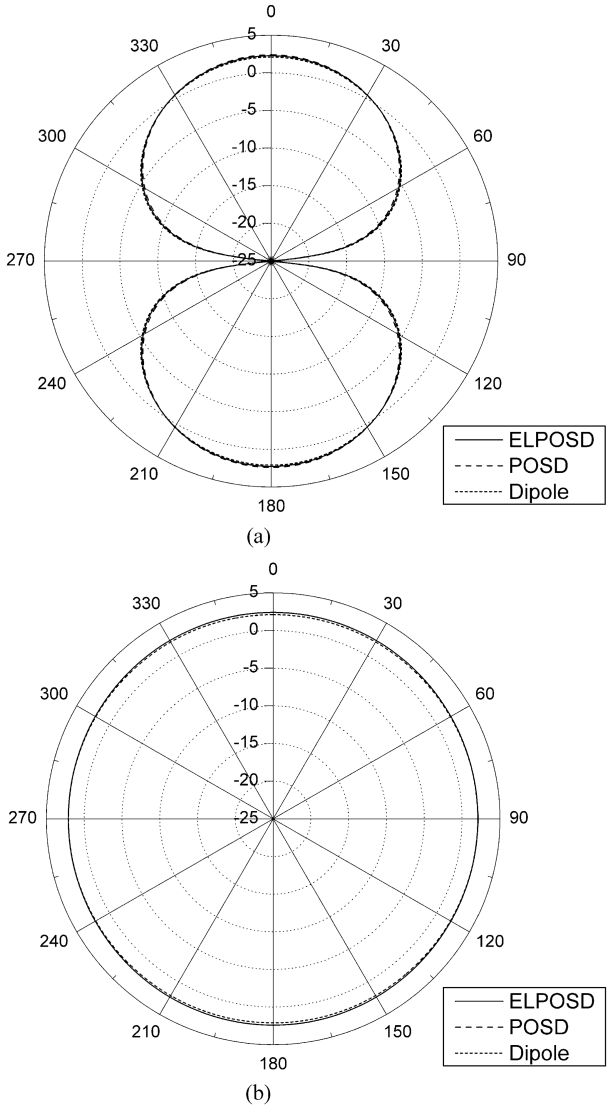

Figure 2-12. (a) E-plane and (b) H-plane cuts of the radiation pattern versus theta (in degrees) at 1 GHz for the narrowband dipole, broadband POSD, and the miniature broadband ELPOSD.

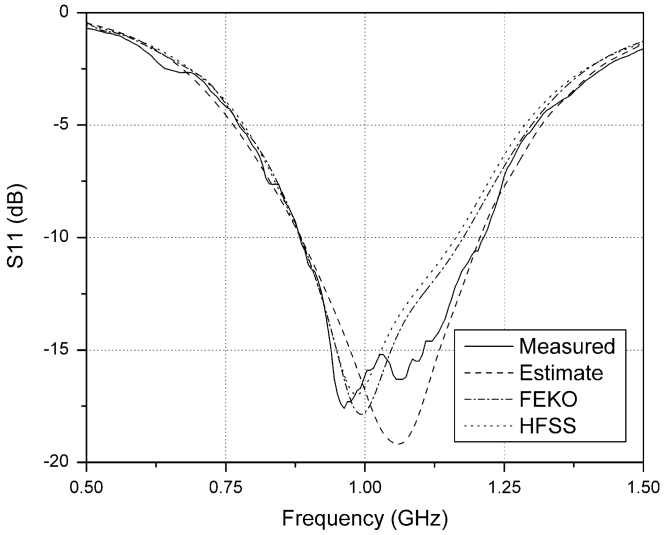

Figure 2-13. S11 versus frequency of the measured results of the ELPOSD antenna.

2.7 . MICROSTRIP PATCH ANTENNA

Microstrip antennas have been the subjects to study for many years. The physical size of a microstrip antenna is small, but the electrical size measured in wavelength λ is not so small. Much research has gone into further reducing the microstrip antenna physical size.

A microstrip patch antenna (MPA) consists of a conducting patch of any planar or nonplanar geometry on one side of a dielectric substrate with a ground plane on the other side. Consider the microstrip antenna shown in Figure 2-14, the patch is of length "L", width "W", and thickness "t", and sitting on top of a substrate of thickness "h" with permittivity "ε_r". The thickness of the ground plane or of the microstrip is not critically important. Typically the height "h" is much smaller than the wavelength of operation, but not much smaller than 0.05 of a wavelength.

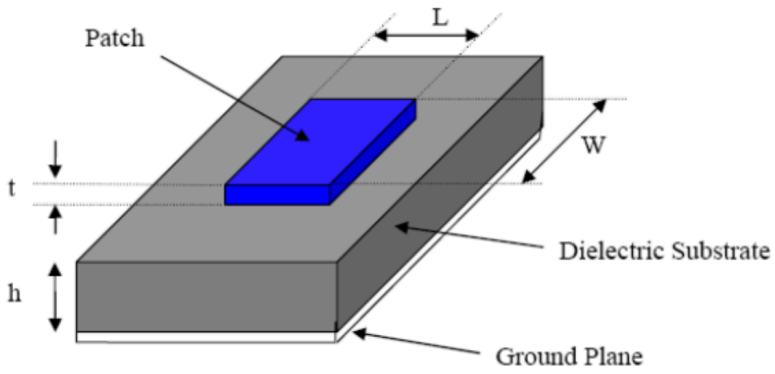

Figure 2-14. Structure of microstrip patch antenna.

Radiation characteristics have been calculated for larger number of patch antenna. The basic configurations used in practice are shown in Figure 2-15. Their radiation characteristics are similar, despite the difference in geometrical shape, because they behave like a dipole. Rectangular microstrip patch antennas have received much attention due to their major advantage of conformability.

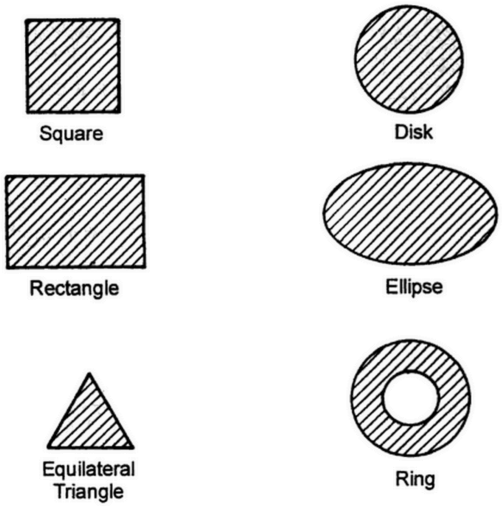

Figure 2-15. Basic microstrip patch antennas shapes commonly used in practice.

Regarding feeding techniques, microstrip line feed is one of the easier methods to fabricate, as it is a just conducting strip connecting to the patch and therefore can be considerer as extension of patch as shown in Figure 2-16. It is simple to model and easy to match by controlling the inset position. The disadvantage of this method is that as substrate thickness increases, surface wave and spurious feed radiation increases which limit the bandwidth.

The microstrip antenna can also be matched using the matching stub. The goal is to match the input impedance to the transmission line.

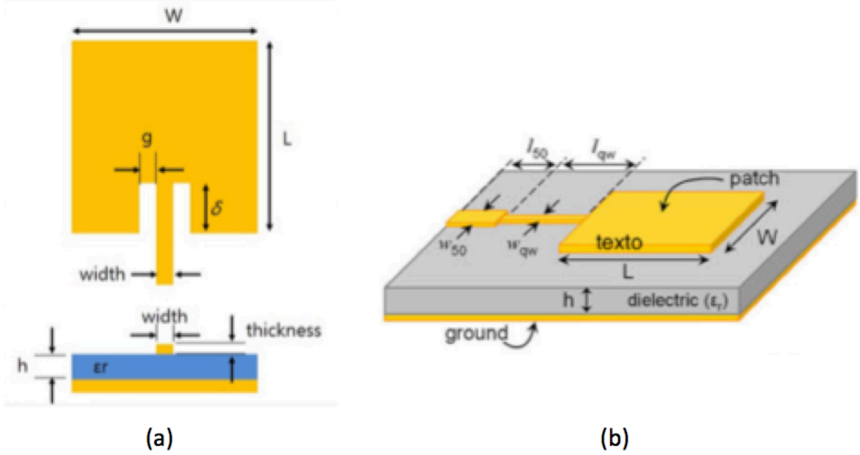

Figure 2-16. (a)Inset feed microstrip patch antenna and (b) Edge feed microstrip patch antenna.

In Coaxial feeding, Figure 2-17, the inner conductor of the coaxial is attached to the radiation patch of the antenna while the outer conductor is connected to the ground plane. The main advantages of this method are easy to fabricate, easy to match and low spurious radiation.

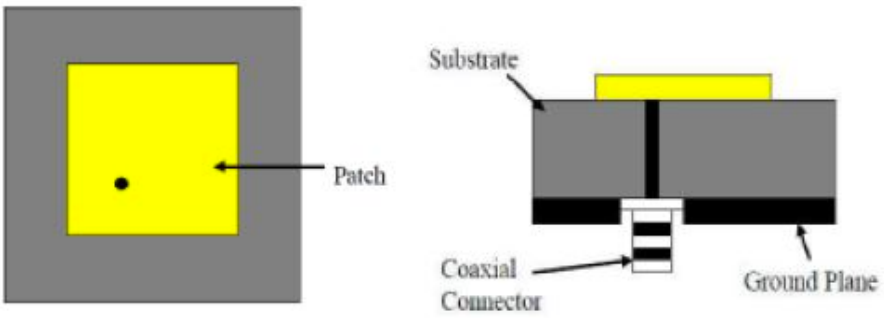

Figure 2-17. Coaxial feed microstrip patch antenna.

Aperture coupling, Figure 2-18, consist of two different substrate separated by a ground plane. On the bottom side of lower substrate there is a microstrip feed line whose energy is coupled to the patch through a slot on the ground plane separating two substrates. Top substrate uses a thick low dielectric constant substrate, and the bottom substrate uses high dielectric substrate. The ground plane, which is in the middle, isolates the feed from radiation element and minimizes interference of spurious radiation for pattern formation and polarization. The main advantage of this method is allows independent of feed mechanism element.

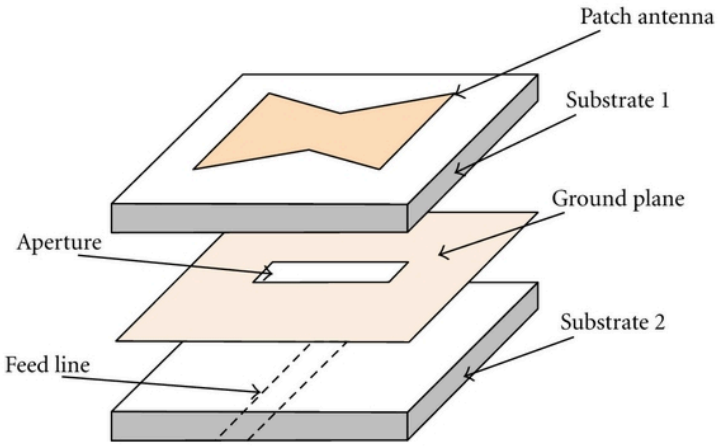

Figure 2-18. Aperture coupling feed microstrip patch antenna.

Proximity coupling, Figure 2-19, has the largest bandwidth, has low spurious radiation. This method consists of two layers on top of each other. A grounded substrate at the bottom layer consists of a microstrip feed line. Above this material is another

dielectric layer with a patch etched on its top surface. Power from the feed network is coupled in between layers, up to the patch electromagnetically.

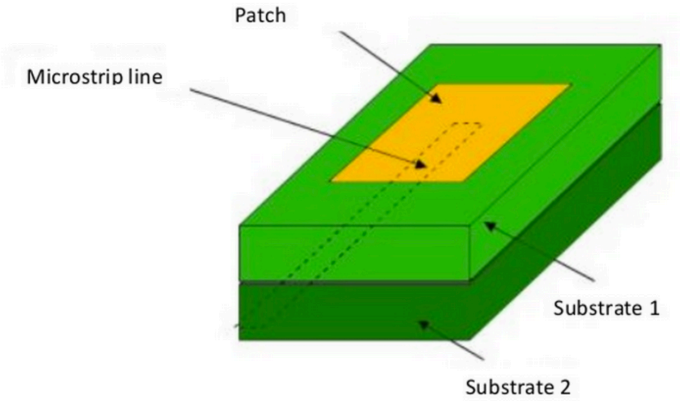

Figure 2-19. Proximity coupled feed microstrip patch antenna.

Figure 2-20 shows the radiation pattern of a Square Patch antenna for a square patch working at 2.6 GHz.

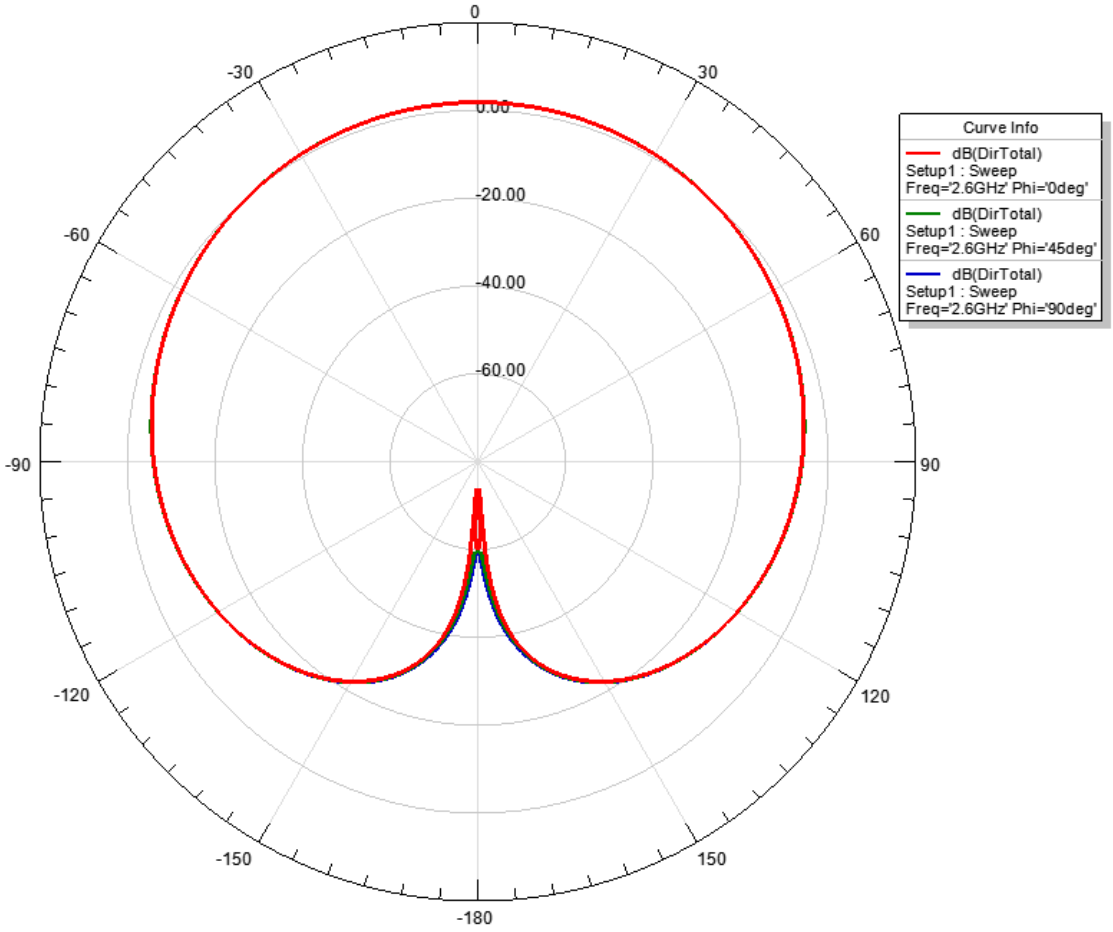

Figure 2-20. Radiation pattern of a microstrip patch antenna.

The return loss of a microstrip Square Patch antenna working at 2.6 GHz is shown in Figure 2-21.

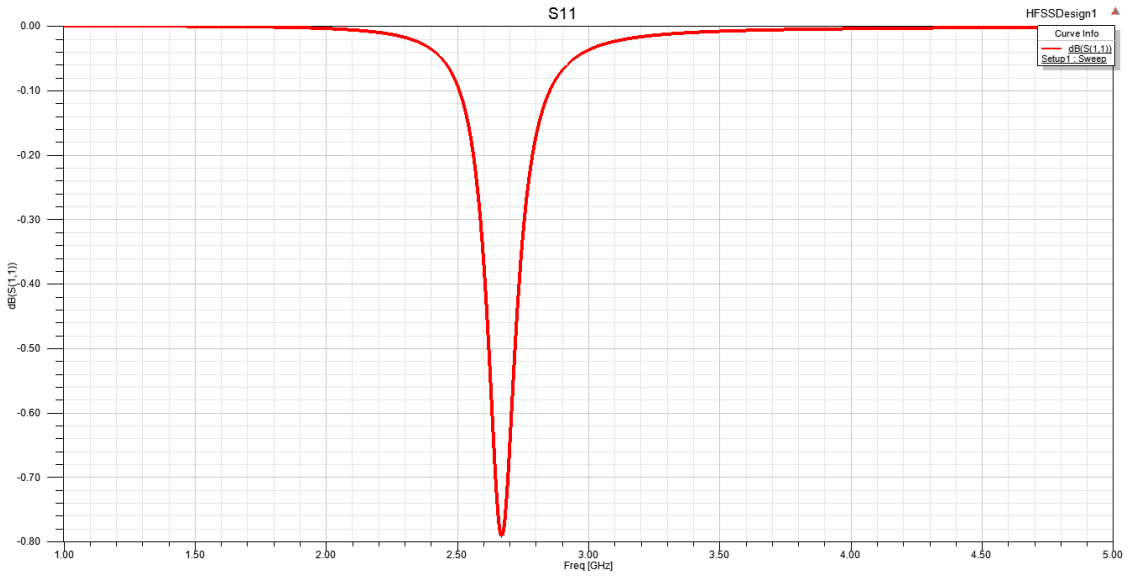

Figure 2-21. Frequency sweep of S11 parameter.

upna Universidad Pública de Navarra Nafarroako Unibertsitate Publikoa

CHAPTER 3. DESIGN OF THE ANTENNA'S ELEMENTS AND RESULTS

In this chapter the parts that compound the overall design are studied and designed separately. First at all, the End-Loaded Open-Sleeve Dipole antenna and the Square Patch antenna are designed working at 2.4 GHz and a comparison between the both antennas is made. Afterwards, BST varactor and Frequency Selective Surface (FSS) are designed and studied.

3.1. DIPOLE ANTENNA DESIGN

The radiator selected for this work consists of an end-loaded planar open sleeve dipole (ELPOSD) using a 1.27-mm-thick Rogers RT6010 substrate with a dielectric constant of 10.2. The geometry of the conventional ELPOSD along with its design parameters is shown in Figure 3-1. There are basically nine design parameters that have an impact on the performance of the antenna. These parameters include the length (L) and width (W) of the dipole, the length (L_p) and the width (W_p) of the parasitic element, the width (F) of the tapered dipole feed and the length (W) of the tapered dipole feed that in this case it is equal to the width of the dipole to simplify the design, and the length (L_s) and the width (W_s) of the end-load stub.

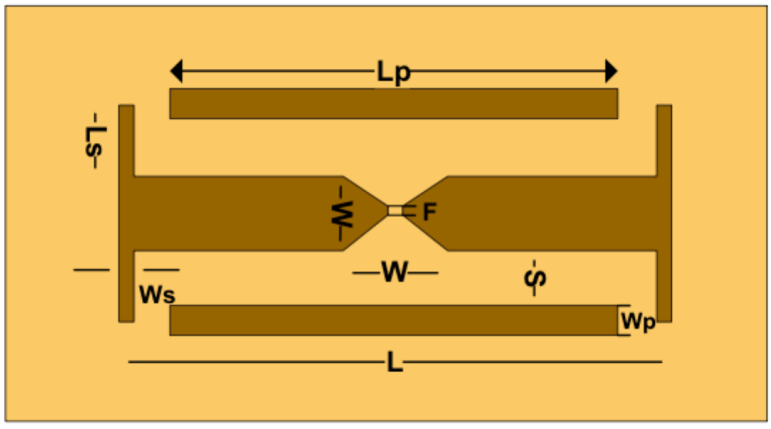

Figure 3-1. ELPOSD geometry.

Due to the boundless combinations of the parameters, dimensions were taken from [Cur10] to have a starting point. The dimensions are L=36, Lp=13.43, Ls=1.99, W=5.8, Wp=4.4, Ws=2.35, S=2.85, F=1 (mm).

First at all, dipole antenna is designed in HFSS with its nine design parameters to modify them in the simulation to adjust the dimensions to operate at 2.4GHz. The overall dimensions of the antenna are 94mm by 70 mm. The HFSS schematic is shown in Figure 3-2.

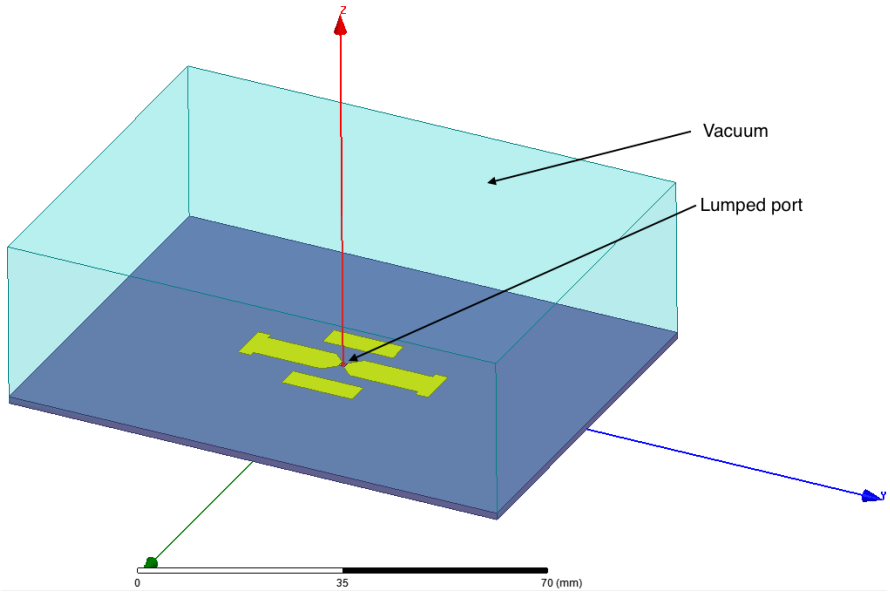

Figure 3-2. ELPOSD design in HFSS software.

A lumped port is being added in the width F of the tapered dipole feed to feed the antenna and a block of vacuum to perform the simulation. According to the requirements of the simulation program, the thickness of the vacuum block must be at least a quarter of the wavelength of the frequency at the operational frequency, which in this case is 2.4 GHz, giving a thickness of 31 mm.

Furthermore, to perform the simulation boundary conditions has been assigned to different parts of the model. The antenna is defined as "Perfect E" because it is a perfect electrical conductor, so that the electric field is perpendicular to its surface. The surfaces that make up the vacuum block are defined as "Radiation", which means that the system will absorb incident electromagnetic waves preventing possible internal reflections, except the ground, which is defined as a "Perfect E". The boundary conditions are shown in Figure 3-4 (a), (b) y (c).

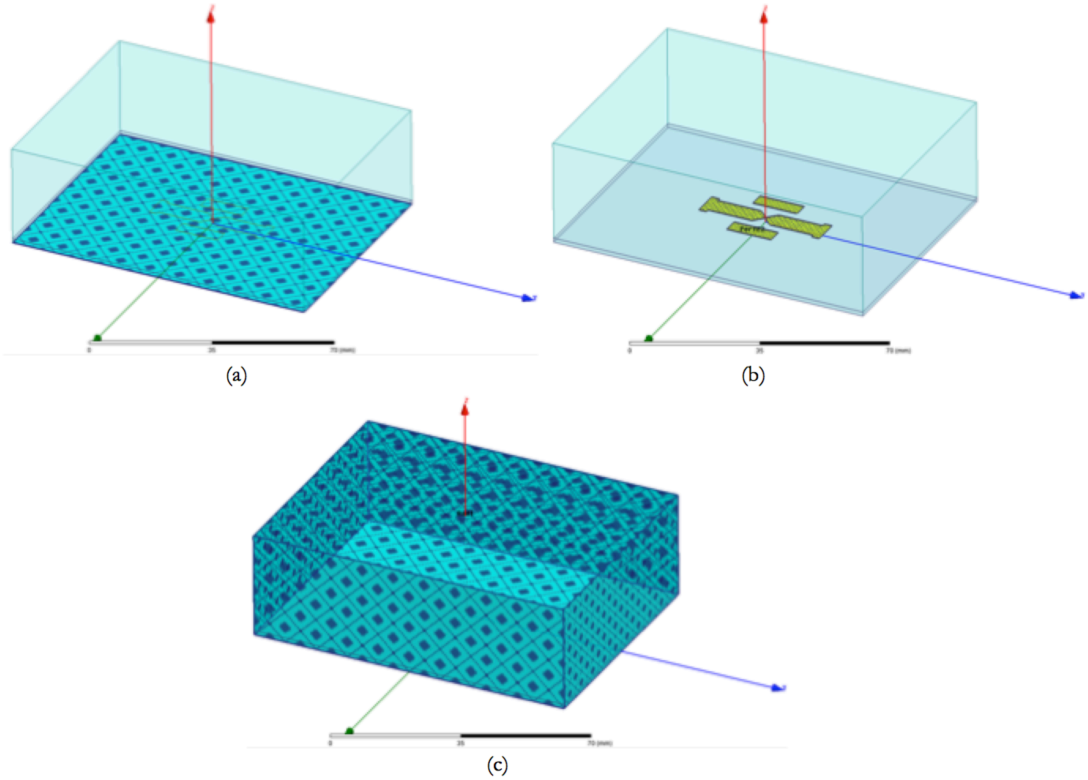

Figure 3-4. (a) Perfect E ground plane. (b) Perfect E dipole antenna. (c) Radiation surface.

The first step is to analyse the dimensions obtained in [Cur10] focusing on the S parameters, especially in the S11 parameter, which gives the simulated return loss. The results are given in Figure 3-5.

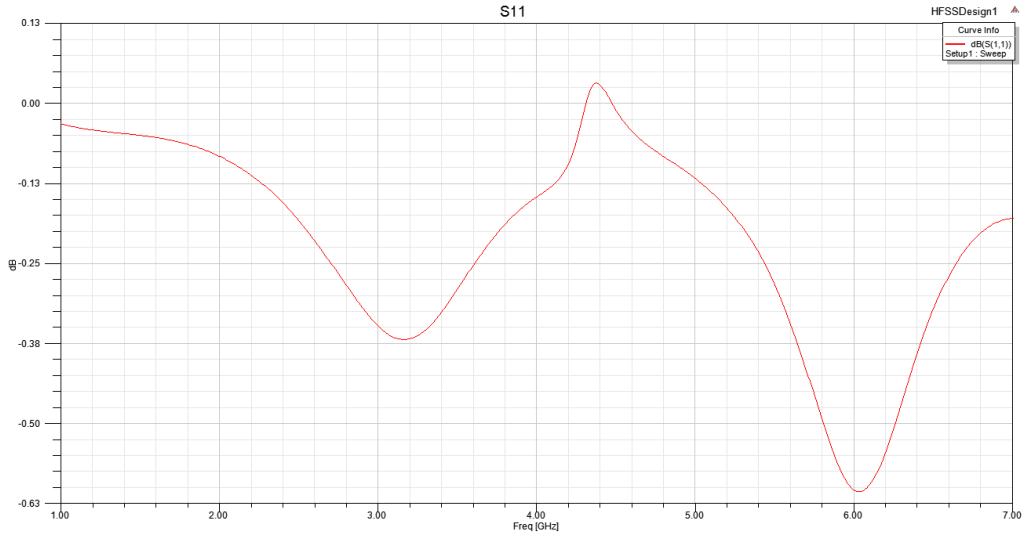

Figure 3-5. Frequency sweep of S11 parameter.

With the dimensions taken from [Cur10] the resonance frequencies are 3.2 GHz and 6 GHz. Both of them are quite far from the operational frequency that is required in this project. Therefore, in a first simulation with HFSS software is set a parametric sweep

upna Universidad Pública de Navarra Nafarroako Unibertsitate Publikoa

with the length and the width of the dipole, which is shown in Figure 3-6. The dipole length takes values between 40 and 120 mm with steps of 5mm, and the dipole width takes values between 20 and 100 mm with steps of 5 mm. The other parameters are set with the following dimensions: Lp=11, Wp=10, Ls=1.99, Ws=2.35, S=1.5, F=1 (mm).

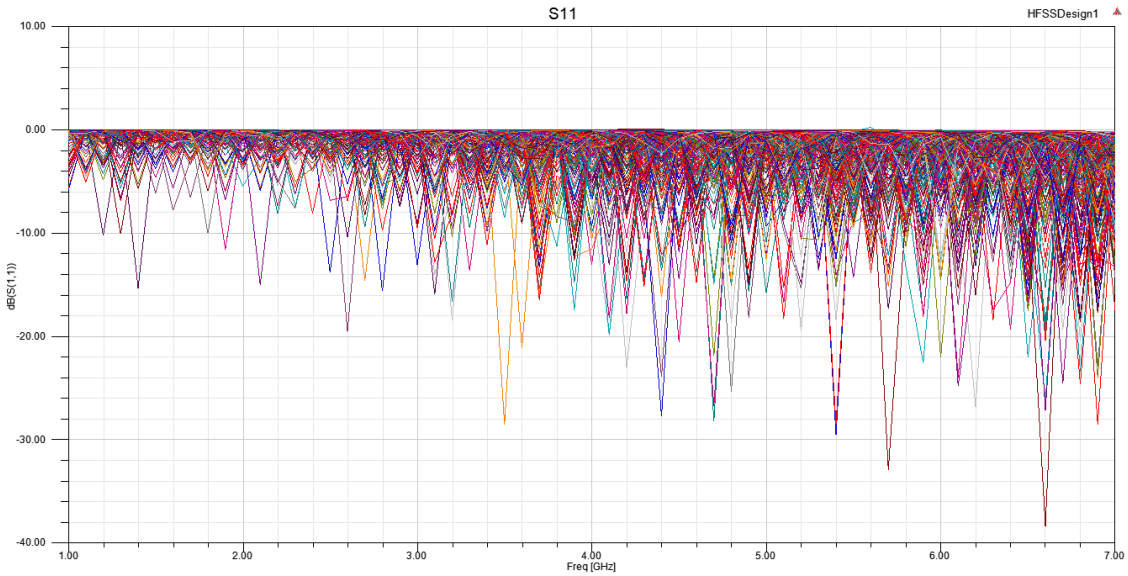

Figure 3-6. Frequency sweep of S11 parameter with dipole length and width variation.

Focusing only in the range of the operational frequency of 2.4 GHz, the different options of the antenna dimensions are shown in Figure 3-7.

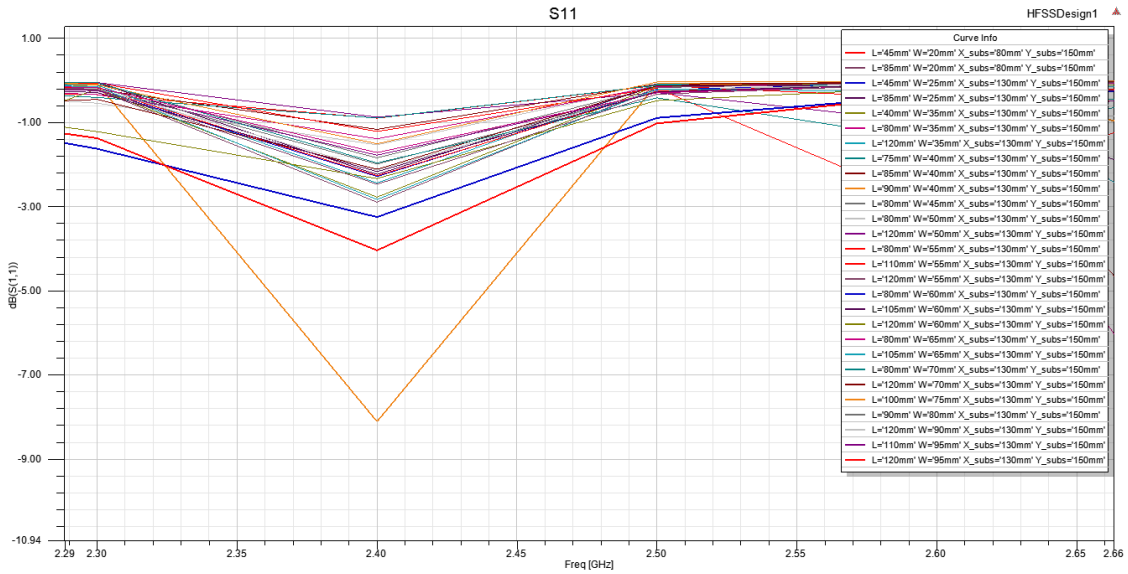

Figure 3-7. Selected results of the frequency sweep.

Once the results are obtained, those that are closest to the operating frequency are chosen to re-run a simulation with the rest of the parameters that define the ELPOSD to adjust them to the desired frequency. The dimension parameters of the dipole antenna that can be acceptable are collected in Table 3-1.

upna Universidad Pública de Navarra Nafarroako Unibertsitate Publikoa

Results at 2.4 GHz		
Dipole length "L" (mm)	Dipole width "W" (mm)	S11 (dB)
100	75	-8.10
45	20	-4.04
45	25	-3.25
120	55	-2.90
120	35	-2.84

Table 3-1. Acceptable dimensions of the ELPOSD antenna.

To reduce simulations only the two best values for the previous simulation have taken to run a global simulation. A simulation with the relevant results modifying the length and the width of the parasitic elements and of the end-load stub is shown in Figure 3-8 for the dipole with length 100 mm and width 75 mm, and in Figure 3-9 for the dipole with length 45 mm and width 20 mm.

Sweeps ranging from 14 to 20 mm for the width and from 10 to 12 mm for the length of the parasitic elements, from 1.5 to 2.5 mm for the width and from 1 to 3 mm from the length of the end-load stub have been carried out. Also it was taken into account the distance between the dipole and the parasitic element varying its value from 1 to 5 mm. All the variations had steps of 1 mm, except the width of the end-load stub and the distance between the dipole and the parasitic element with steps of 0.5 mm.

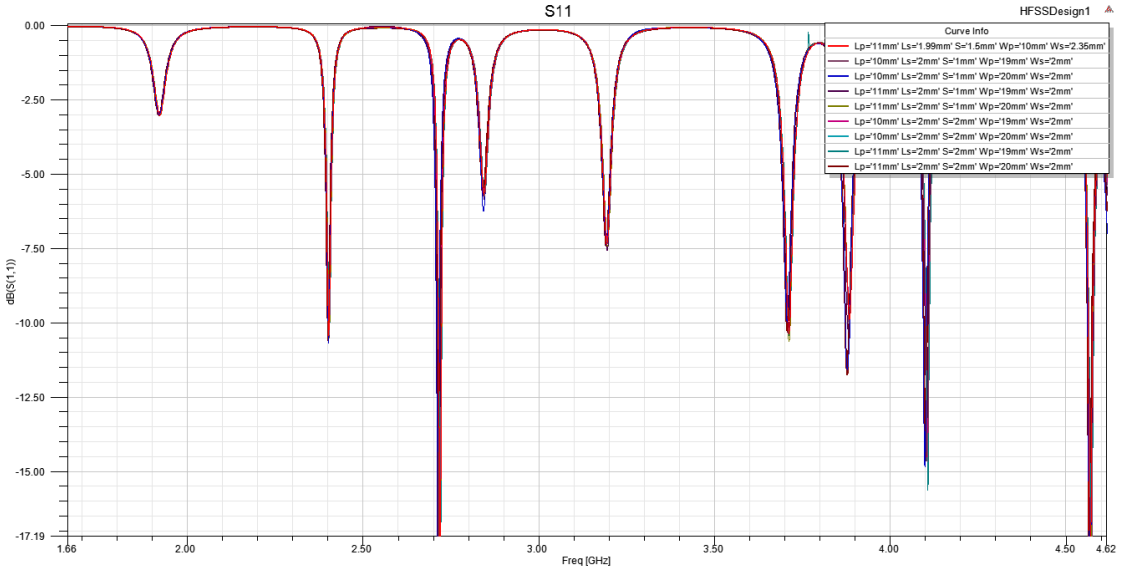

Figure 3-8. S11 frequency Sweep modifying the length and width of the parasitic elements and end-load stub for the Antenna1 with dimensions of L=100mm and W=75mm.

upna Universidad Pública de Navarra Nafarroako Unibertsitate Publikoa

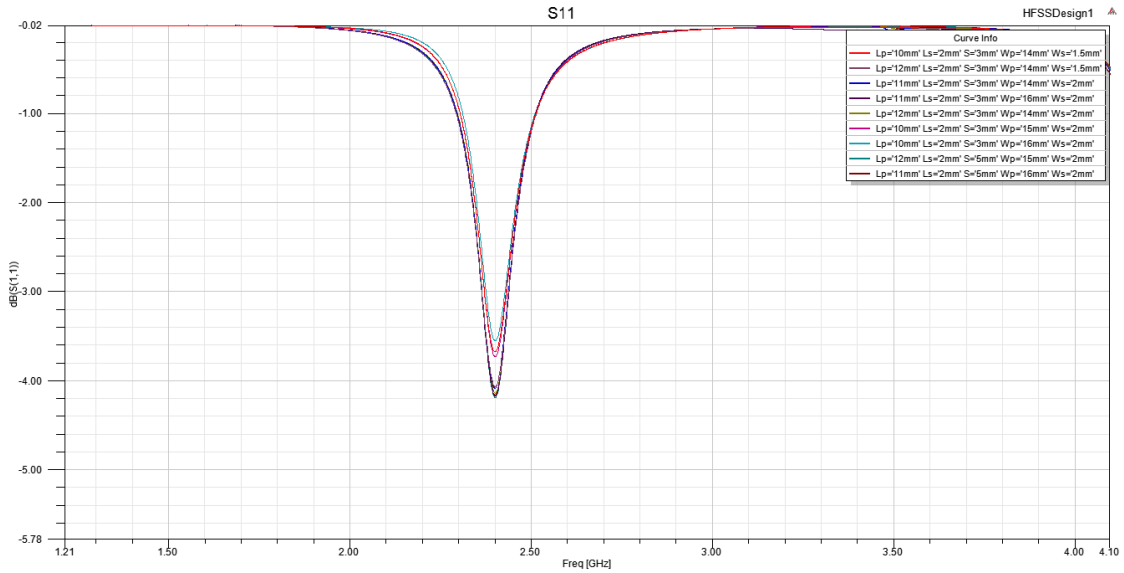

Figure 3-9. S11 frequency Sweep modifying the length and width of the parasitic elements and end-load stub for the Antenna2 with dimensions of L=45mm and W=20mm.

From the S11 parameter plots is concluded that the best dimensions are L=100, W=75, Lp=11, Wp=20, Ls=2, Ws=2 and S=1,5 (mm) obtaining a S11 of -10.70 dB and L=45, W=20, Lp=11, Wp=16; Ls=2, Ws=2 and S=5 (mm) obtaining a S11 of -3.90 dB.

In the following figures (Figure 3-10, Figure 3-11 and Figure 3-12) the comparison of S11 between the two selected solutions and radiation patterns are shown. In view of the results it can be observed quite significant differences. Firstly, the reflection parameter is best for the first antenna with regards to the second, having a difference of about 6 dB. Otherwise the bandwidth is greater in the second antenna than in the first one. Also Antenna1 exhibits many more resonant frequencies than Antenna2, which can be disadvantageous as they are close to the working frequency.

These larger numbers of resonances are due to the characteristics of the end-loaded open sleeve dipole antenna. As discussed in the chapter on the theoretical basis, as the difference between the length of the dipole and the parasitic elements is increased, more resonances appear, and a wideband VSWR response results.

Regarding the radiation pattern, the directivity is higher in the second antenna (with a value of 6.61 dB) than in the first (with a value of 1.55 dB). Moreover, the shape of the radiation pattern is the expected, but for the first antenna the shape is less symmetric than for the second one. The pattern for the first antenna is rotated around 25° and its shape is less similar than the typical dipole radiation pattern shape.

upna Universidad Pública de Navarra Nafarroako Unibertsitate Publikoa

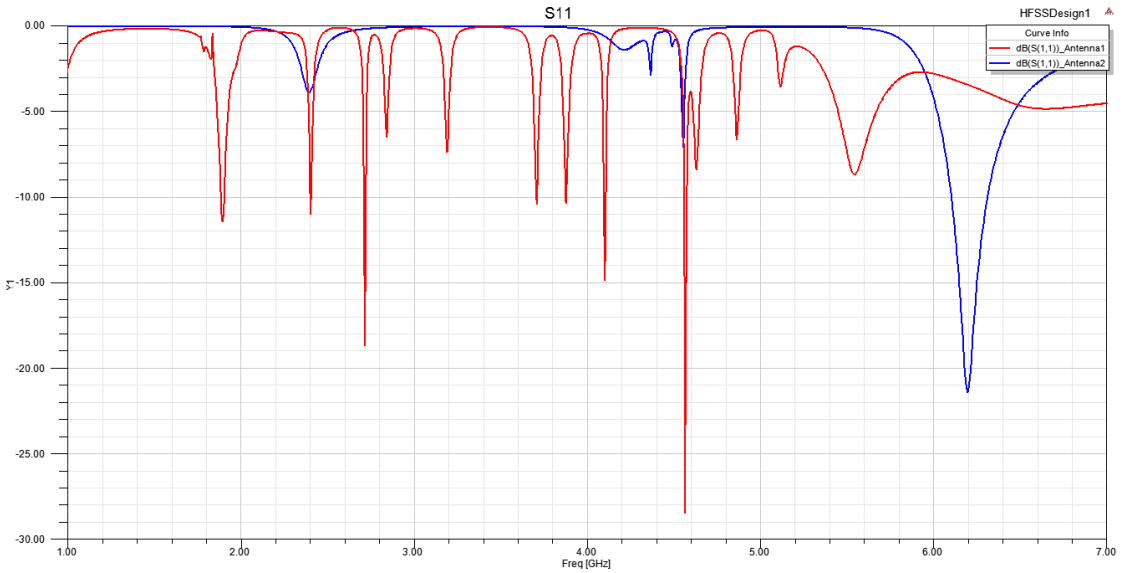

Figure 3-10. Comparison between the S11 parameter of Antenna1 (L=100mm, W=75mm) and Antenna2 (L=45mm, W=20mm).

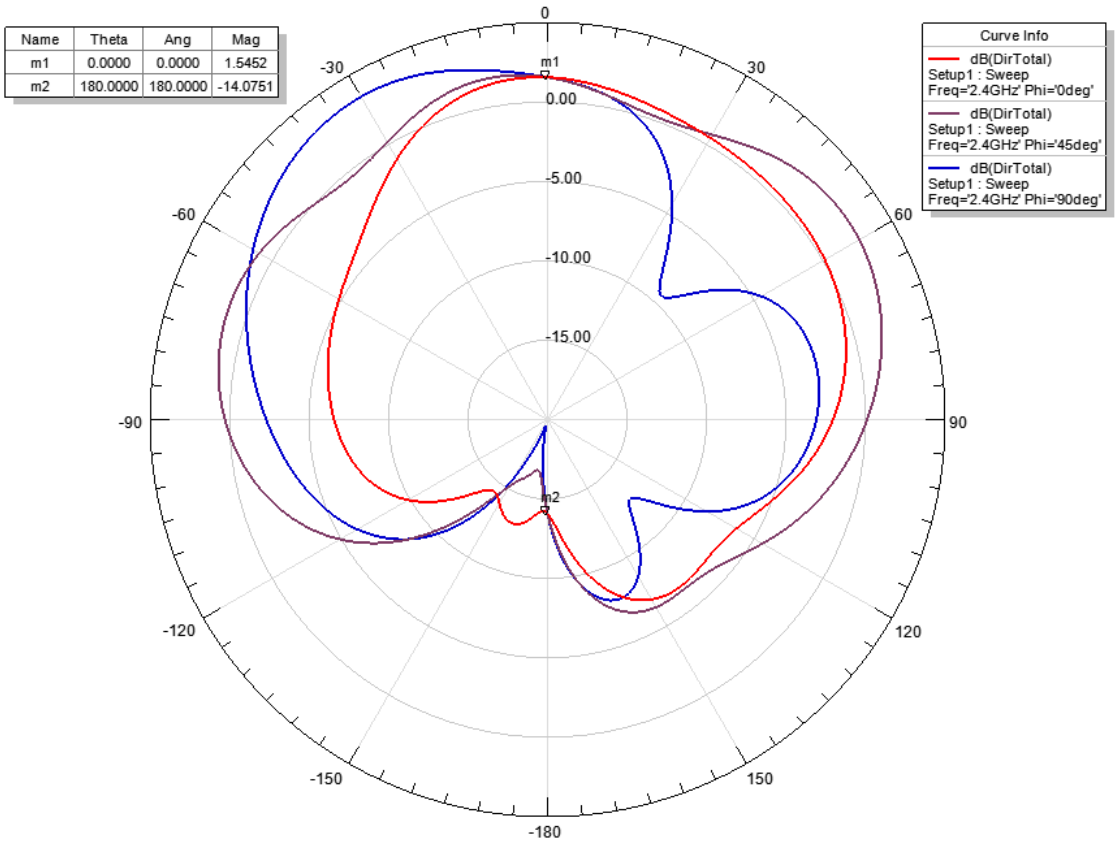

Figure 3-11. Radiation pattern of Antenna1.

upna Universidad Pública de Navarra Nafarroako Unibertsitate Publikoa

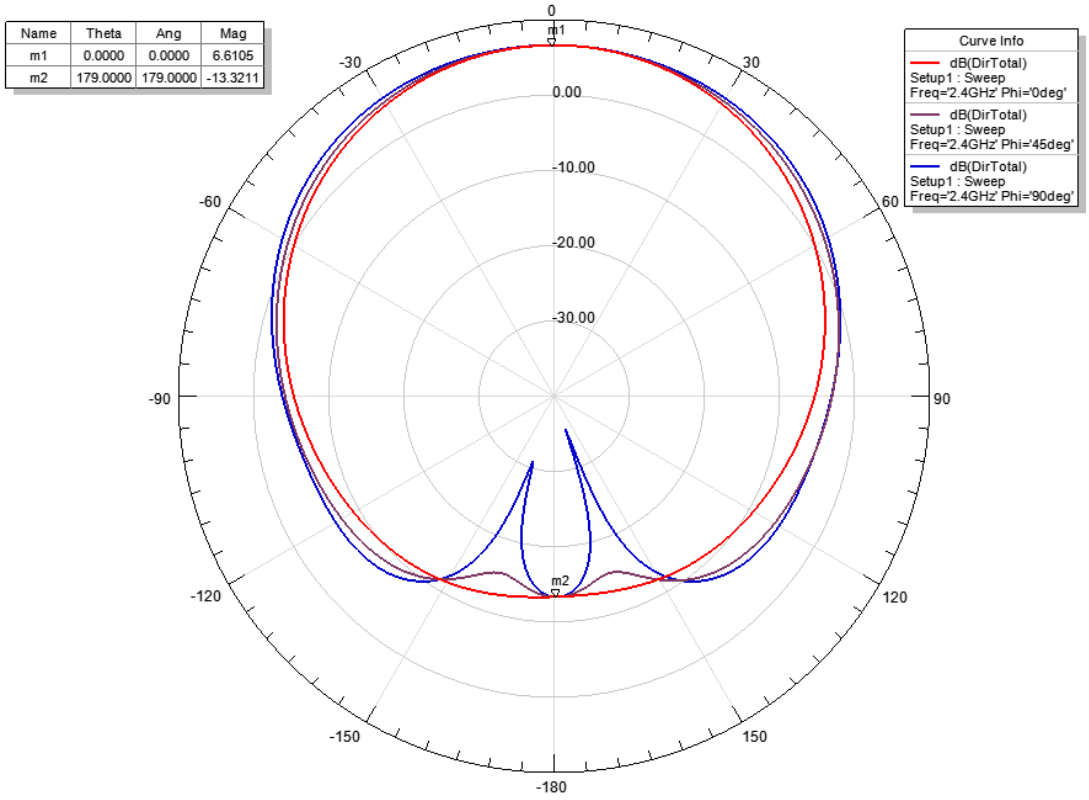

Figure 3-12. Radiation pattern of Antenna2.

In view of the radiation patterns and the frequency sweep of the S11 for both antennas, the second antenna was chosen to develop the final design. The dimensions for the low profile antenna are: L=45, W=20, Lp=11, Wp=16; Ls=2, Ws=2 and S=5 (mm).

Although it was found that the value of the S11 parameter was not very high, it is estimated that this value will be improved when adding the frequency selective surface into the design.

upna Universidad Pública de Navarra Nafarroako Unibertsitate Publikoa

3.2. SQUARE PATCH ANTENNA DESIGN

Although this work has the end-loaded open sleeve dipole as main antenna, another planar antenna is chosen in order to compare the final structure with both combinations and decide which benefits most.

Therefore, the radiator selected in this section consists of a square patch antenna with a microstrip line feed shown in Figure 3-14. First at all, the square patch is design at 2.4 GHz and after that the inset position is adjusted to match the antenna to the operating frequency. The dimensions of the square patch antenna are 19.25 mm for the width and length of the square patch, 1 mm for the width of the microstrip line and 7.5 mm for the inset position.

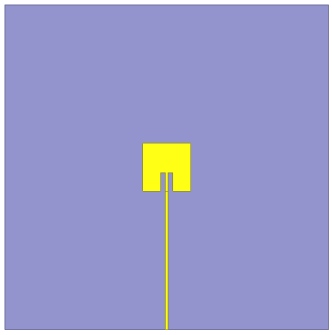

Figure 3-14. Square patch antenna.

The microstrip patch antenna is designed in HFSS software. A wave port is being added in one of the vacuum box surfaces, which ended the microstrip line, and the rest of surfaces of the vacuum box are defined as radiation boundary. Also boundary conditions as "Perfect E" has been assigned in the metal layer and in the ground plane. Figure 3-15 shows the configuration with the boundaries and excitations conditions.

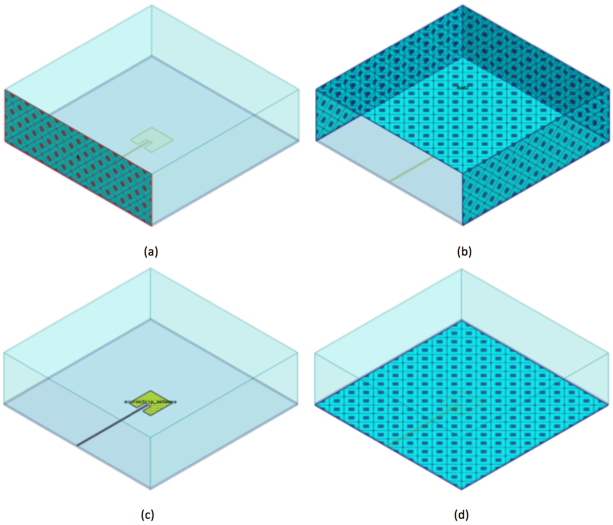

Figure 3-15. (a) Waveport. (b) Radiation surface. (c) Perfect E layer. (d) Ground plane.

In Figure 3-16 the S11 parameter versus frequency is shown. The S11 plot shows that this microstrip patch does not have too many resonance frequencies, which is good. Also, the value of the S11 parameter is -9.80 dB, which is higher than the S11 parameter of the end-loaded open sleeve dipole shown in the previous section with a value of -3.90 dB.

Therefore, using the microstrip patch antenna a better result for the S11 parameter is obtained and furthermore the design process is simpler in this case. Even so, only with the final configuration it will be tested if the microstrip antenna is a better candidate than the dipole antenna.

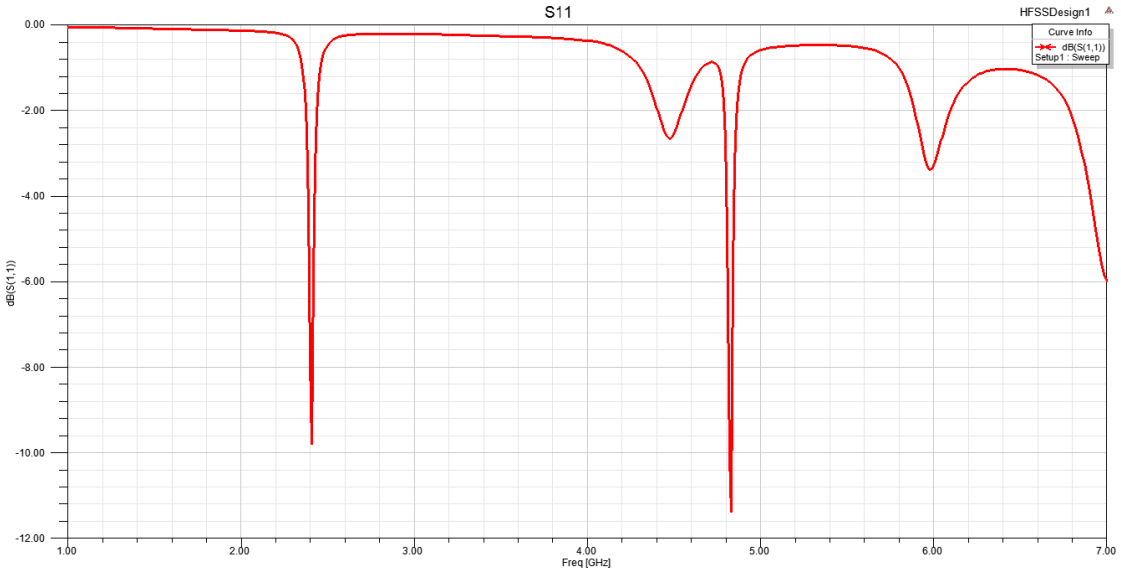

Figure 3-16. Frequency sweep of S11 parameter.

Regarding the radiation pattern shown in Figure 3-17, the directivity is lower in the microstrip patch antenna than in the end-loaded open sleeve dipole. Nevertheless, the difference is not very significant; the directivity of the microstrip antenna is 5.57 dB while the directivity of the ELPOSD is 6.61 dB.

In addition, the shape of the radiation pattern is the expected for a microstrip antenna. If the radiation patterns of the two antennas (microstrip patch and ELPOSD) are compared it can be seen that are very similar. Therefore, there is not a better option for the radiation pattern, both options are good, so only with the final structure it will be seen the performances.

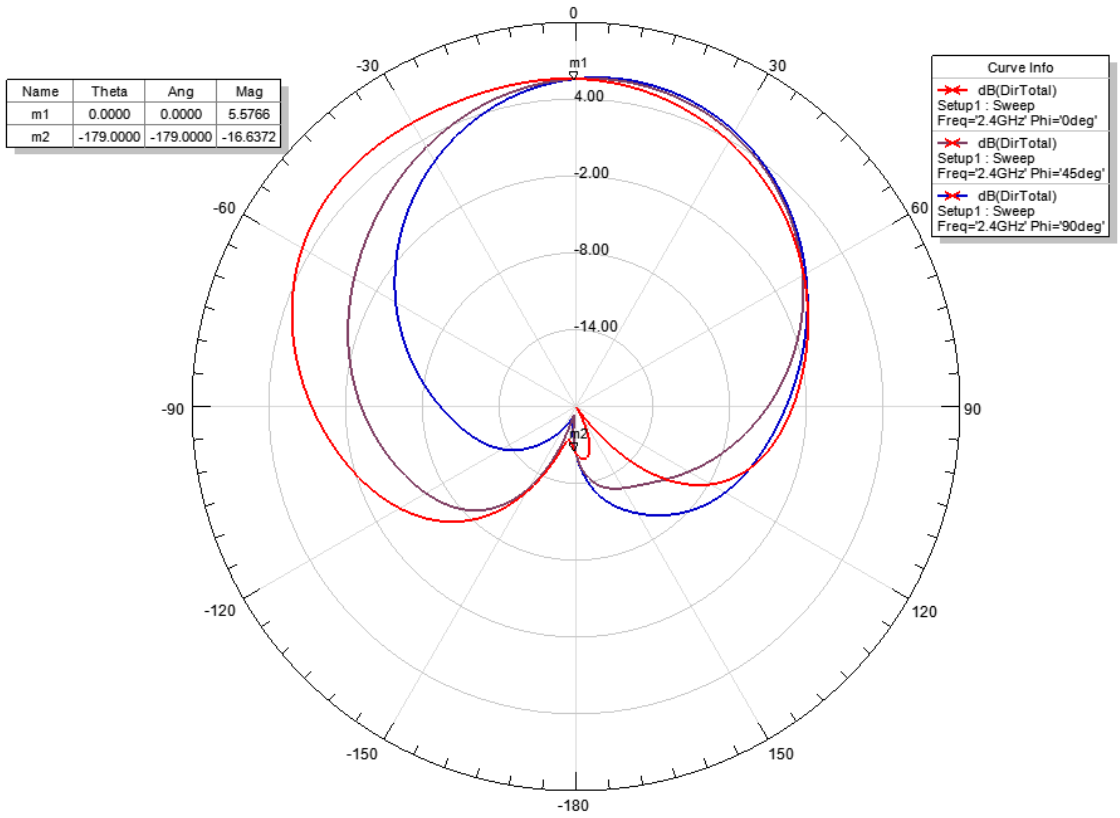

Figure 3-17. Radiation pattern of microstrip patch antenna.

For a better understanding of the properties of the two antennas with which this work is focused, in Figure 3-18 the comparison of the parameter S11 is shown and Figure 3-19 shows the comparison between the radiation patterns. The results of the ELPOSD are shown with short dash lines.

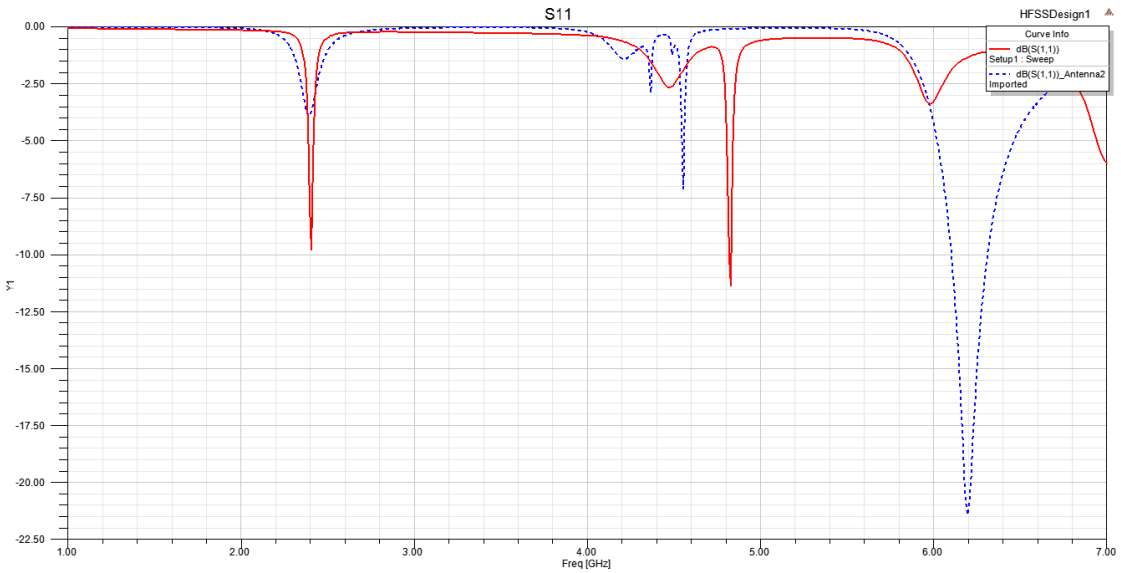

Figure 3-18. Comparison between Square Patch antenna and ELPOSD antenna of the S11 parameter.

upna Universidad Pública de Navarra Nafarroako Unibertsitate Publikoa

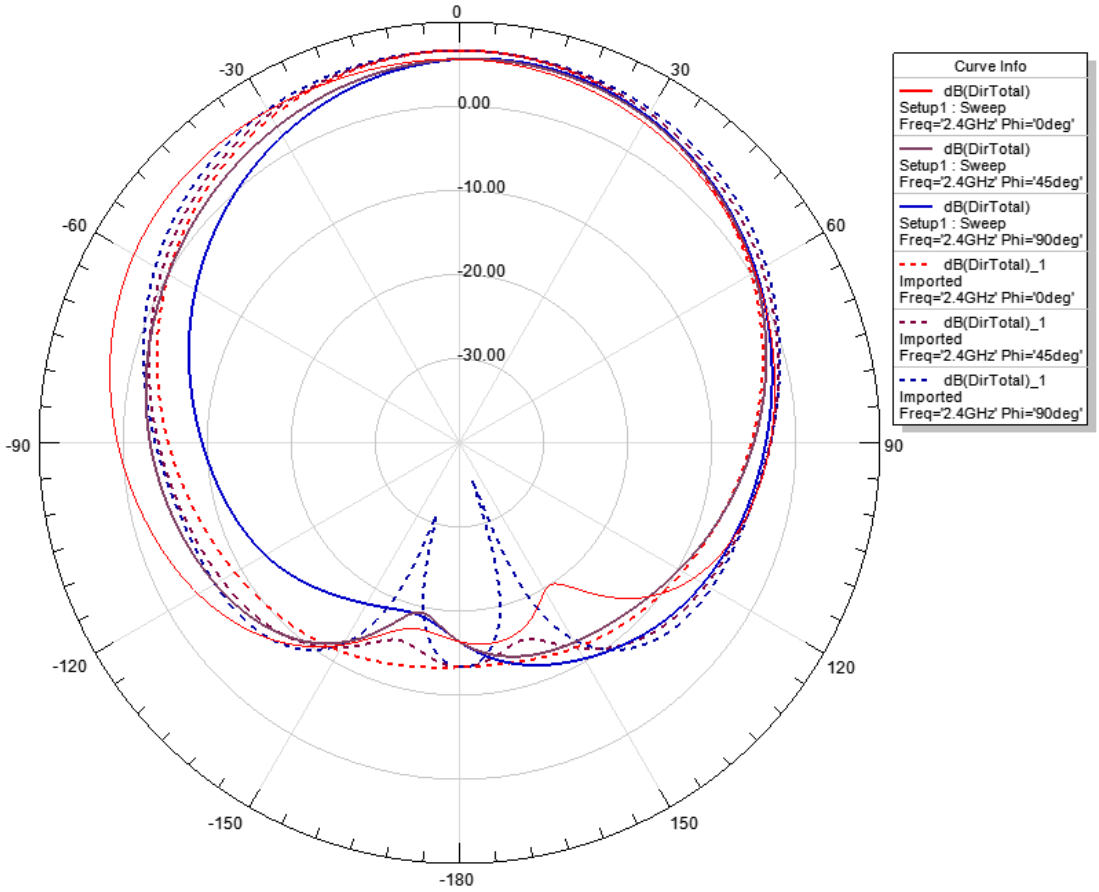

Figure 3-19. Comparison between Square Patch antenna and ELPOSD antenna of the radiation patterns.

upna Universidad Pública de Navarra Nafarroako Unibertsitate Publikoa

3.3. BST VARACTOR DESIGN

In this section, the design of the BST varactors is explained, along with the selection of the geometry used in the metal layer.

As stated above, Barium Strontium Titanate (BST) is a well-known ferroelectric material and up to now, one of the most promising tunable ceramics fro microwave applications. Applying an external electrostatic field across the material can change the relative permittivity of this material. The BST material used in this design is a $Ba_{0.6}Sr_{0.4}TiO_3$, taken from [Cur14].

Interdigital capacitors (IDCs) using coplanar waveguide (CPW) feedlines were initially design with 800 nm of thickness. The BST was deposited onto 500- μm-thick polycrystalline alumina substrate and its thickness was approximately 350 nm. The CPW devices have dimensions of $1.05 \times 0.9\ mm^2$. Figure 3-20 depicts a 3D schematic diagram of the multilayer IDC structure identifying its layers, dielectric constants, and thickness.

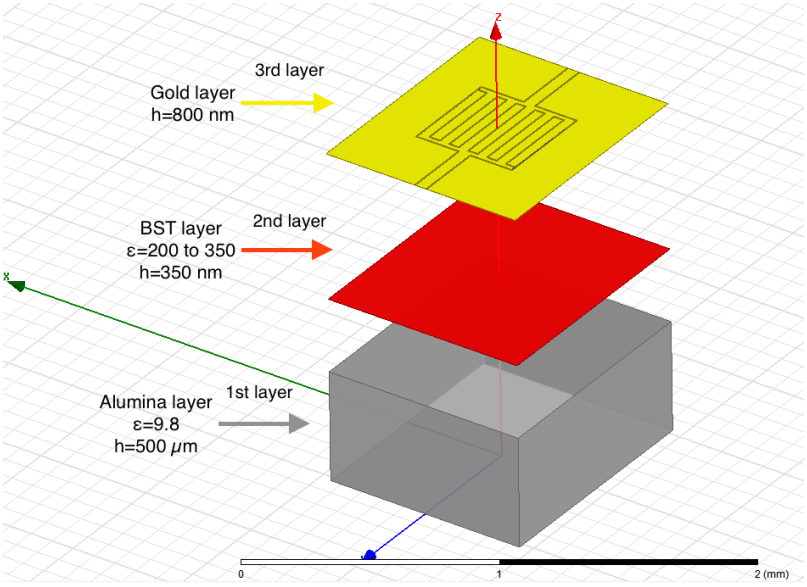

Figure 3-20. Schematic diagram of the CPW multilayer IDC.

To characterize the BST varactors, IDCs consisting of three, five and seven pairs of fingers were designed on top of the patterned BST thin film. The fingers are 400 μm long by 50 μm wide and are separated by a 5 μm gap. These values were taken from [Cur14]. The three different configurations are shown in Figure 3-21.

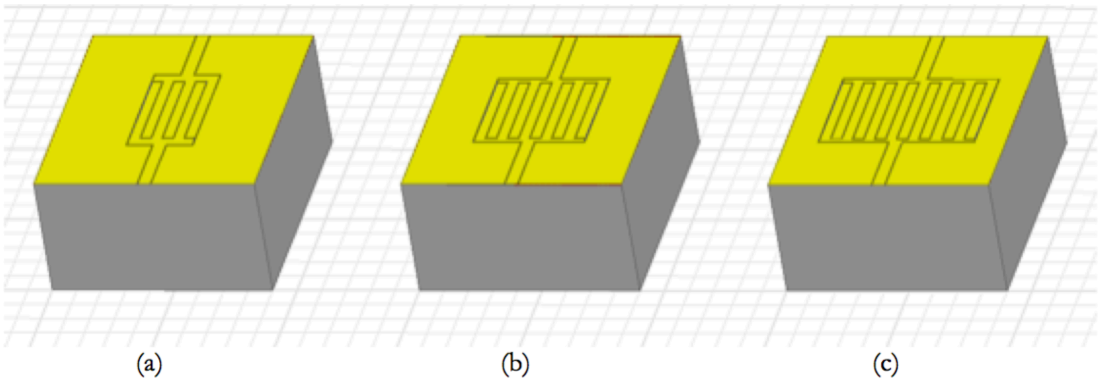

Figure 3-21. (a) Three, (b) five and (c) seven fingers configurations.

To perform the simulation of any of the configurations boundary conditions and excitations have been assigned. The surfaces were the coplanar waveguide (CPW) feedlines end are defined as waveport to feed the design. The surface where the finger are printed is defined as "Perfect E", the gaps between the fingers and the ones that make the feedline are define as "vacuum", the surfaces that make up the vacuum block are defined as "Radiation" except the surfaces that behave as waveports, and the ground plane is defined as "Perfect E". The boundary conditions for a three fingers BST varactor are shown in Figure 3-22.

In order to decide which configuration is most suitable for the design of the Selective Frequency Surface (FSS) a comparison of the S parameters, namely the input port voltage reflection coefficient and the forward voltage gain, of the three models is shown in Figure 3-23.

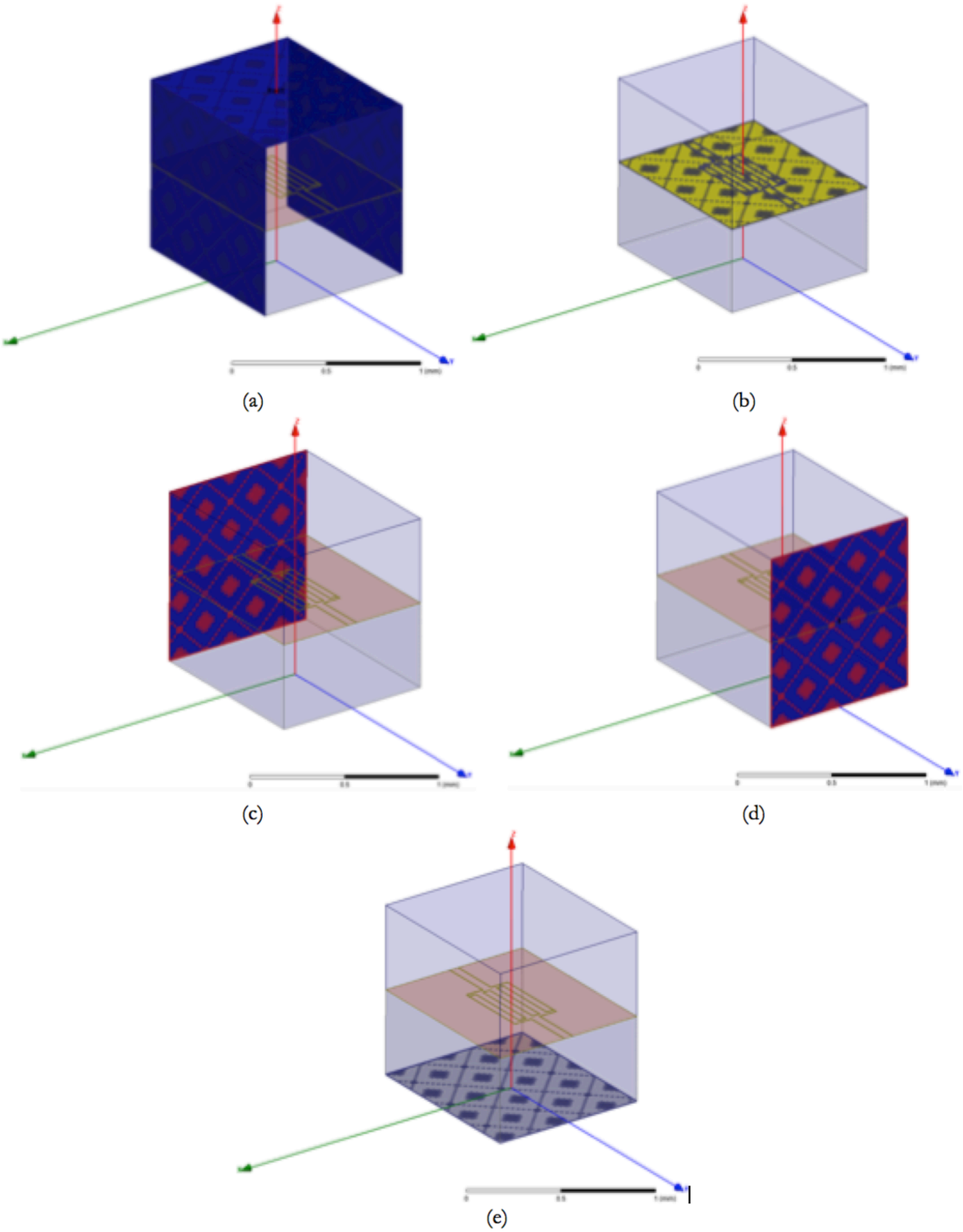

Figure 3-22. (a) Radiation surface, (b) Perfect E interdigital capacitors, (c) Output and (d) input waveport surfaces, and (e) Perfect E ground plane.

upna Universidad Pública de Navarra Nafarroako Unibertsitate Publikoa

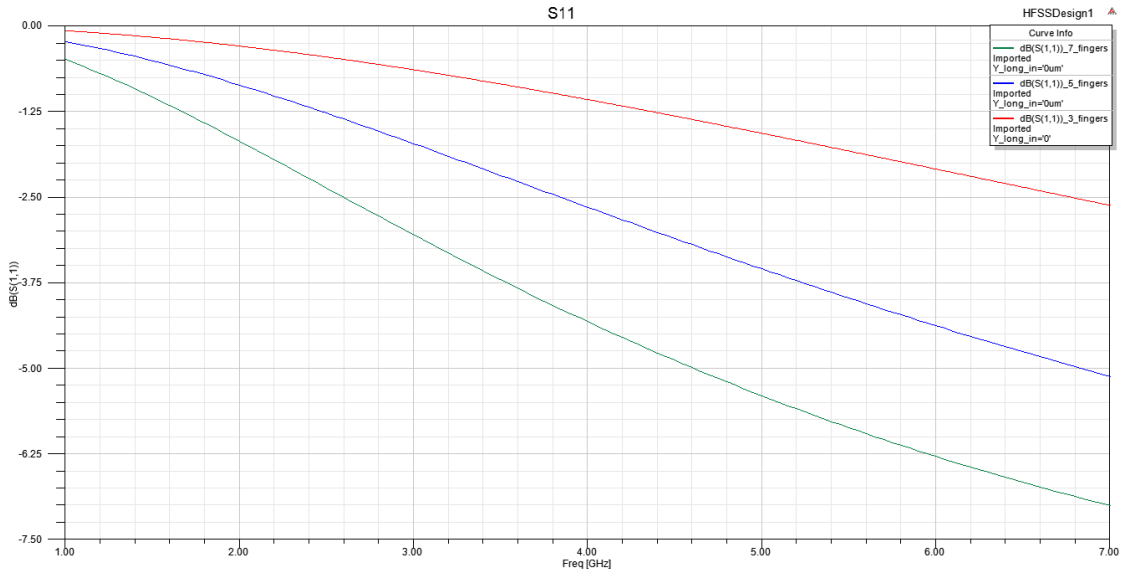

(a)

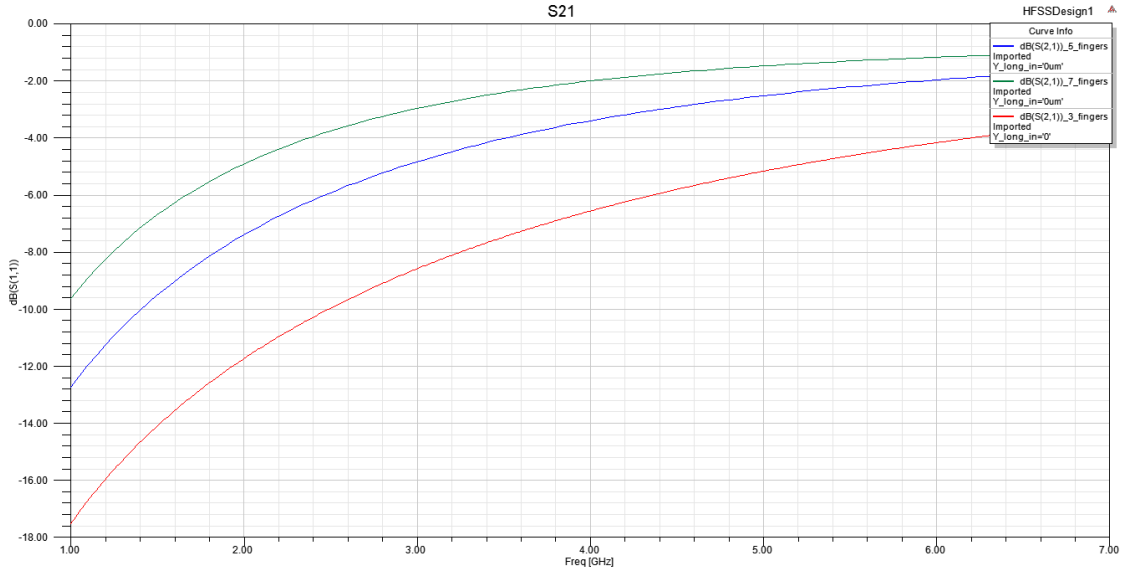

(b)

Figure 3-23. (a) S11 parameter frequency sweep and (b) S21 parameter frequency sweep.

As can be seen the matching improves as with the number of fingers. Therefore the best choice is the 7 fingers configuration, but it must be taken into consideration that the higher number of fingers will lead to a larger complexity in its fabrication. Thus the option chosen is the 5 fingers configuration with which the fabrication complexity is reduced without losing too much in matching performances.

In order to feed the interdigital capacitors, a waveguide feedline is added. This feedline can be closer or further from the top of the fingers and that distance will influence over the interdigital capacitors performance. Hence a simulation is run in which the width of the area is varied, taking the minimum value the width of the finger (50 μm)

upna Universidad Pública de Navarra Nafarroako Unibertsitate Publikoa

up to 200 µm with steps of 50 µm. Figure 3-24 (a) shows the results of the S11 parameter with the simulated variation and Figure 3-24 (b) shows the same results focusing on the operational frequency of 2.4 GHz.

In view of the results the best option is a space of 125 µm, but the differences between the values taken are not very far at 2.4 GHz. So it is found that at this frequency is not so important the distance between the fingers and the feedline. Even though at higher frequencies the S11 parameter varies more significantly when the distance between the top of the fingers and the feedline is improved.

Therefore the value taken for the distance between the fingers and the feedline is the minimum (50 μm) and it will used for the rest of the simulations.

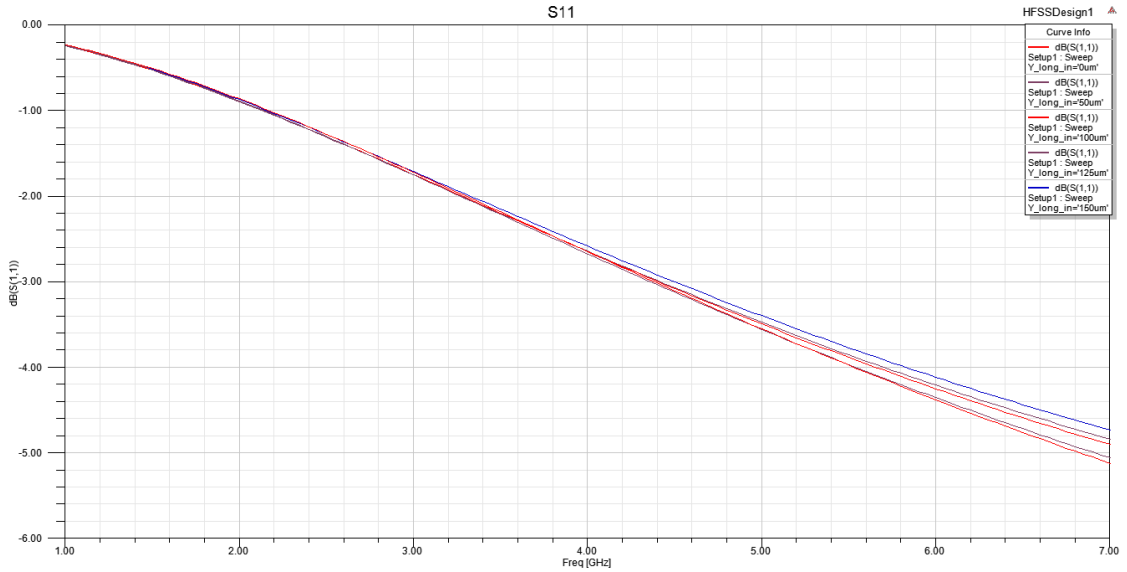

(a)

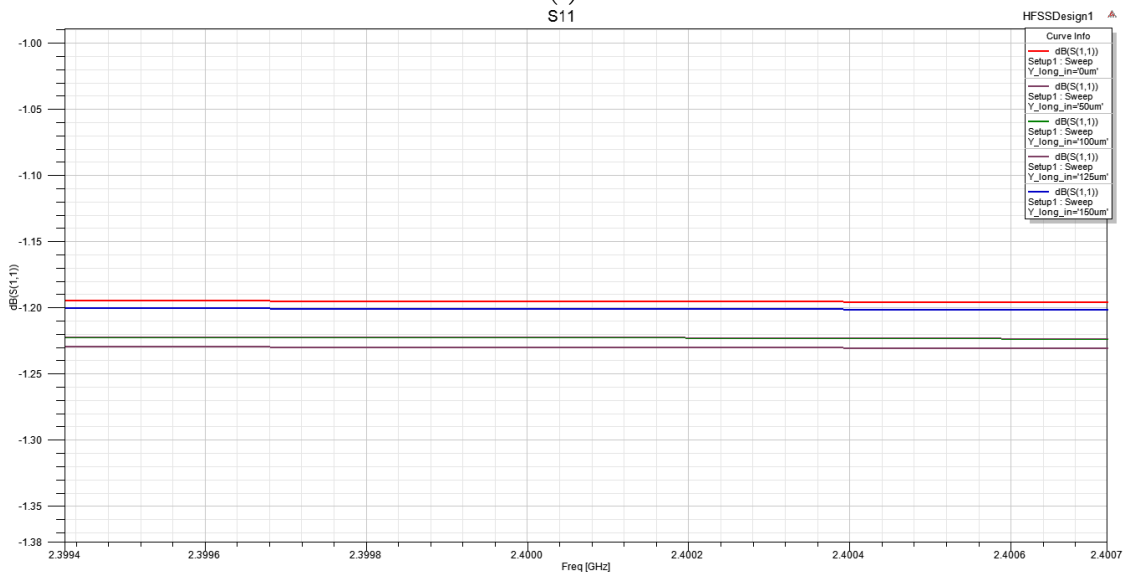

(b)

Figure 3-24. (a) 11 parameter of five fingers capacitor with variations of the space to the feedline and (b) zoom around 2.4 GHz of S11 parameter of five fingers capacitor.

upna Universidad Pública de Navarra Nafarroako Unibertsitate Publikoa

The previous designed process described was modified in order to accommodate integration of the varactors into the FSS layer. First, the ground-signal-ground (CPW) feed lines were removed and replaced with bonding pads on each end. As the final design step, the alumina substrate on which the varactors were designed was assembled into individual chips measuring 2.4 x 0.7 mm^2; this includes the two 0.7 x 0.7 mm^2 bonding pads. Notice that the planar size of the chips can be further reduced by decreasing the bonding pad area. Figure 3-25 depicts the top view of a fabricated BST chip and its 3D schematic diagram identifying its layers, dielectric constants and thicknesses.

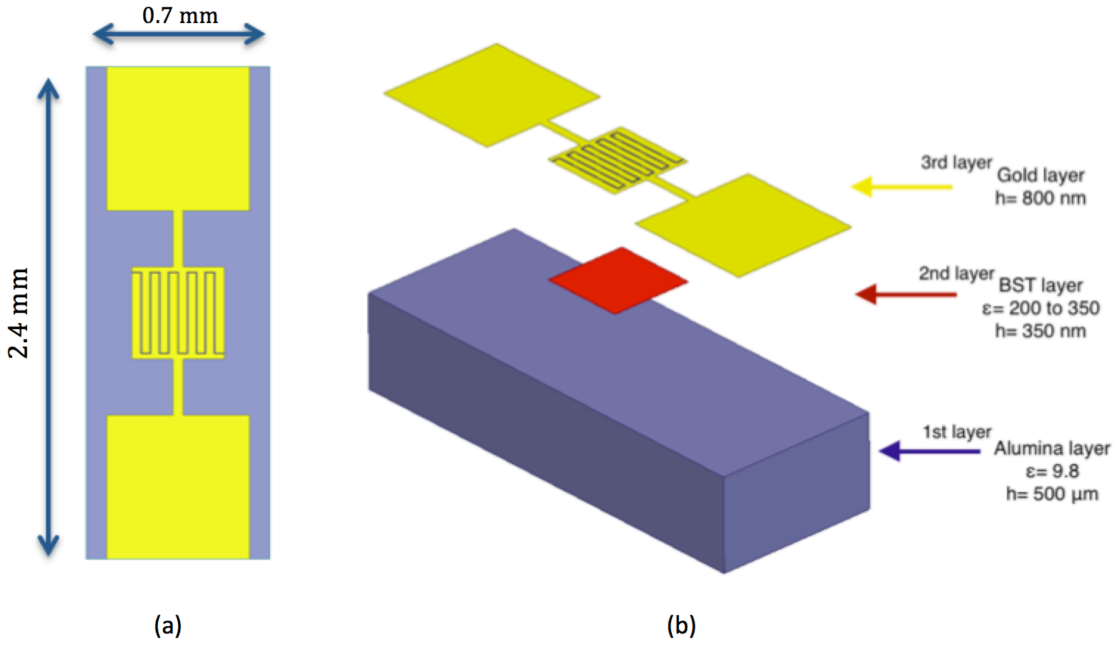

Figure 3-25. (a) Top view of the BST chip. (b) 3D schematic diagram of the multilayer IDC identifying all its layers, dielectric constants and their thickness.

In order to check the correct operation of the BST chip a simulation was run varying the permittivity of the BST material from 200 to 350. These values were taken from [Cur14] considering that the only way to calculate these values is measuring the material.

As in the latter simulation, vacuum box, boundary conditions and excitations has been assigned. Figure 3-26 shows the HFSS chip design, radiation surfaces, perfect E surface and ground plane boundaries and the excitation ports.

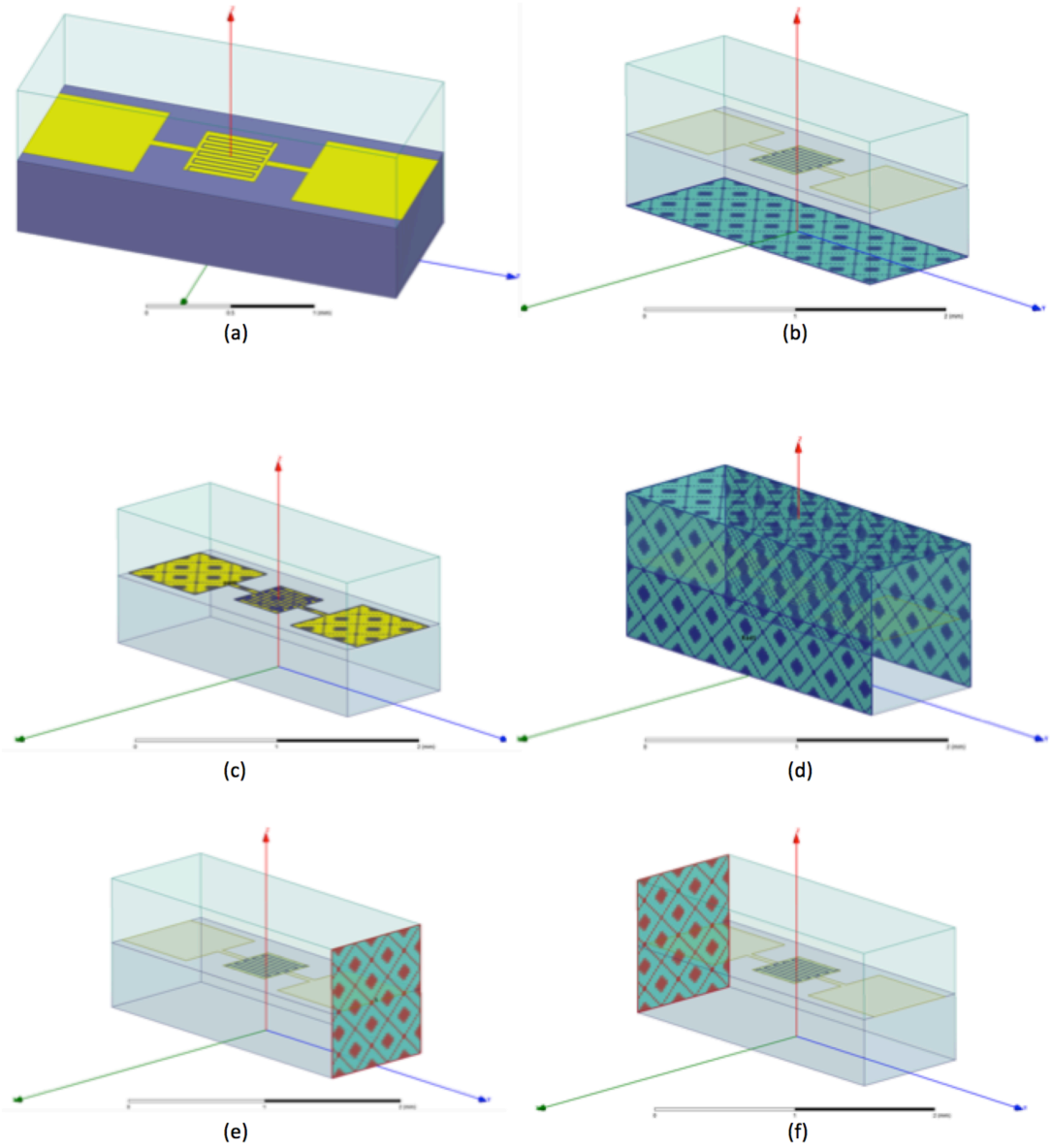

Figure 3-26. (a) HFSS design. (b) Perfect E ground plane. (c) Perfect E metal layer. (d) Radiation surfaces. (e) and (f) Input and output waveports.

As it can be seen in Figure 3-27, S11 parameter varies with changing the permittivity value. Table 3-1 shows the permittivities, the value of the S11 parameter of each one and the distance between the minimums values of the S11. It is clear that the design of the varactor changes its adaptation when permittivity is varied. Thus affects to the capacitance of the BST chip, which is the main purpose of this structure.

BST permittivity	Operational frequency (GHz)	S11 parameter (dB)	Δ frequency (MHz)
200	4.15	-21.1	0
275	3.8	-22.2	370
300	3.5	-23.5	290

Table 3-1. S11 parameter of the permittivity variation.

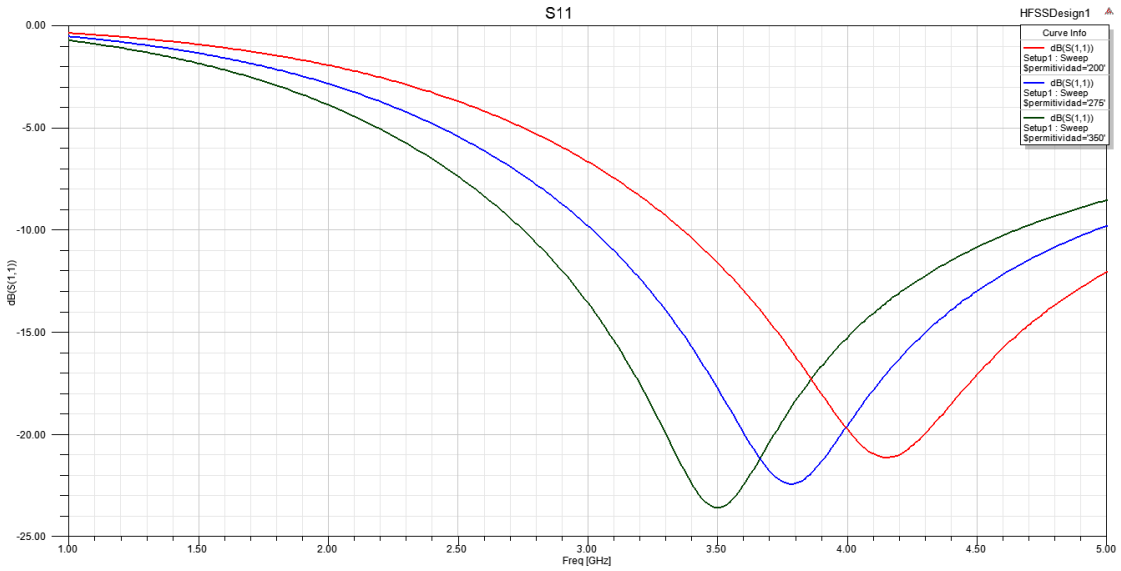

Figure 3-27. S11 parameter as function of the permittivity variation.

upna Universidad Pública de Navarra Nafarroako Unibertsitate Publikoa

3.4. FREQUENCY SELECTIVE SURFACE DESIGN

In this section the frequency selective surface is developed. In Chapter 2, 'Background theory', was demonstrated that the distance between the square patches in a frequency selective surface is crucial (See Figure 2-5). For that reason, the square patch dimensions and the dimensions of the substrate is obtained by a simulation where the distance between the patches is varied, ie the dimensions of the substrate are varied in order to adjust the square patch antenna to the operating frequency.

The square patch is designed in HFSS software. A floquet port is being added on the top of the vacuum box and the rest of surfaces of the vacuum box are defined as master-slave boundaries respectively. Also has been assigned other boundary conditions as "Perfect E" in the metal layer and in the ground plane. Figure 3-40 shows the configuration of the floquet port and the master-slave surfaces.

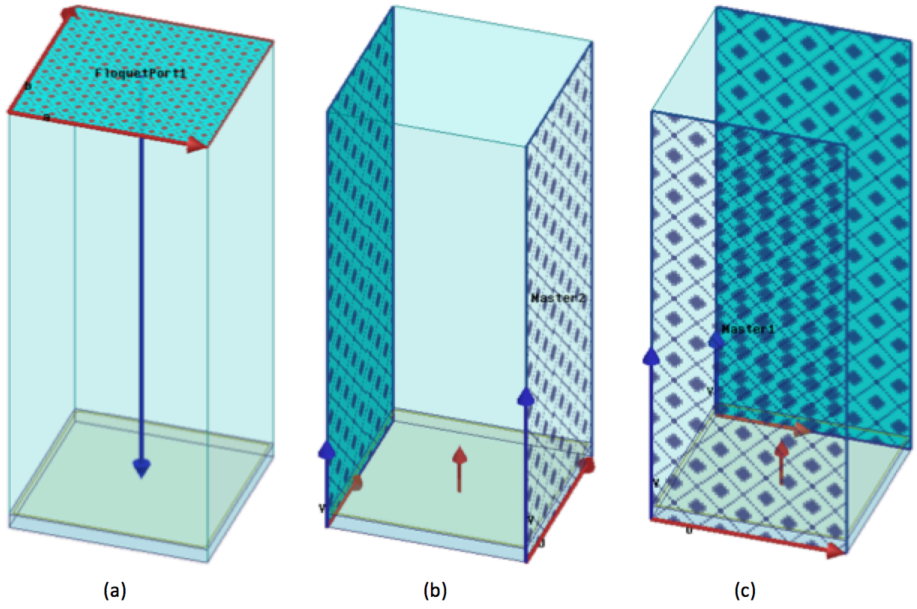

Figure 3-40. (a) Floquet port. (b) and (c) Master-Slave surfaces.

Figure 3-41 shows the S11 parameter where the Square Patches dimensions vary from 16 mm to 17 mm, and the dimensions of the substrate vary from 17mm to 18 mm. As can be seen the most suitable result for the square patch dimensions is 16.5 mm, the others dimensions move away from the operating frequency of 2.4 GHz.

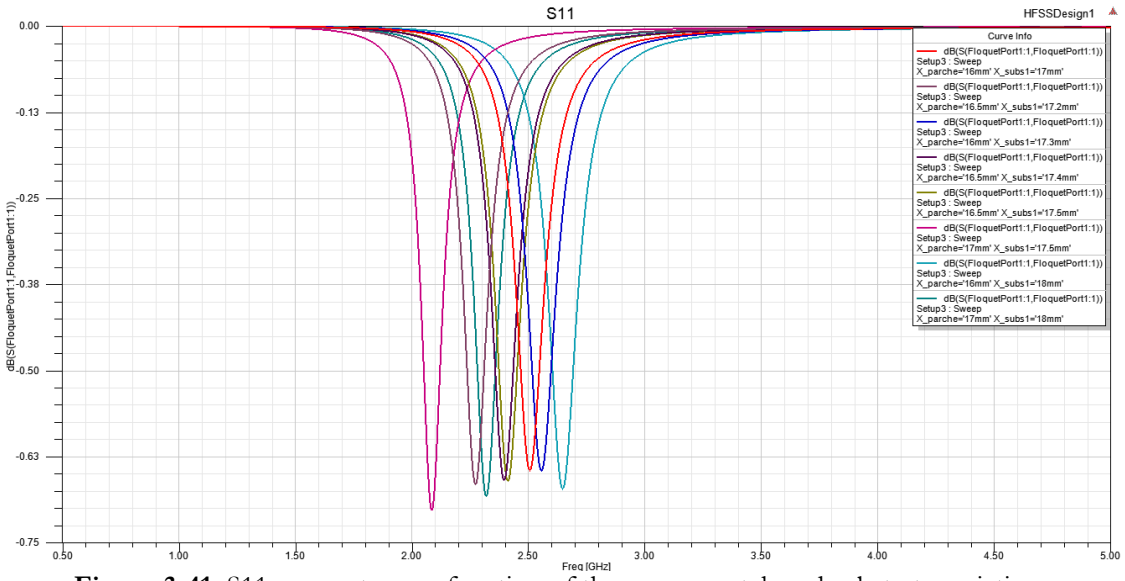

Figure 3-41. S11 parameter as a function of the square match and substrate variation.

Regarding to the substrate's dimensions it is clear that with a patch of 16.5 mm the substrate is between the values 17.4 mm and 17.5 mm. Therefore a simulation with a patch of 16.5 mm and a parametric which the dimensions of the substrate varies from 17.4 mm to 17.5 mm with steps of 0.001 mm. Considering that the steps are too small, the simulation results will have 100 solutions so the plot of the S11 parameter it will be not shown. For the 100 solutions the best solution is for a substrate dimensions of 17.405 mm.

With these two values of the dimensions the distance between the patches is known and has a value of 1.81 mm. This value is the one that makes 0 degrees in the phase at 2.4 GHz, which is shown in Figure 3-42. Moreover, Figure 3-43 shows the S11 parameter versus frequency, which gives the expected result considering that the square patch is a Partial Reflective Surface (PRS). The value of the S11 parameter is near zero because the square patch reflects most of the incident wave.

upna Universidad Pública de Navarra Nafarroako Unibertsitate Publikoa

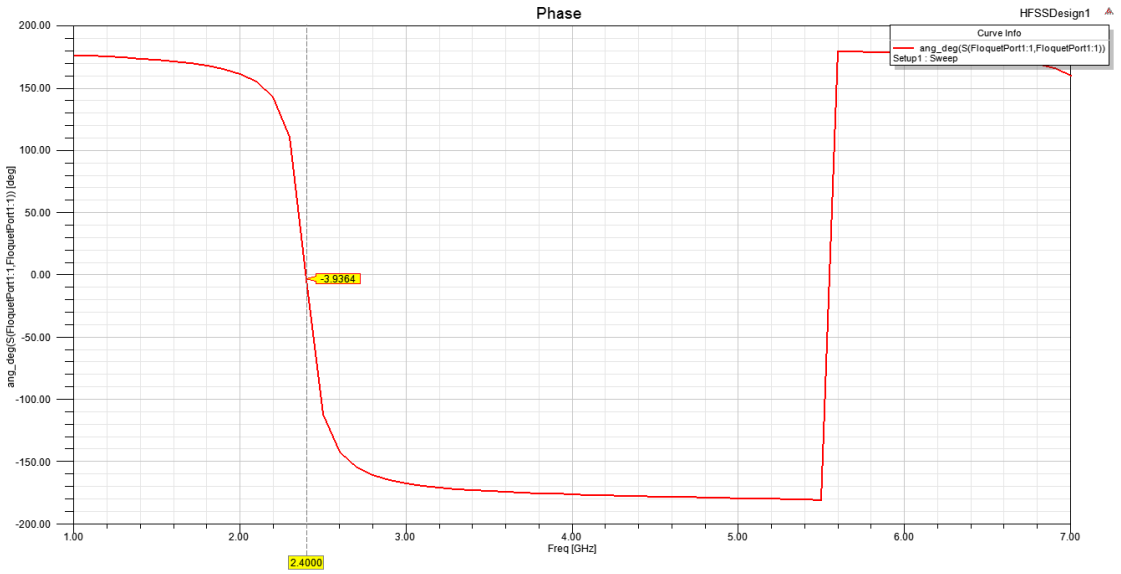

Figure 3-42. Phase vs frequency of the FSS.

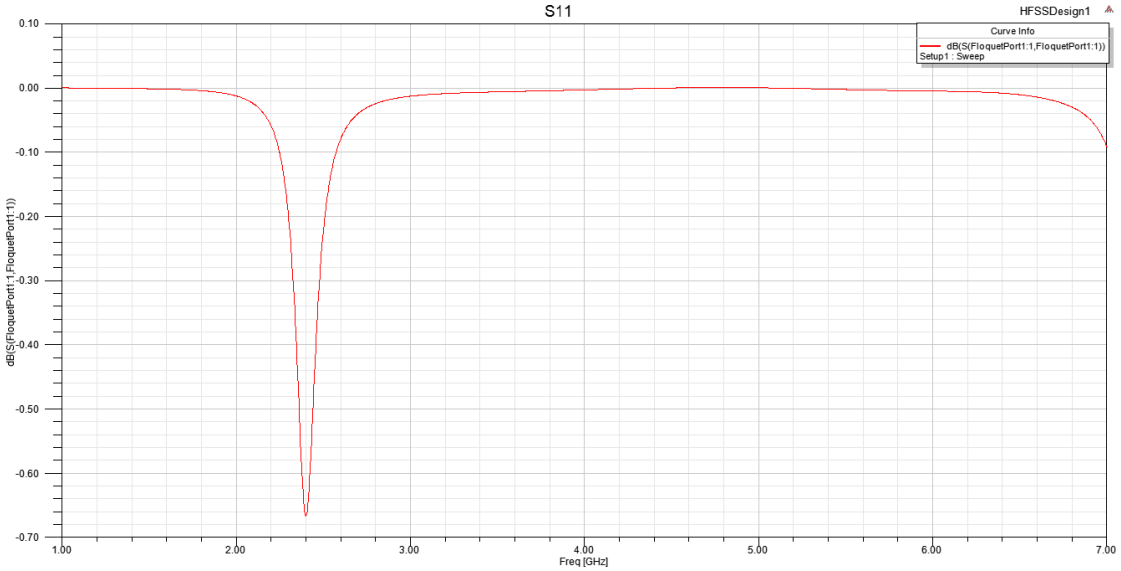

Figure 3-43. S11 parameter of the FSS.

The overall dimensions of the frequency selective surface are 130 mm by 130 mm. With that dimensions it can be located an array of 7x7 square patches with dimensions 16.5x16.5 mm. When End-Loaded Open Sleeve Dipole Antenna was designed the overall dimensions were 94 mm by 70 mm, but now the dimensions of the substrate have been changed in order to place the array of square patches.

In [Cur14], the square patches have a dimension of 8.9 mm and the array consisted of 8x8 square patches. A simulation with a square patch of 8.9 mm was run in order to verify that the patch was working at the required frequency. In view of the results shown in Figure 3-44 was demonstrated that the dimensions of that patch has a resonance

frequency around 4.8 GHz, which is not useful for this design. For that reason the overall dimensions are larger than in the design made in [Cur14].

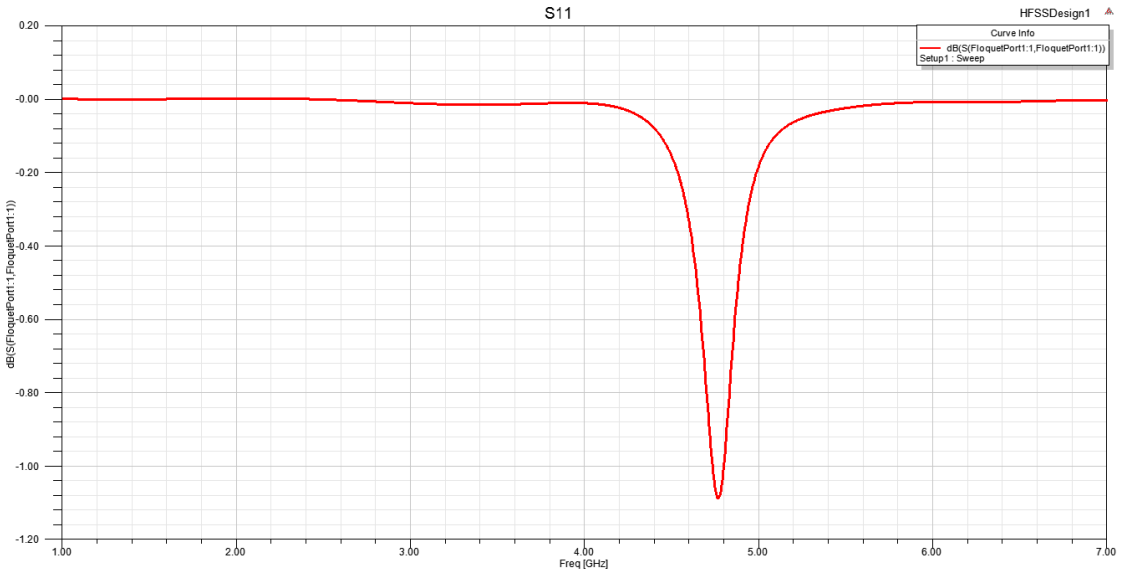

Figure 3-44. S11 parameter of the square patch of 8.9 mm.

Once designed the square patches that are placed on the frequency selective surface, the BST varactors are added between them. Figure 3-45 shows the square patches with the BST varactors and in Figure 3-46 a zoom of the same design is shown.

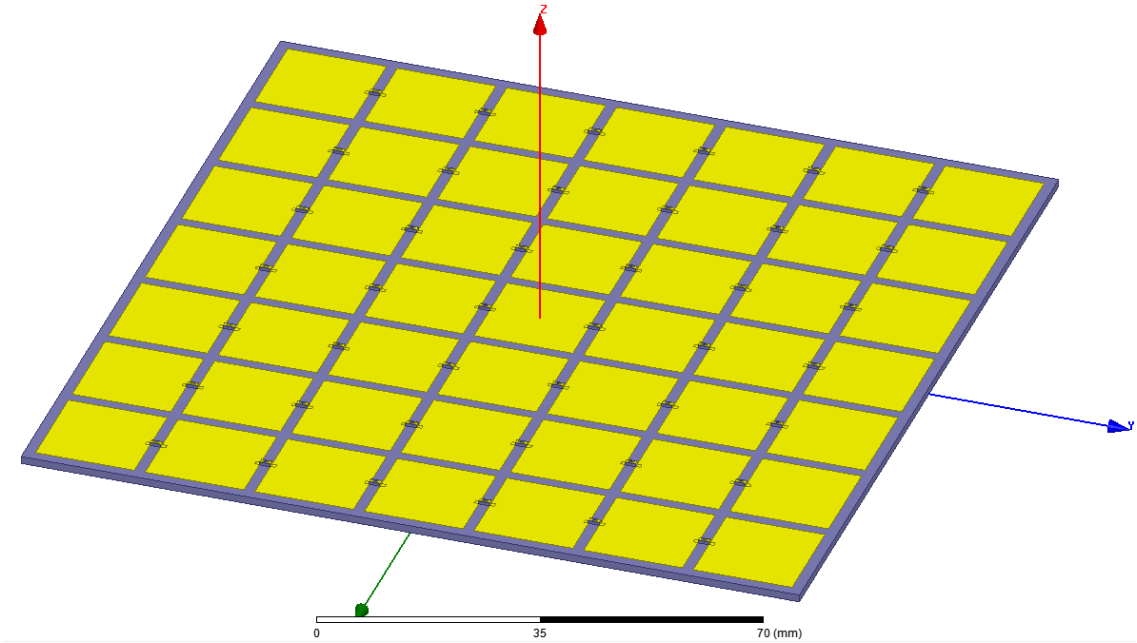

Figure 3-45. FSS with the square patches and BST varactors design.

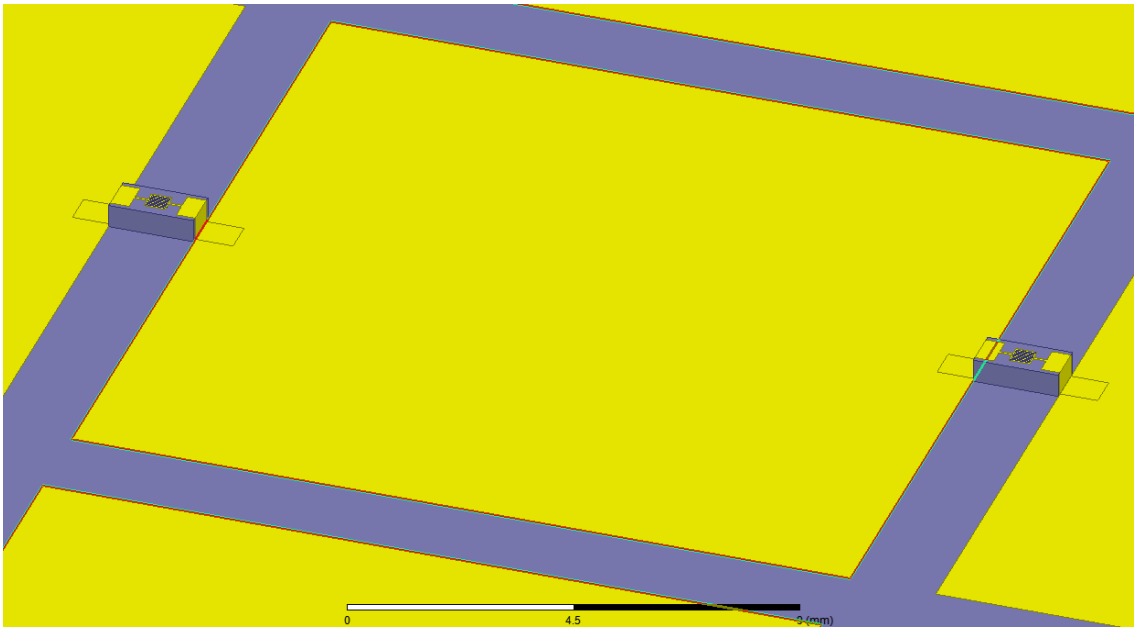

Figure 3-46. Zoom of FSS design.

upna Universidad Pública de Navarra Nafarroako Unibertsitate Publikoa

CHAPTER 4. FINAL ANTENNA DESIGN

In this chapter the final antenna design is presented. Three results are presented; in the first case the return loss together with the radiation pattern of the antenna on top of the FSS configuration are plotted. Two different antennas are used; i.e. the ELPOSD and the patch antenna. A comparison between results is driven. Afterwards, an artificial lumped load with a capacitive value emulating the BST varactors is introduced; different values are used in order to check the behaviour of the overall configuration. Finally, the BST structure is modelled and included together with the FSS. The return loss and radiation pattern are obtained. The results are commented.

4.1. DESIGN AND RESULTS OF THE ELPOSD AND SQUARE PATCH ANTENNA TOGETHER WITH THE FSS STRUCTURE

In this first section, the results of the two different antennas used in this project; i.e. the ELPOSD and the patch antenna on top of the FSS configuration are analyzed. In both cases, the return loss and the radiation pattern are obtained. A comparison between results is given. The design with the ELPOSD antenna is shown in Figure 4-1 and for the Square patch antenna is shown in Figure 4-2.

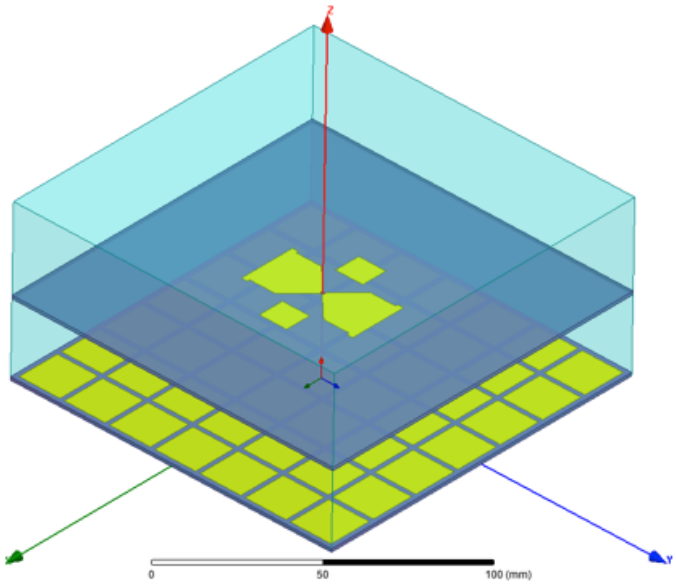

Figure 4-1. Schematic of the ELPOSD antenna together with the square patches FSS structure.

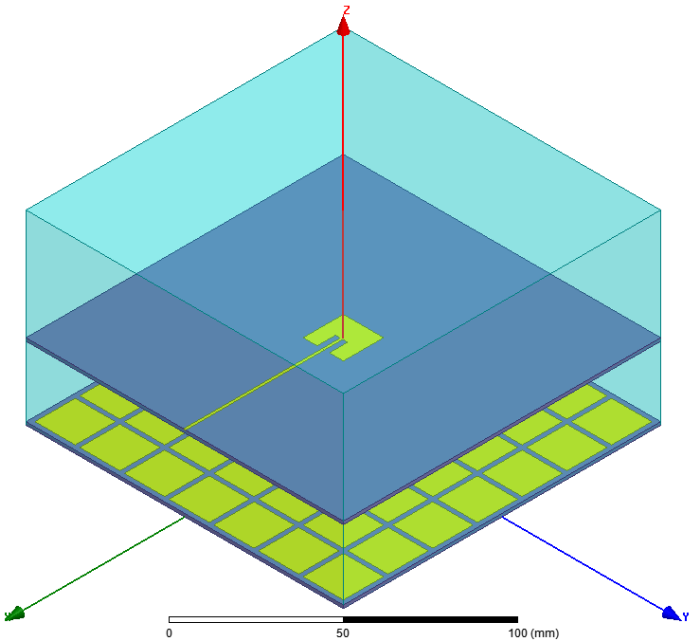

Figure 4-2. Schematic of the Square Patch antenna together with the square patches FSS structure.

In [Cur14] holes of approximately 0.5 mm in depth were drilled into the substrate to accommodate the BST varactors and maintain the low-profile characteristic. In this work, instead of complicating the design in HFSS software, the chips are placed on top of the FSS without doing any hole to locate them. For that reason, there will be an air gap between the FSS and the antenna substrate. A simulation with a variation of the gap between the two layers was run for the ELPOSD antenna in order to obtain the best air gap distance for the structure. The simulated values vary from 0.2 to 0.8 mm.

The value of the gap was set to 0.5 mm. This value is a compromise between the achieved S11 and a reasonable air gap value.

Figure 4-3 shows the S11 parameter of the ELPOSD antenna without the BST varactors varying the gap between the two substrates. Notice that the resonance frequency changes in every value of the gap, at a distance of 0.2 mm is around 2 GHz, with a 0.5 mm gap is 2.2 GHz and at a distance of 0.8 mm is close to 2.3 GHz. That is clearly the result of the combination of the antenna and the FSS. Even when both parts were design to work at 2.4 GHZ, they interfere between them a greater or lesser degree depending of the distance between them.

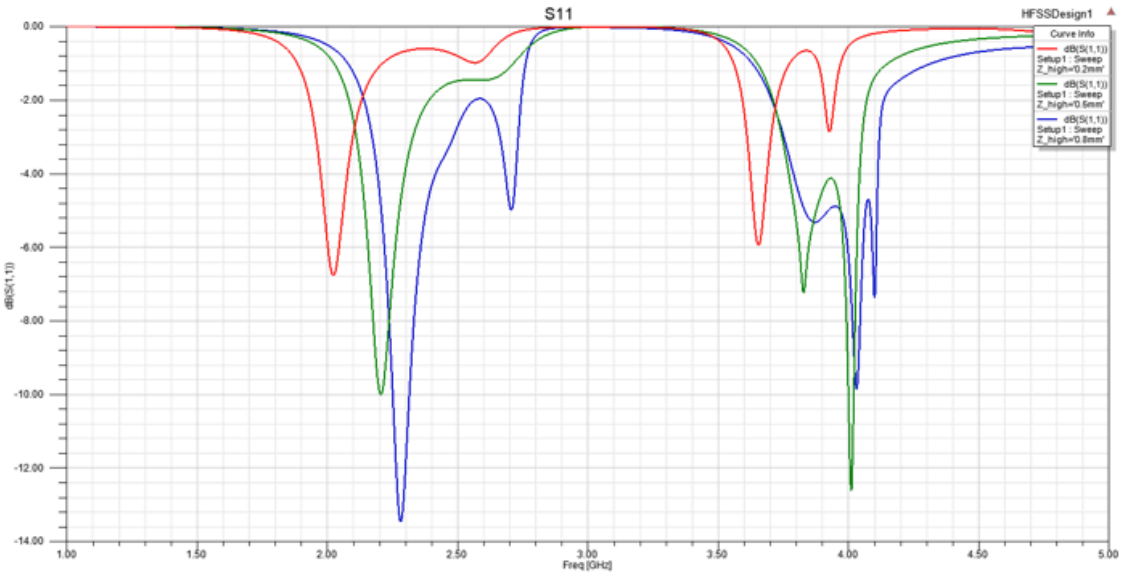

Figure 4-3. S11 parameter for different gap values.

Once the distance between the FSS and the antenna substrate is set, the simulations for the ELPOSD and the square patch antenna with the frequency selective surface without the BST chips are run. In Figure 4-4 the S11 comparison for the two types of antennas is shown.

As it can be seen in Figure 4-4 the S11 parameter is better with the patch antenna than with the ELPOSD antenna. The resonance frequency has moved from 2.4GHz in both cases. For the antenna ELPOSD the operating frequency is now at 2.21 GHz, while for the Square Patch antenna is at 2.83 GHz. Therefore, the impedance that the FSS entails to the set affects much on the Square Patch antenna because it has the same dimensions as the metallic elements of the FSS. The ELPOSD antenna is less influenced by the impedance of the Frequency Selective Surface because their design does not have the same shape or dimensions as the metallic elements of the FSS. Also be noted that the bandwidth for the ELPOSD is higher than for the Square patch antenna. This was also happening in the case the isolate antennas. Adding the FSS to the design, the bandwidth is greater for the ELPOSD antenna. However, there has not been much variation in the bandwidth in either of the two antennas. Note also that the ELPOSD antenna presents a higher resonant frequency around 4GHz.

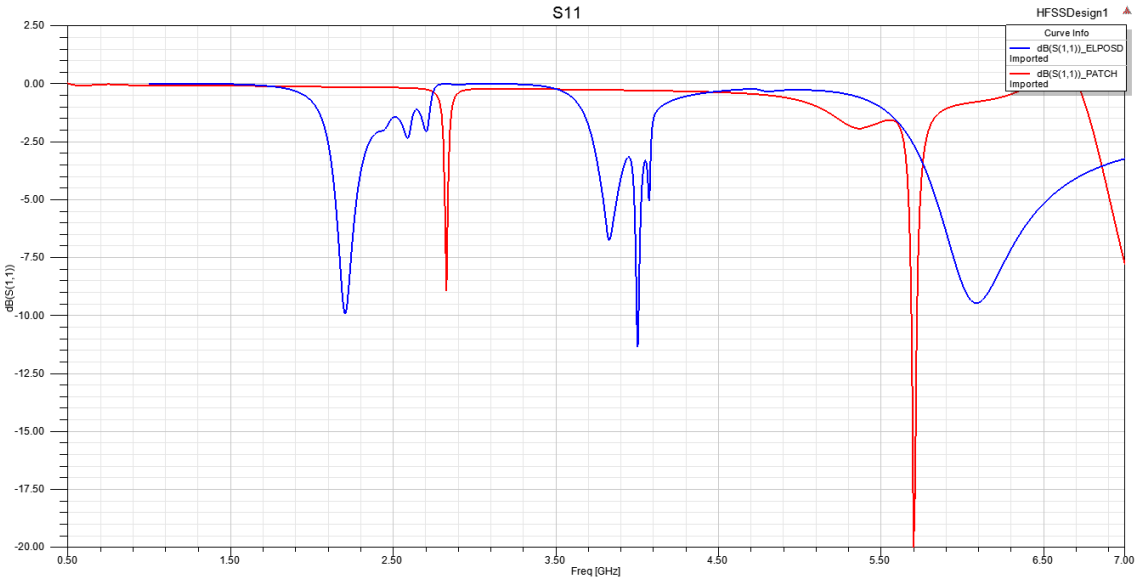

Figure 4-4. S11 parameter comparison between the ELPOSD antenna (blue line) and the Square Patch antenna (red line).

If Figure 4-4 is compared with the S11 parameter of the single ELPOSD (Figure 3-9 in section 3.1) and the single Square patch (Figure 3-16 in section 3.2) it is notice that the results are similar without the Frequency Selective Surface without BST varactors, but the S11 parameter is better with it for the ELPOSD antenna.

At this point, the results for the two main antennas are quite good and the case of the Square Patch antenna has its resonance frequency far from the operating frequency, which differs from the dipole antenna having its next resonant frequency 1.6 GHz away from the operational frequency.

Figure 4-5 shows the E field of the ELPOSD antenna at 2,2 GHz where it can be seen that the field is mainly located along the dipole antenna and the parasitic elements do not couple too much power.

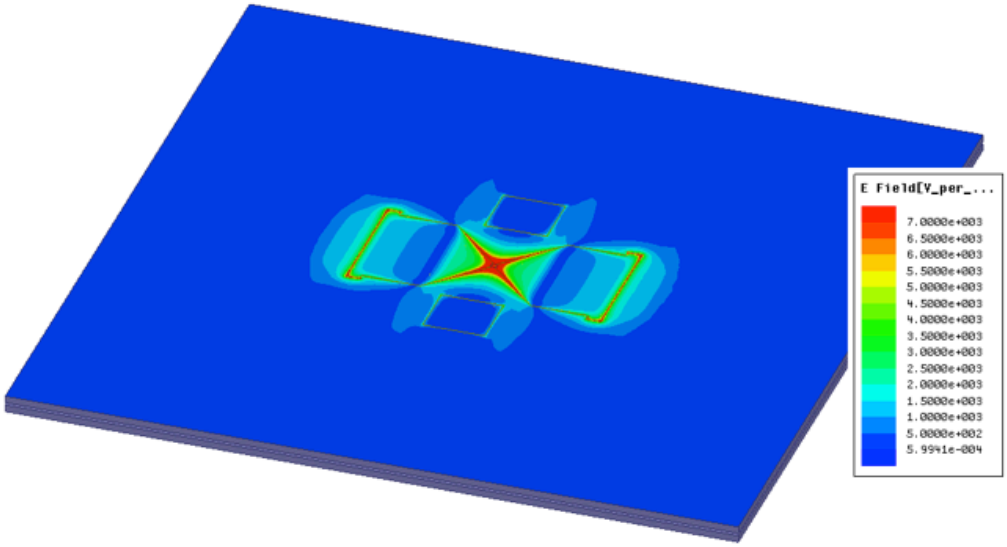

Figure 4-5. E-field at 2.7 GHz of the ELPOSD antenna.

upna Universidad Pública de Navarra Nafarroako Unibertsitate Publikoa

The E-field of the Square Patch antenna at 2.8 GHz is shown in Figure 4-6. It can be seen how the field goes through the microstrip and reaching the square patch. Notice that the field is greater in the ELPOSD antenna than in the Square Patch antenna.

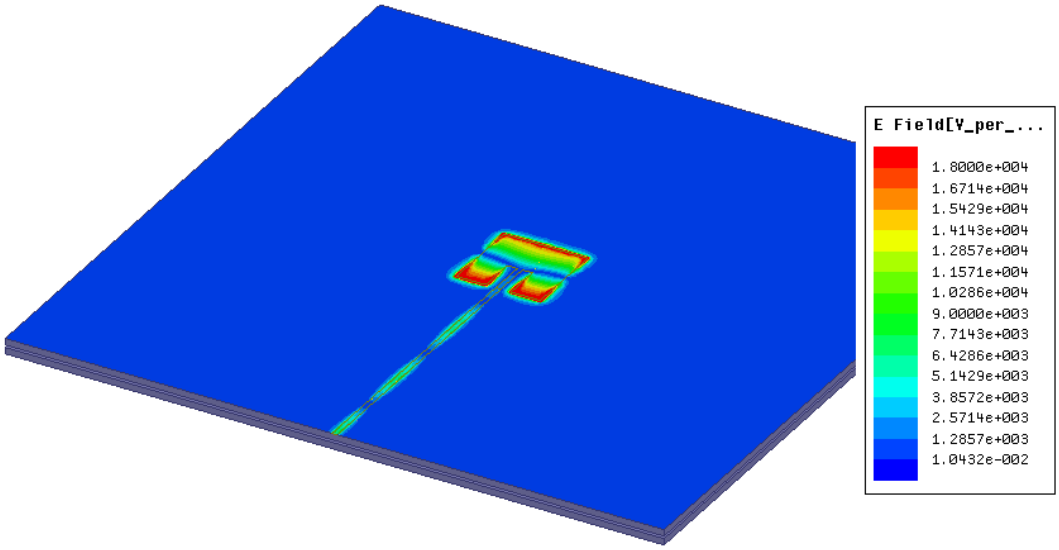

Figure 4-6. E-field at 2.8 GHz of the Square Patch antenna.

Regarding to the radiation pattern for the ELPOSD antenna with the FSS without the varactors, the shape is quite similar to the single antenna. Figure 4-7 shows the radiation pattern of this last combination. If the directivity is compared between the ELPOSD antenna with and without the FSS (see Figure 3-12 in section 3.1), a reduction in the directivity value from 6.6 dB to 5.6 dB is obtained. Even though the results obtained are still good.

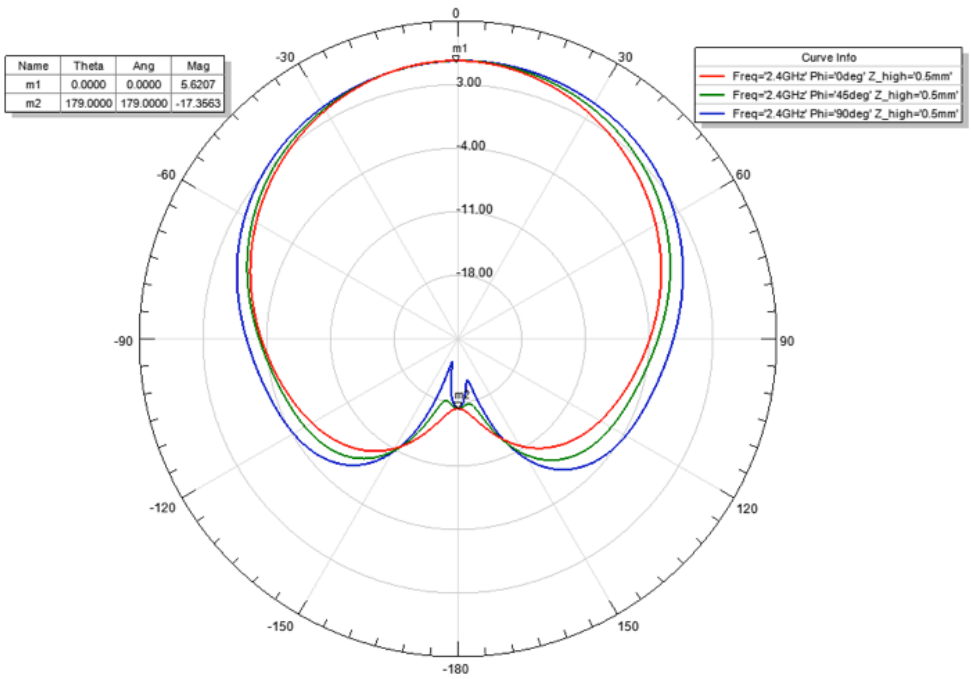

Figure 4-7. Radiation pattern of the ELPOSD antenna with the FSS.

The radiation pattern of the Square Patch antenna with the FSS without the varactors is shown in Figure 4-8. If the directivity of the Patch antenna with the FSS is compared with the single antenna shown in Figure 3-17 in Section 3.2, it is noticed that there is no improvement on the value of the directivity from 5.57 dB to 6.26 dB, but it is noted that there has been a change in the shape regarding the single antenna. Now the radiation pattern is more symmetric, the influence of the feeding line in the pattern has been mitigated.

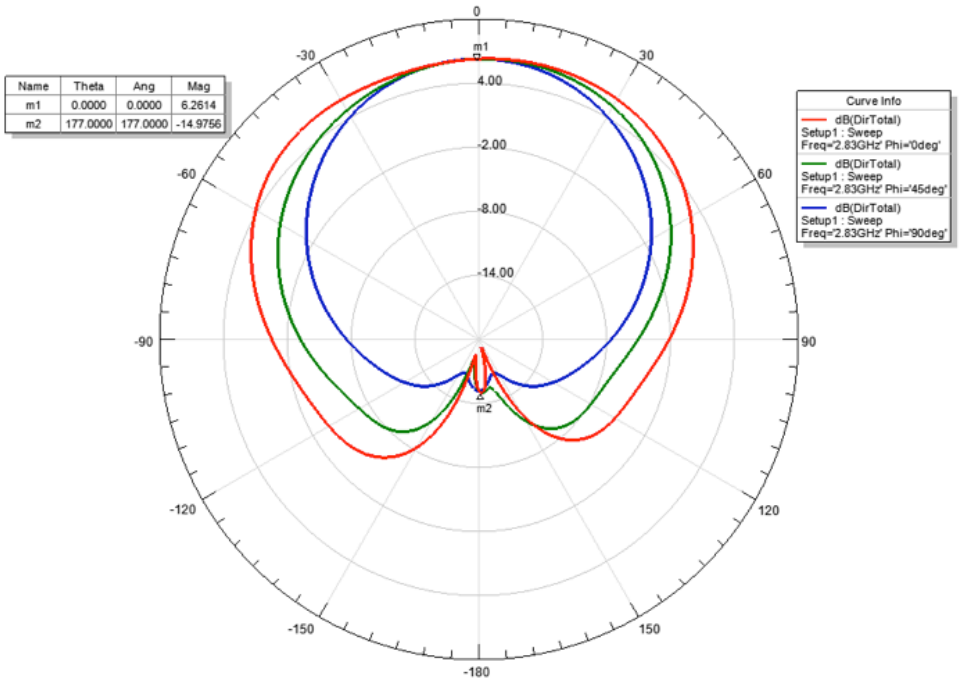

Figure 4-8. Radiation pattern of the Square Patch antenna with the FSS.

4.2. DESIGN AND RESULTS OF BOTH ANTENNAS WITH THE FSS REPLACING THE BST VARACTORS BY LUMPED CAPACITORS

Before the BST varactors are introduce into the design, they will be replaced for rectangle elements defined as "Lumped RLC". This design is made to verify that varying the capacitance of these added elements, the resonance frequency changes as expected. The capacitance values for these lumped elements are taken from [Cur14] and shown in Figure 4-9. The effective capacitances were extracted using an optimization of the measured and modelled results. The measure of the interdigital capacitors is beyond the scope of this work; therefore the effective capacitances values for the five-fingers interdigital capacitor are taken from Figure 4-9.

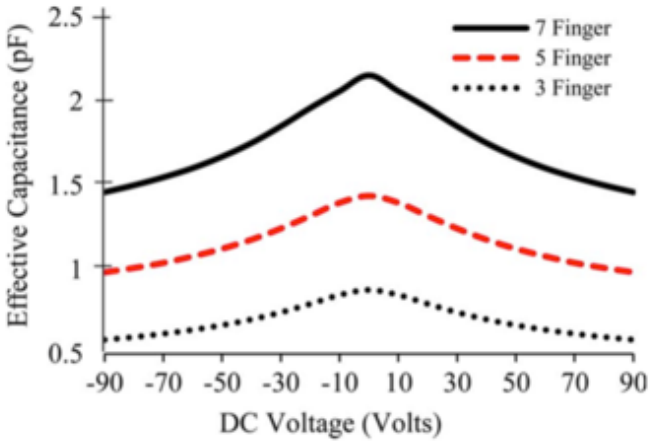

Figure 4-9. Measured capacitance versus voltage for three-,five-, and seven-finger IDCs at 1GHz.

The capacitance values simulated were 1 pF, 1.2 pF and 1.4 pF for five-finger interdigital capacitors. In Figure 4-10 the FSS design layer with these lumped elements is shown and Figure 4-11 shows the two designs for each case of radiating antenna and a zoom of the frequency selective surface layer.

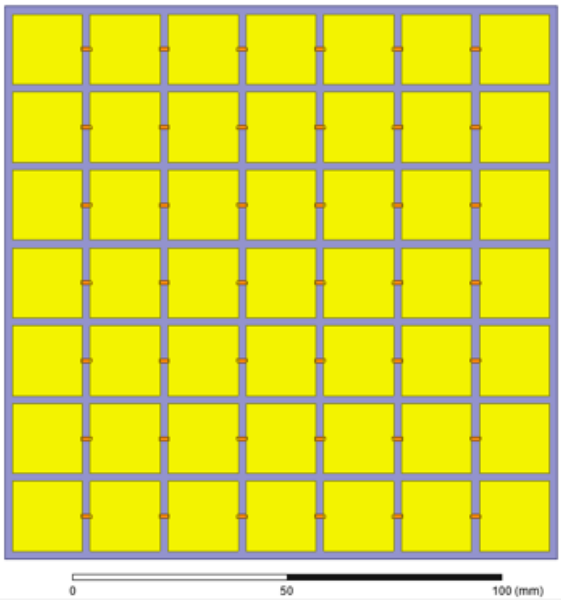

Figure 4-10. Schematic of the lumped RLC design.

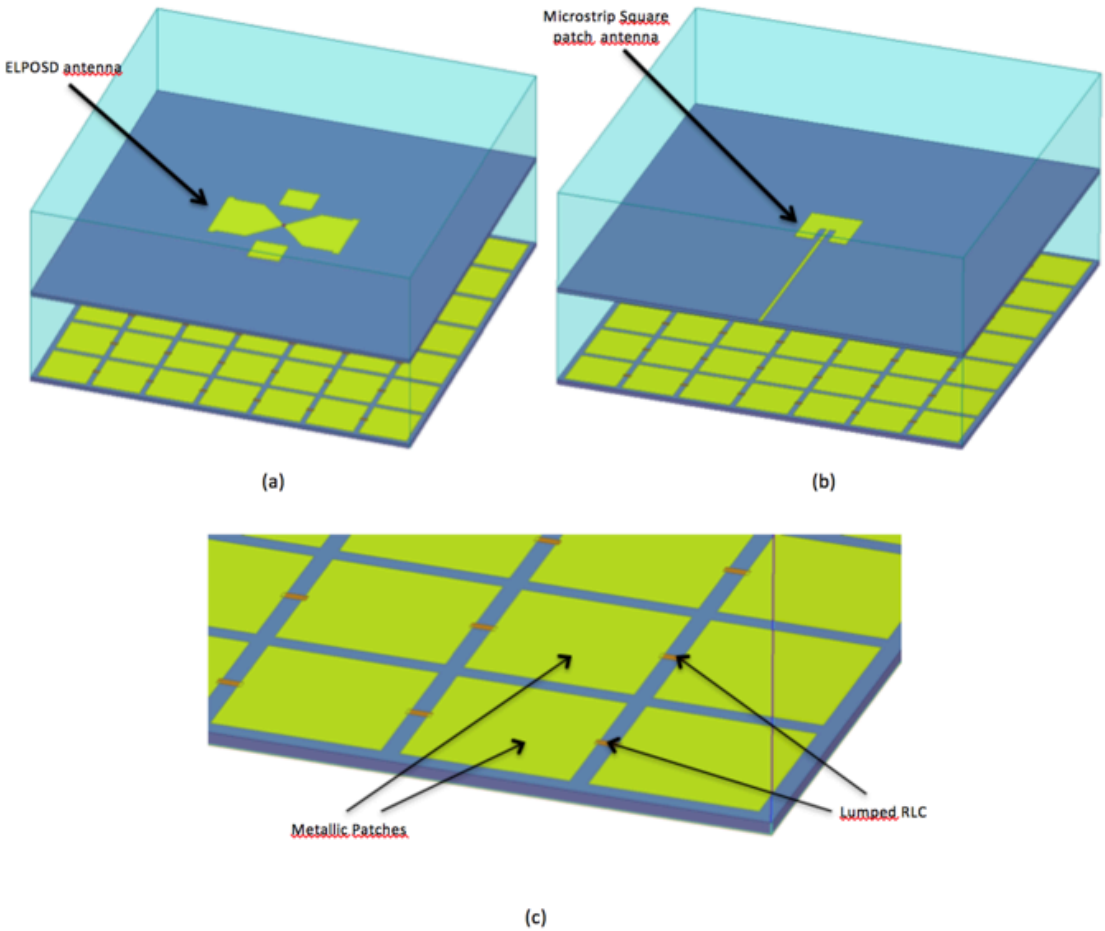

Figure 4-11. (a) ELPOSD antenna design. (b) Microstrip Patch antenna design. (c) Zoom of the FSS layer with the lumped capacitor elements and the metallic patches.

First at all, the S11 parameter versus frequency of the ELPOSD antenna will be shown. As can be seen in Figure 4-12, the resonance frequency changes by varying the capacitance of the lumped elements. For a capacity of 1 pF the resonance frequency is 1,97 GHz and the value of the S11 parameter is almost -20 dB. On the other variations of the lumped element's capacitances the S11 parameter worsens slightly, but still keeps a good values. For a capacity of 1,2 pF the resonance frequency is 1,91 GHz and for a capacitance of 1,4 pF is 1,85 GHz. The S11 parameter for the last two capacitances is around -15 dB. The results are gathered in Table 4-1 for better understanding.

Therefore, the design works as expected and the distance between frequencies moves around 60 MHz for each capacitance value.

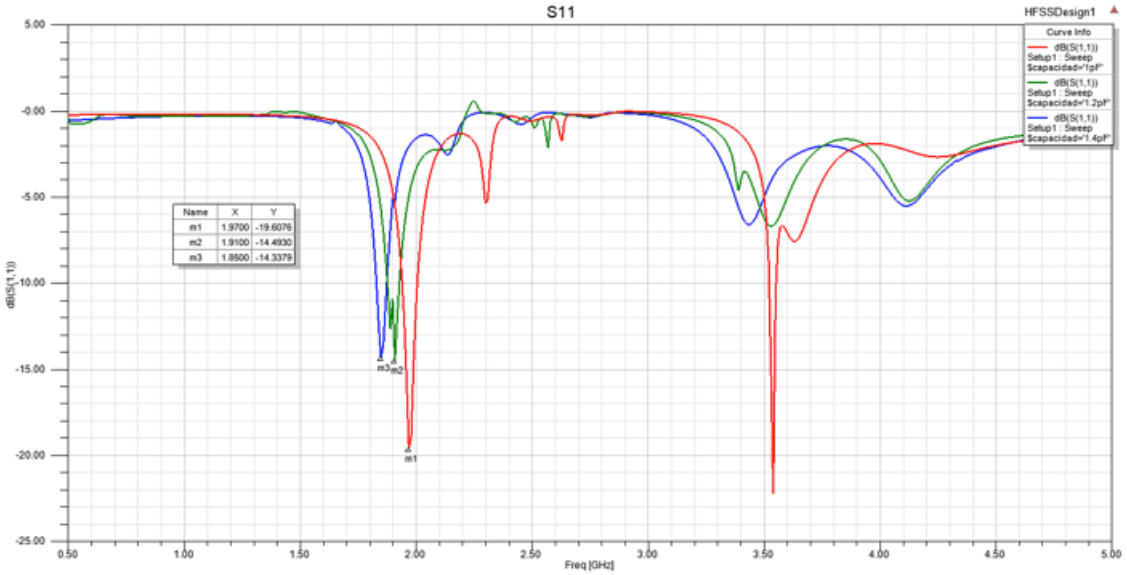

Figure 4-12. S11 parameter versus frequency of the ELPOSD antenna.

Element's capacitance (pF)	Operating frequency (GHz)	S11 parameter (dB)
1	1.97	-20
1.2	1.91	-15
1.4	1.85	-15

Table 4-1. Results varying the capacitance of the lumped elements.

The following figures (Figure 4-13, Figure 4-14 and Figure 4-15) show the radiation pattern of the ELPOSD antenna for every value of capacitance simulated. As can be observed the directivities values are similar to the one obtained in Figure 4-7 Section 4.1 (around 5 dB).

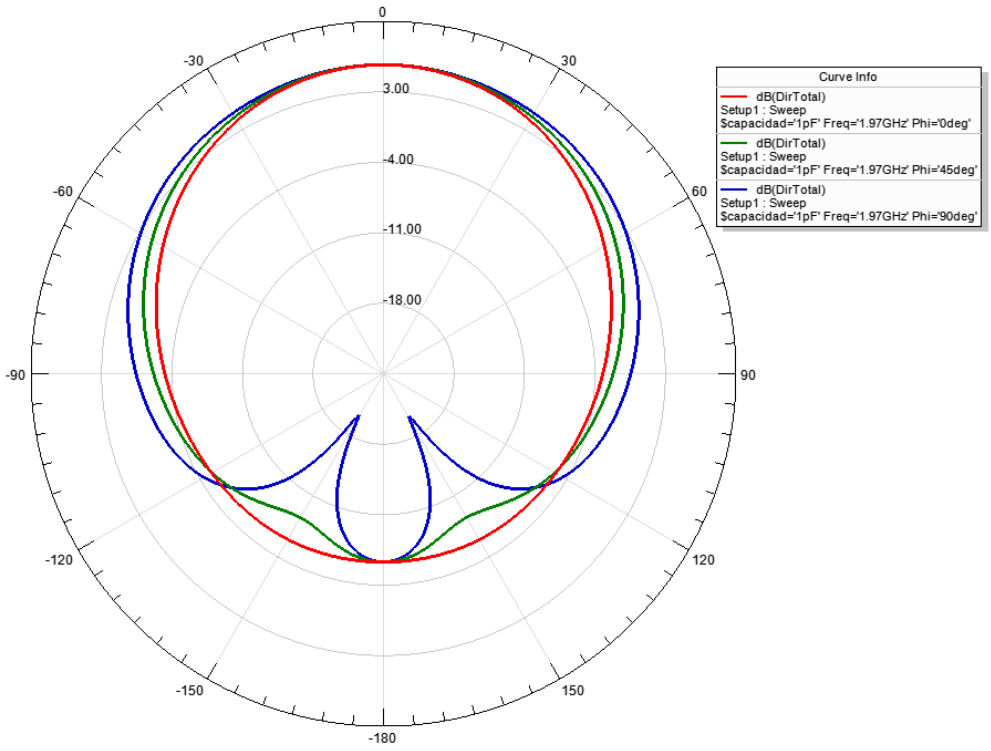

Figure 4-13. Radiation pattern of the ELPOSD antenna at 1.97 GHz with a 1 pF of capacitance.

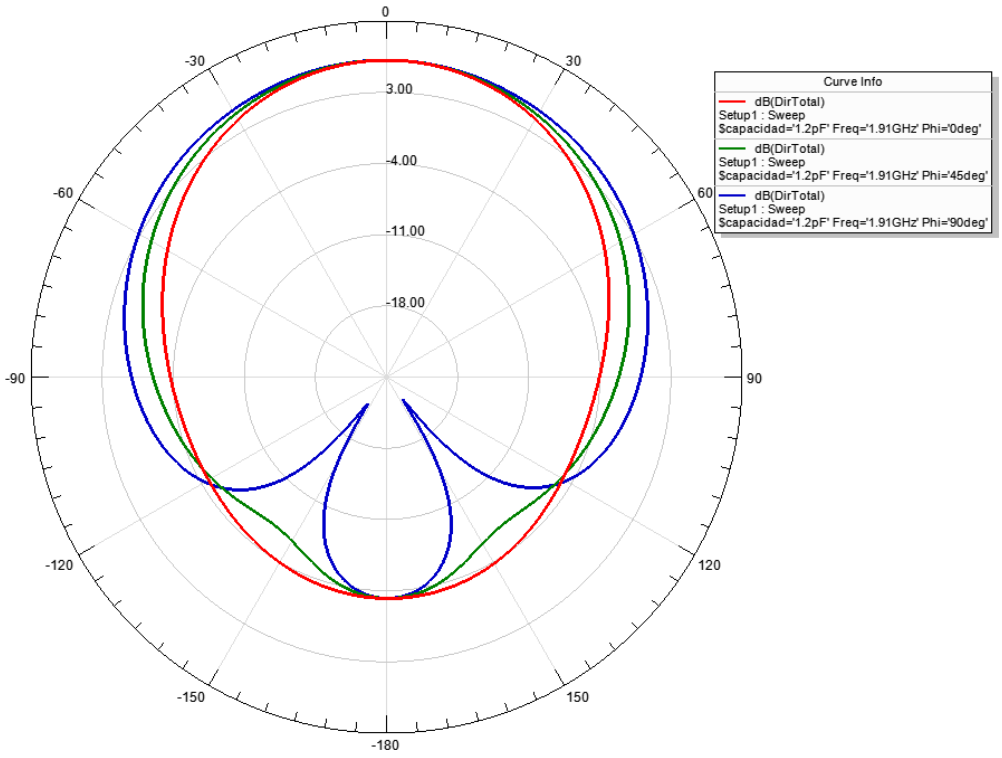

Figure 4-14. Radiation pattern of the ELPOSD antenna at 1.91 GHz with a 1.2 pF of capacitance.

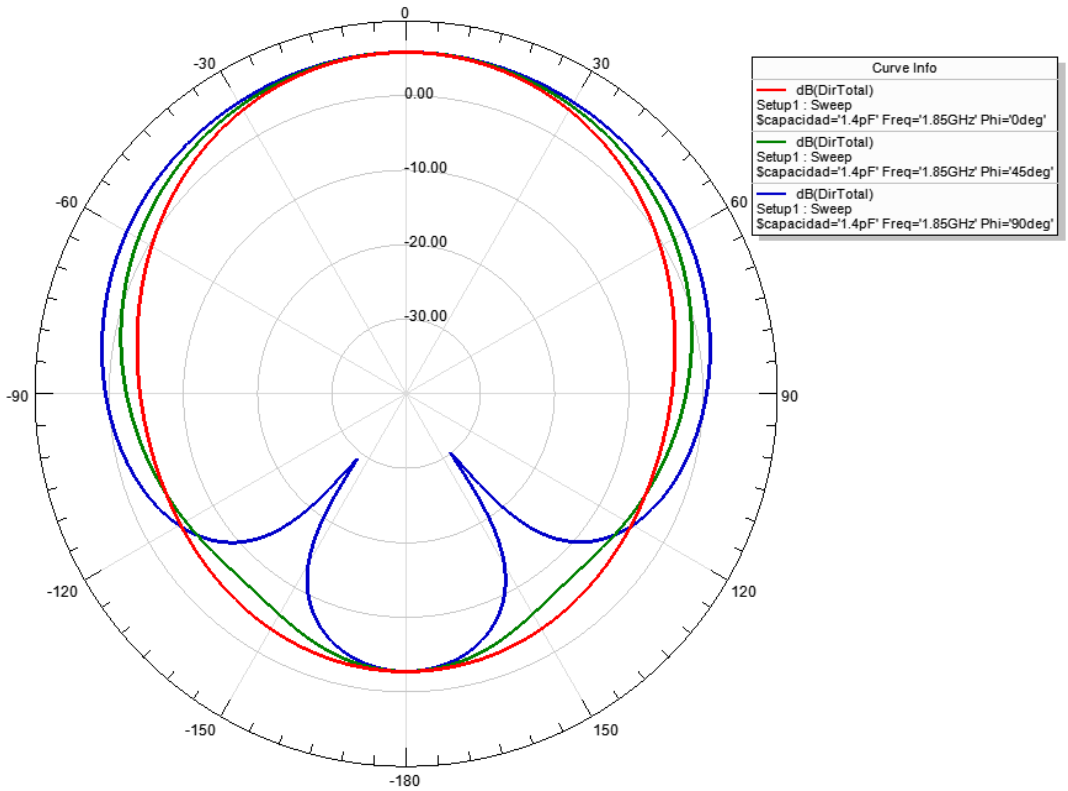

Figure 4-15. Radiation pattern of the ELPOSD antenna at 1.85 GHz with a 1.4 pF of capacitance.

The same simulation was performed for the case of the Square patch antenna. Figure 4-16 shows the reflection spectrum as a function of frequency and Figure 4-17 shows the E-field at 2.7 GHz of half of the Square Patch antenna.

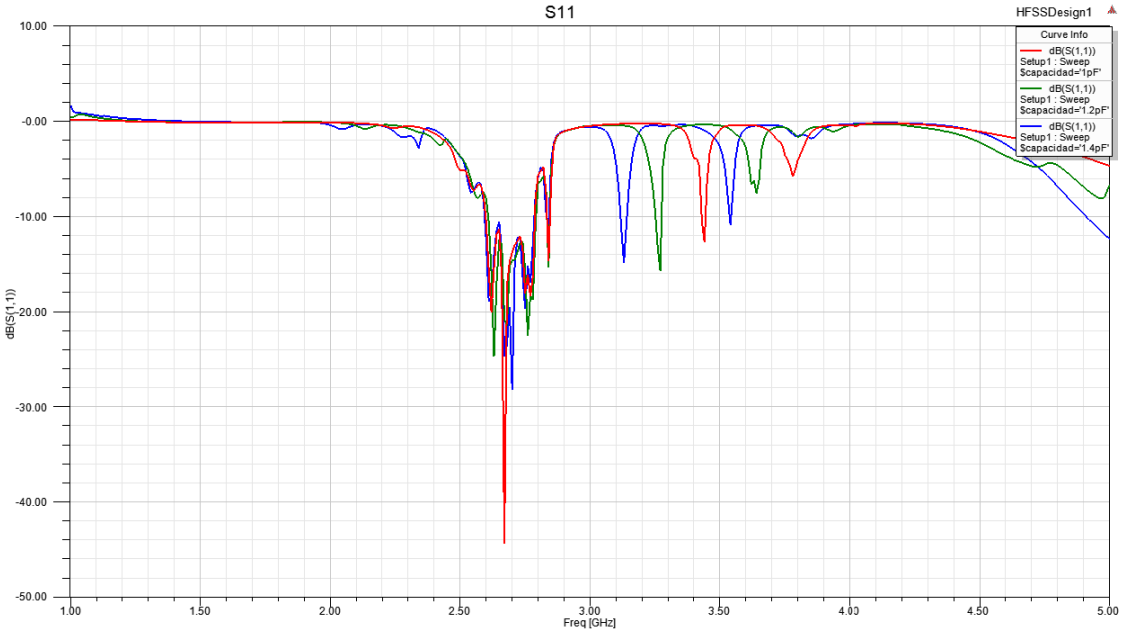

Figure 4-16. S11 parameter versus frequency of the Square Patch antenna.

upna Universidad Pública de Navarra Nafarroako Unibertsitate Publikoa

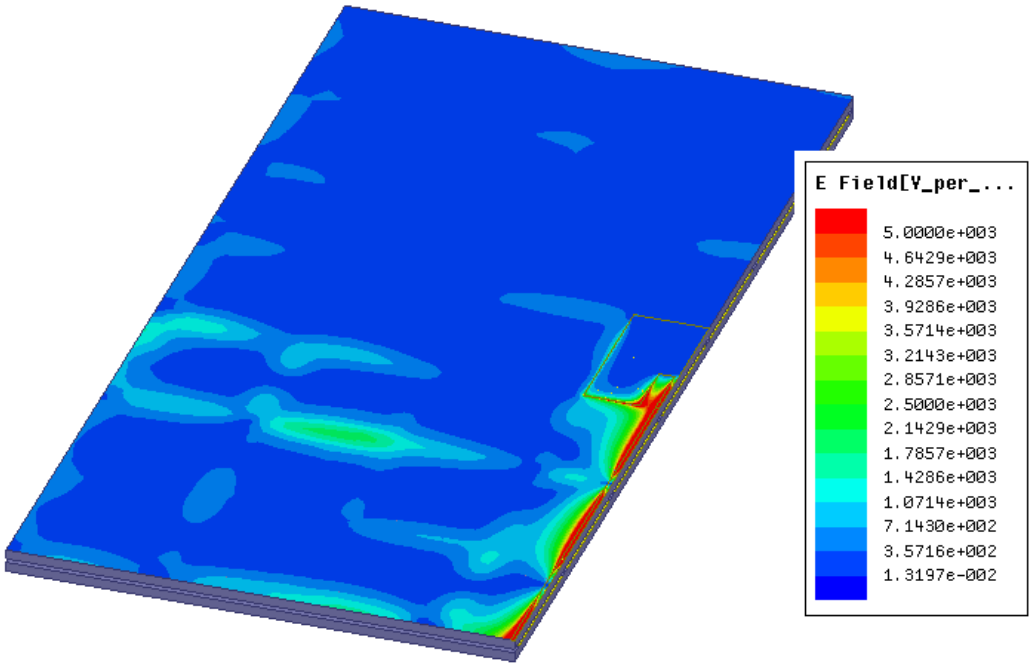

Figure 4-17. E-field at 2.7 GHz of the Square Patch antenna.

As can be seen in Figure 4-17 around 2.7 GHz appears a series of resonances, which makes the bandwidth larger. The point is that at 2.7 GHz the frequency does not vary, as can be seen in other frequency resonances. This fact suggest that the frequency selective surface (FSS) affects more to the main antenna, as the FSS is designed to that frequency, especially because the metallic elements of the FSS and the Square Patch antenna have almost the same shape and the same dimensions. Figure 4-17 shows how the E-field does not reach the patch antenna. The E-field cuts through the microstrip line to the substrate at 2.7 GHz. Figure 4-18 shows the E-field at 2.7 GHz of the Frequency Selective surface where it is observed that the E-field is coupled to the FSS before reaching the Square Patch antenna.

One of the possible causes of these results in the S11 parameter is the way that the patch antenna has been fed. While in the case of the patch antenna with the FSS with square patches has achieved successful results; in this configuration the FSS square patches are bound to each other by the capacitive elements and this causes the E-field couple to the square patches of the FSS instead of the main antenna.

Although at the estimated frequency has not been a frequency variation due to this phenomenon, a frequency variation occurs in the following harmonics. The distance between adjacent resonance frequencies is around 150 MHz. Therefore, it can be said that including the lumped elements a tunable antenna is achieved.

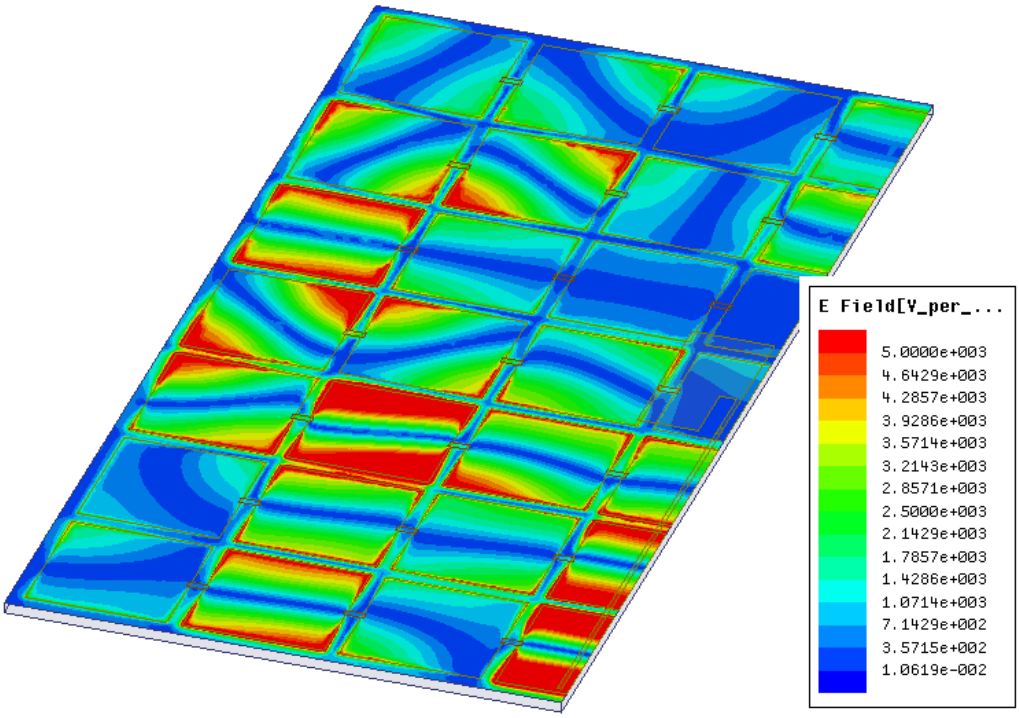

Figure 4-18. E-field at 2.7 GHz of the Frequency Selective Surface (FSS) with a capacitance value of 1 pF.

The radiation patterns of the Square Patch antenna with the FSS are not shown since no significant data have been obtained.

upna Universidad Pública de Navarra Nafarroako Unibertsitate Publikoa

4.3. DESIGN AND RESULTS OF THE MAIN ANTENNAS WITH THE FSS WITH BST VARACTORS

Once it is demonstrated that the structure works as planned, the lumped elements are replaced for the BST varactors, which have to work similar as these elements. In order to reduce the complexity of the design in HFSS software, instead of include a centered aperture on either side of the patch unit cell to fit the BST varactors, the procedure carried out was to allocate the BST varactor on the FSS substrate without subtracting part of thereof. Thus it is designed simpler and the results obtained will be equal or similar than if the design is done with an aperture for the BST varactors. In addition to attach the varactor with the patch unit cells, a metal has been added between them that simulates the fusion part that would occur in the fabrication.

Since the difference in size between the BST chip varactors and the dimension of the main antenna or the square patches of the FSS is so huge, to make the HFSS software simulation more accurate, the final structure of the antenna will be divided into as many parts as can be made symmetries. In the case of the End-Loaded Open-Sleeve dipole antenna may be split into the ZX and ZY plane, being a quarter of the antenna. On the contrary, in the case of the Square patch antenna only the ZX plane is capable to create symmetry, being half of the antenna. Therefore, these new faces appearing after splitting the antenna will become a so-called symmetry boundary condition, which may be E or H type.

Figure 4-19 show the whole ELPOSD antenna, the quarter of antenna that results of the split process and the two faces that become symmetry E and symmetry H respectively. The whole Square patch antenna, the half of the square patch antenna and the symmetry H face are shown in Figure 4-20.

upna Universidad Pública de Navarra Nafarroako Unibertsitate Publikoa

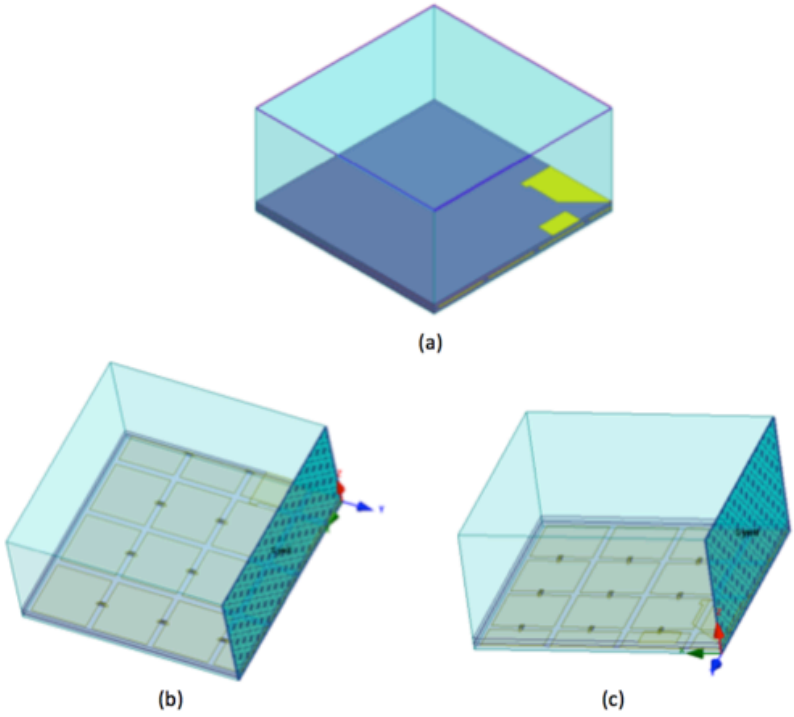

Figure 4-19. (a) Quarter of the ELPOSD antenna. (b) Symmetry E face. (c) Symmetry H face.

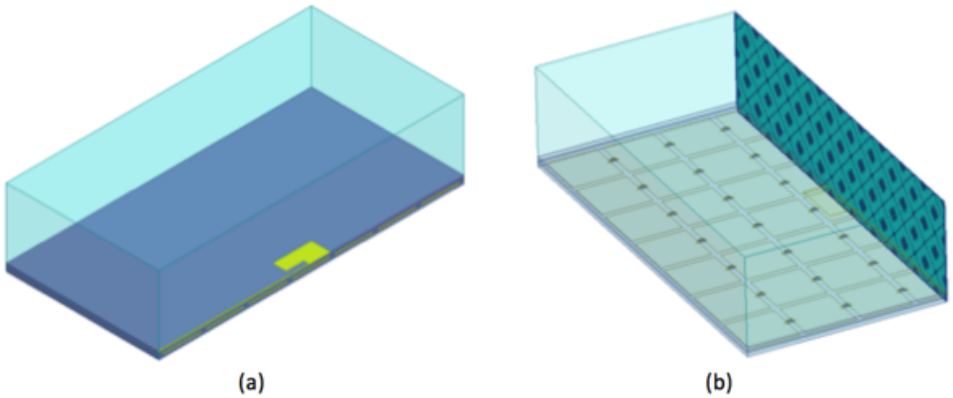

Figure 4-20. (a) Half of the Square Patch antenna. (b) Symmetry H face.

The BST material's permittivity was probed in [Cur08] that can be varied from 200 to 350. In a first simulation with each main antenna it will be made a parametric with three values of the permittivity of the BST, that values are 200, 275 and 300. Simulation is performed only with these three values to check first that the structure works as expected. As can be seen in Figure 4-21 where the S11 parameter versus frequency of the ELPOSD antenna is shown there is no variation of the resonance frequency, which means that the final structure does not work or the software is not able to see the effect of a 350 nm film thickness by changing its permittivity because for the software it is a minimal part of the

overall design. The simulation with patch antenna will not be performed to save time because the result will be the same, without variation in the resonance frequency.

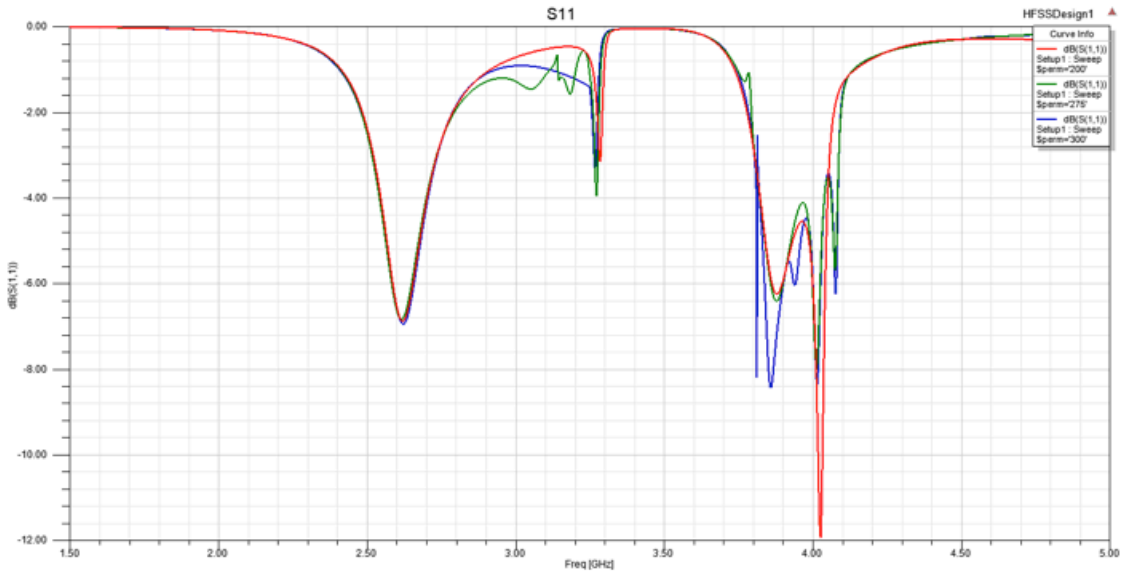

Figure 4-21. S11 parameter vs frequency as function of the permittivity variation.

It is clear that although the BST film is so small affects more to the varactor that what affects the alumina substrate. The field lines are higher near the interdigital capacitors, ie near the BST film than in the rest of the BST varactor chip. Therefore, it is decided that the software is not working properly and that previous simulations should not be taken into account.

In order to explain the results, a useful analytical constraint for the effective dielectric constant is provided by the Weiner bounds, as in Aspnes (1982), taken from [Joa08]. Specifically, for a two-material composite, each effective dielectric constant ε_α is bounded by

$$(f_1\varepsilon_1^{-1} + f_2\varepsilon_2^{-1})^{-1} \leq \varepsilon_\alpha \leq f_1\varepsilon_1 + f_2\varepsilon_2$$

where f_1 and f_2 are the volume fractions of the materials with dielectric constants ε_1 and ε_2.

If we use this equation with the permittivities and the volume fractions of the alumina substrate and the BST material the following boundaries for the effective dielectric constant are obtained and gathered in Table 4-2 and Table 4-3:

Material	Volume fraction	Permittivity
Alumina	0.999	9.8
BST	0.001	200-350

Table 4-2. Volume fraction for the Alumina substrate and BST film.

Effective dielectric constant			
BST permittivity	Lower boundary		Upper boundary
200	9.80061845	$\leq \varepsilon_\alpha \leq$	9.81262056
250	9.80062482	$\leq \varepsilon_\alpha \leq$	9.81593827
300	9.80062907	$\leq \varepsilon_\alpha \leq$	9.81925598

Table 4-3. Effective dielectrics constant with the volume fractions of Table 4-2.

As can be seen the effective dielectric constant varies almost nothing, which means that for the HFSS software the BST film does not affect to the whole design. For this reason, to make sure the system works properly, ie that changing the permittivity of the material BST the resonance frequency varies, it is going to carry out a study in which the volume of BST material will be increased and also it will be given more weight or more importance that it actually has. Thus, the volume fractions are altered to give more value to the BST film than the rest of the alumina substrate. This will be done because the field is concentrated in the area where the interdigital capacitors are, hence the changes in the capacity will occur there; the rest of the BST chip acts like a microstrip line.

With this change in the importance of BST film is intended to justify the mean values of the dielectric constant taken, seeing that by using the above equation and using the permittivities simulated before (200, 275 and 300), a range for the effective permittivity is obtained in which values are used in the simulation.

In Table 4-4 the filling factor equation is used with some values of the dielectric of the BST material (200, 250 and 300) and the volume fractions are altered to make the simulation seems closer of what would be the reality.

BST permittivity	BST volumen fraction	Alumina volume fraction	Effective dielectric constant boundaries		
200	0,2	0,8	12,10	$\leq \varepsilon_\alpha \leq$	47,84
250	0,3	0,7	13,77	$\leq \varepsilon_\alpha \leq$	81,86
300	0,4	0,6	15,99	$\leq \varepsilon_\alpha \leq$	125,88
350	0,83	0,17	50,71	$\leq \varepsilon_\alpha \leq$	292,17

Table 4-4. Effective dielectrics constant with the volume fractions altered.

upna Universidad Pública de Navarra Nafarroako Unibertsitate Publikoa

As can be seen, if the volume fraction of the BST is increased the effective dielectric constant boundaries vary more with the same BST permittivity. Therefore, a value for every bounded range is taken in order to run a simulation with these values.

The BST chip will be performed with a volume fraction of the BST that is not any of those presented in the table above. This volume fraction covers the area where the interdigital capacitors are and the thickness will be as the alumina substrate. The altered BST chip is shown in Figure 4-22, where the red volume is the BST volume.

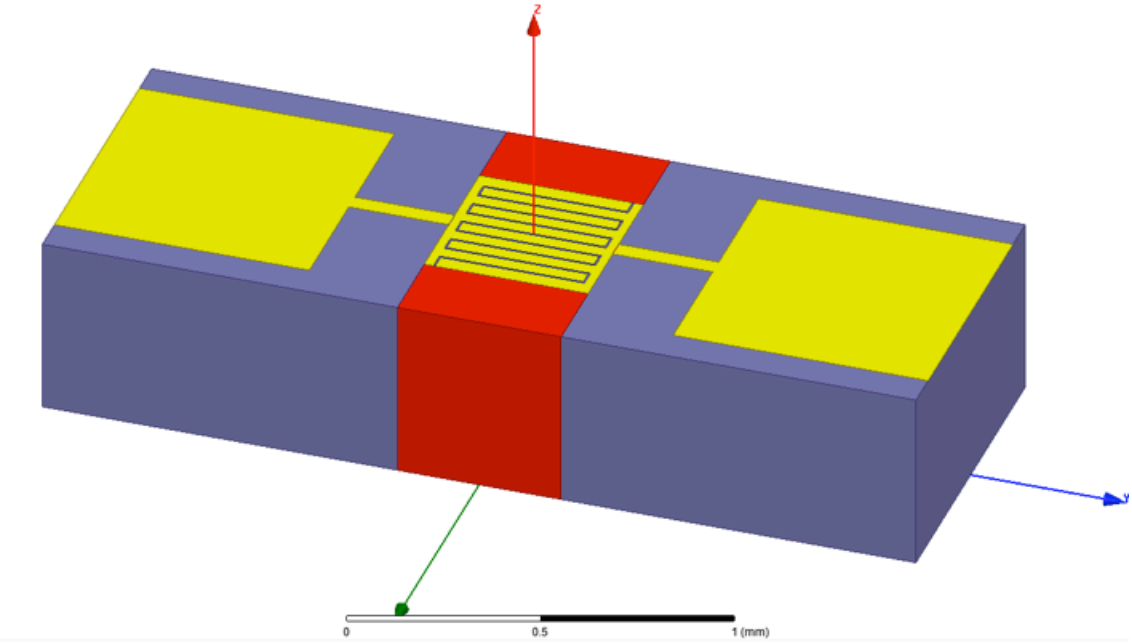

Figure 4-22. Schematic of the altered BST chip.

Now the volume fraction of the BST material corresponds to an 18% of the total volume. Even so it is simulated as if their weight was greater than the 18% and the values of the effective permittivity are gathered in Table 4-5:

BST permittivity	Effective permittivity
200	20
250	30
300	49

Table 4-5. Effective dielectric constants used in the simulation.

New simulations were run with the effective dielectric constants gathered in Table 4-5 and with the BST varactors replaced with the altered BST chips. The S11 parameter as a function of the effective permittivity variation for the ELPOSD antenna is shown in Figure 4-23 and for the Square Patch antenna is shown in Figure 4-24. In addition to permittivity values of the Table 4-5, an effective permittivity value is added corresponding to the value of the permittivity of the Alumina substrate (ie 9.8). This value is added in order to the whole substrate (including the BST material) have the same permittivity, ie the BST varactor is simulated without the BST material.

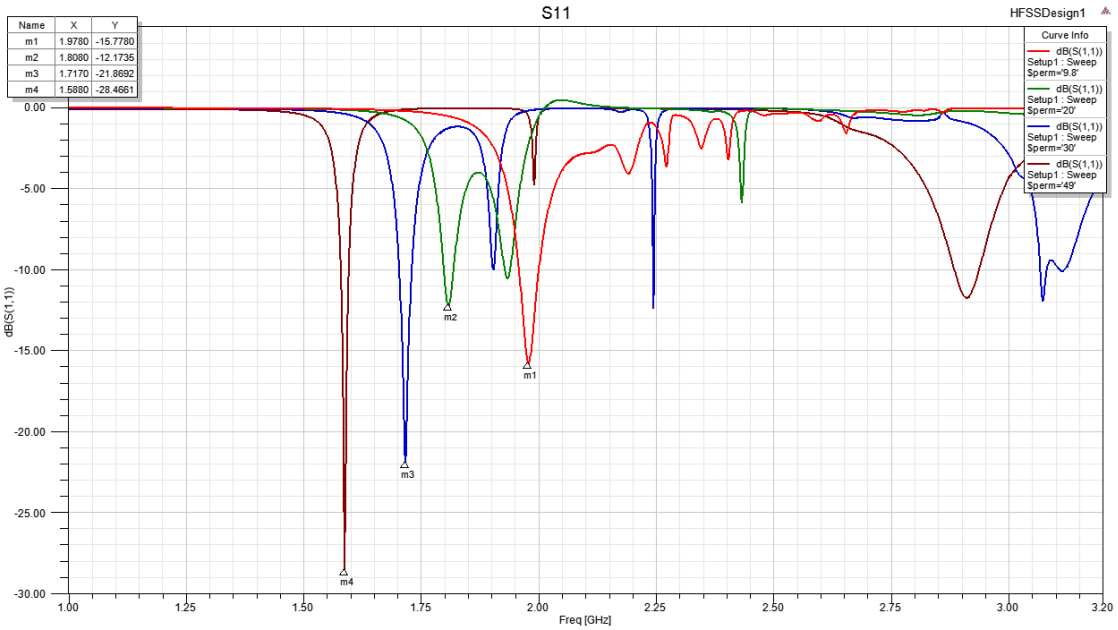

Figure 4-23. S11 parameter for the ELPOSD antenna with the FSS and the altered BST varactors.

As can be seen in the figure 4-23, varying the permittivity of the BST varactor the operational frequency changes, which means that the designed antenna is a tunable antenna. Also note that in the case of a permittivity of 20 and 30 the bandwidth is increased considering that new resonances appear. The resonance frequencies have moved from 2.4 GHz to lower frequencies instead of remain closer to the operational frequency.

Table 4-6 gathered the frequency variation and the S11 value for each permittivity. The distance between operating frequencies is around 100 MHz, which is more than with the Lumped elements used in section 3.5.2, where the distance between operating frequencies were around 60 MHz.

BST permittivity	Operating frequency (GHz)	S11 parameter (dB)
9.8	1.98	-16
20	1.81	-12
30	1.72	-22
49	1.59	-28

Table 4-6. Results for the ELPOSD antenna with the FSS with the altered BST varactors.

The following figures (Figure 4-25, Figure 4-26, Figure 4-27 and Figure 4-28) show the radiation pattern of the ELPOSD antenna for every value of capacitance simulated.

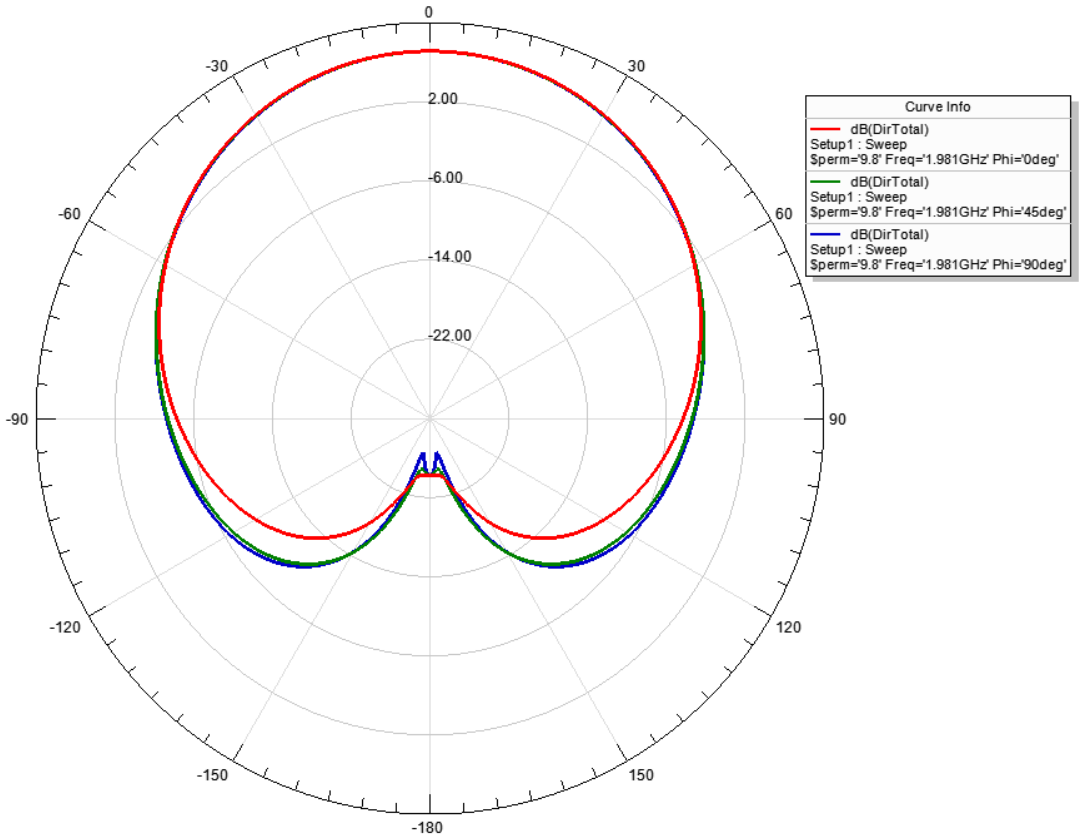

Figure 4-25. Radiation pattern of the ELPOSD antenna at 1.98 GHz with a permittivity value of 9.8.

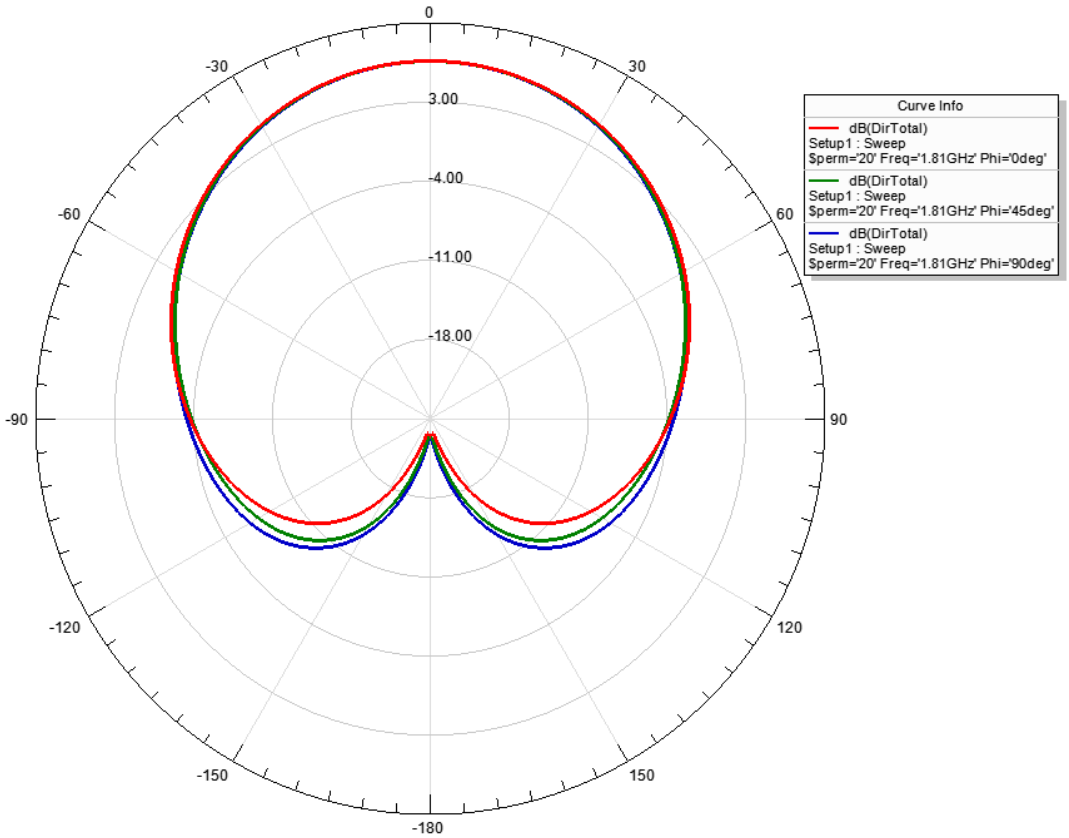

Figure 4-26. Radiation pattern of the ELPOSD antenna at 1.81 GHz with a permittivity value of 20.

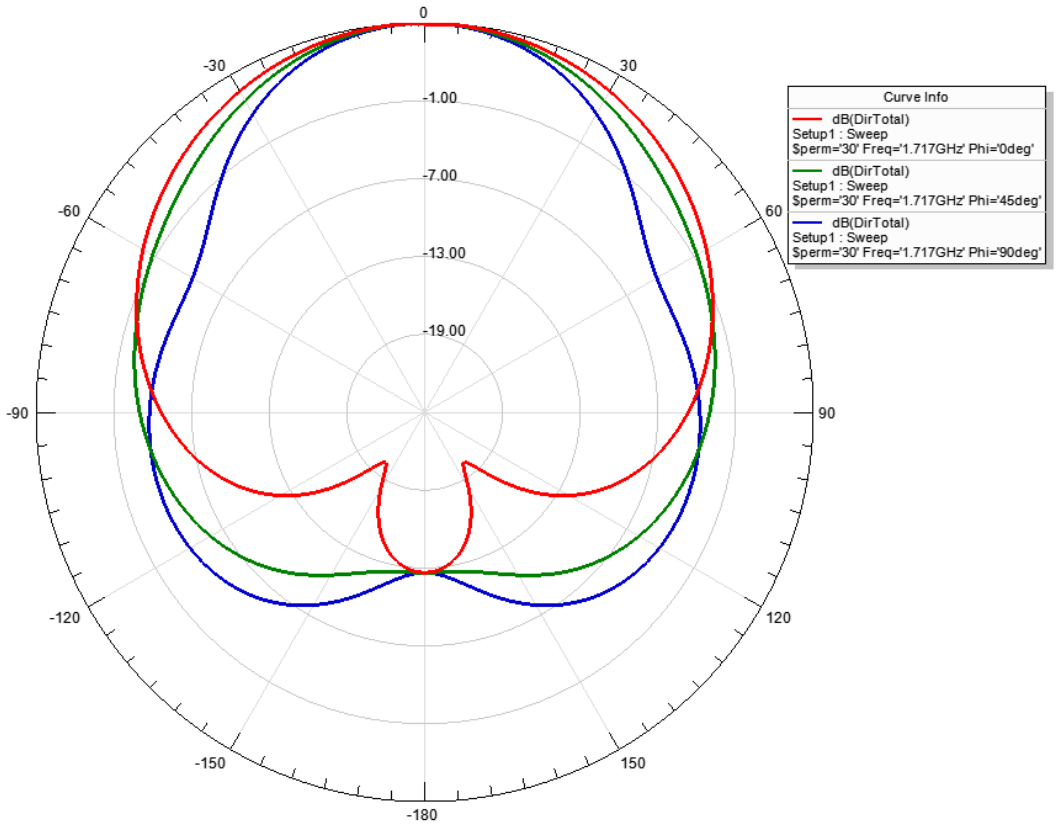

Figure 4-27. Radiation pattern of the ELPOSD antenna at 1.717 GHz with a permittivity value of 30.

upna Universidad Pública de Navarra Nafarroako Unibertsitate Publikoa

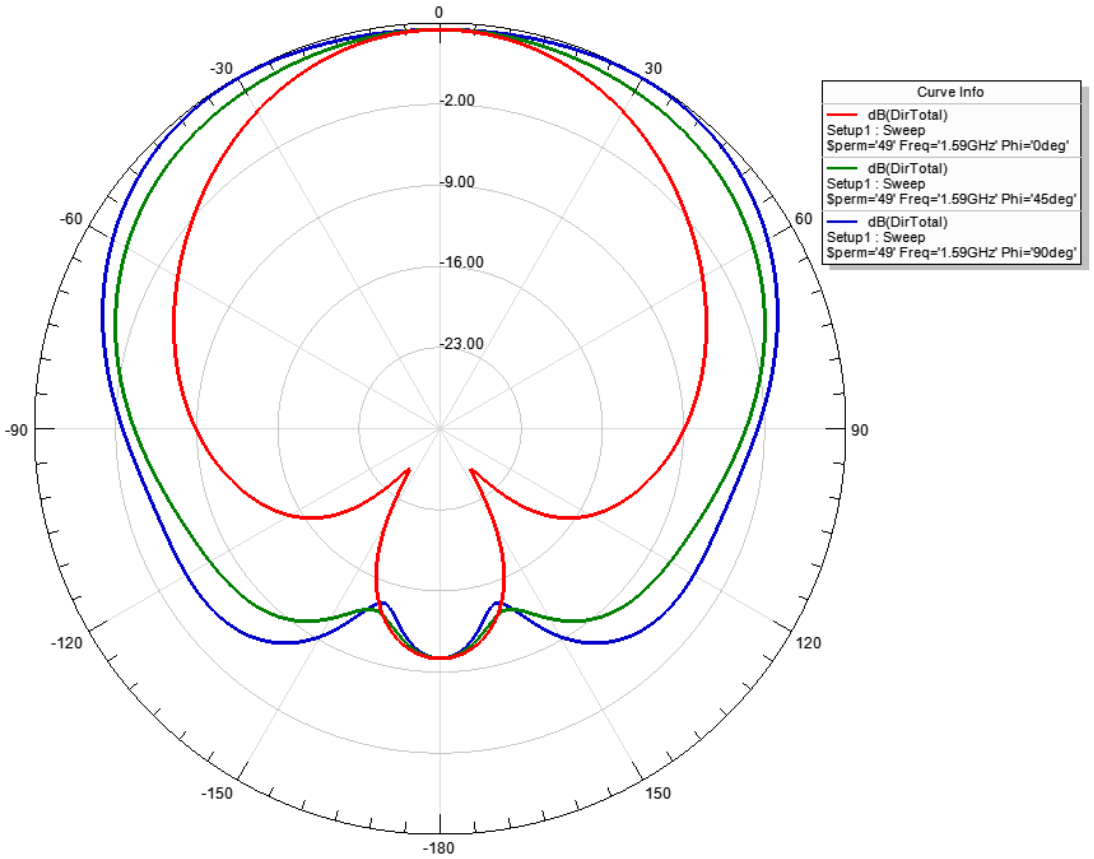

Figure 4-28. Radiation pattern of the ELPOSD antenna at 1.59 GHz with a permittivity value of 49.

As can be seen in the previous radiation patterns, the shape remains similar to the single ELPOSD antenna except for the two last frequencies (1.717 GHz and 1.59 GHz). The directivity is similar as in the case of the FSS with the square patches; it is around 6dB except for the radiation pattern at 1.717 GHz where the directivity is 0 dB. The last radiation pattern has a negative directivity, which does not make much sense since the simulation performed had a ground plane in the FSS substrate.

The same simulation was performed for the case of the Square patch antenna. Figure 4-24 shows the reflection spectrum as a function of frequency. As mention above this S11 parameter results can be caused due to the way the Square patch antenna is fed. Unlike the case with the capacitance element in Section 4.2, the simulation with the altered BST varactors has not occurred a variation of the frequency. However, this result is attributed to an inappropriate operation of the HFSS software and also to an insufficient number of tetrahedrons that is generated in the simulation.

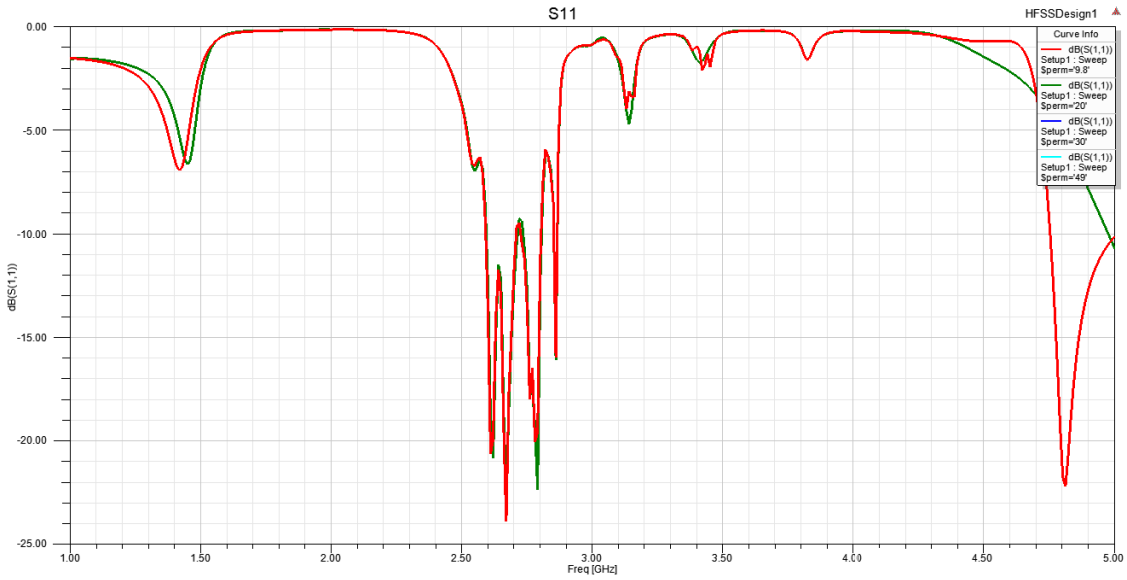

Figure 4-24. S11 parameter for the Square Patch antenna with the FSS and the altered BST varactors.

upna Universidad Pública de Navarra Nafarroako Unibertsitate Publikoa

CHAPTER 5. CONCLUSIONS AND GUIDELINES FOR FUTURE RESEARCH

This work has achieved a tunable antenna with a frequency selective surface (FSS) considered metamaterial and with BST varactors, which have made possible a change in the capacitance of the FSS and therefore a variation in the resonant frequency of the antenna.

In the case of the End-Loaded Planar Open-Sleeve Dipole antenna has achieved a frequency variation of 100 MHz by varying the permittivity of BST material from 200 to 300. The resonance frequencies variation goes from 1.98 GHz to 1.717 GHz with a distance around 100 MHz between resonance frequencies, which equal a variation of the frequency about 8% in the adjacent permittivity values.

In the case of the patch antenna has been achieve a tunable antenna, although the feed line has not been the appropriated one. It should be studied other way of feeding the antenna from beneath the substrate.

As future research should be appointed to study the same structure to achieve a beam steering antenna instead of a tunable one by varying the capacitance of BST varactors unevenly.

To complete the study of this project would be proceed to the manufacture of the dipole antenna and the patch antenna to compare the measured results with the simulation results.

upna Universidad Pública de Navarra Nafarroako Unibertsitate Publikoa

REFERENCES

[Bay09] F. Bayatpur and K. Sarabandi, "A tunable metamaterial frequency-selective surface with variable modes of operation," IEEE Transactions on Microwave Theory and Techniques, vol. 57, no. 6, pp. 1433–1438, 2009.

[Bos08] J. A. Bossard, X. Liang, L. Li et al., "Tunable frequency selective surfaces and negative-zero-positive index metamaterials based on liquid crystals," IEEE Transactions on Antennas and Propagation, vol. 56, no. 5, pp. 1308–1320, 2008.

[Bou08] K. A. Boulais, D. W. Rule, S. Simmons et al., "Tunable split-ring resonator for metamaterials using photocapacitance of semi-insulating GaAs," Applied Physics Letters, vol. 93, no. 4, Article ID 043518, 3 pages, 2008.

[Bou09] D. Bouyge, A. Crunteanu, J.-C. Orlianges et al., "Reconfigurable bandpass filter based on split ring resonators and vanadium dioxide (VO2) microwave switches," in Proceedings of the Asia Pacific Microwave Conference (APMC '09), pp. 2332–2335, Singapore, December 2009.

[Bou10] D. Bouyge, A. Crunteanu, O. Massagué et al., "Applications of vanadium dioxide (VO2)-loaded electrically small resonators in the design of tunable filters," in Proceedings of the 40th European Microwave Conference (EuMC '10), pp. 822-825, September 2010.

[Bra04] M. G. Bray and D. H. Werner, "A broadband open-sleeve dipole antenna mounted above a tunable EBG AMC ground plane," in Proceedings of the IEEE Antennas and Propagation Society Symposium, pp. 1147–1150, Monterey, Calif, USA, June 2004.

[Che06] H.-T. Chen, W. J. Padilla, J. M. O. Zide, A. C. Gossard, A. J. Taylor, and R. D. Averitt, "Active terahertz metamaterial devices," Nature, vol. 444, no. 7119, pp. 597–600, 2006.

upna Universidad Pública de Navarra Nafarroako Unibertsitate Publikoa

[Chi11] D. Chicherin, M. Sterner, D. Lioubtchenko, J. Oberhammer, and A. V. Räisänen, "Analog-type millimeter-wave phase shifters based on MEMS tunable high-impedance surface and dielectric rod waveguide," International Journal of Microwave and Wireless Technologies, vol. 3, no. 5, pp. 533–538, 2011.

[Cho09] J. Choi and S. Lim, "Frequency reconfigurable metamaterial resonant antenna," in Proceedings of the Asia Pacific Microwave Conference (APMC '09), pp. 798–801, Singapore, December 2009.

[Cos08] F. Costa, S. Talarico, A. Monorchio, and M. F. Valeri, "An active AMC ground plane for tunable low-profile antennas," in Proceedings of the IEEE International Symposium on Antennas and Propagation, pp. 1–4, San Diego, Calif, USA, July 2008.

[Cui10] Tie Jun Cui, Ruopeng Liu, David R. Smith, "Metamaterials: theory, design and applications", ed. New York: Springer Science + Business Media, 2010.

[Cur10] D. Cure, S. Melais, T. Weller, P. Herzig and R. Roeder, "2.45 GHz end-loaded dipole backed by a high impedance surface", Antennas and Propagation Society International Symposium (APSURSI), pp. 1-4, 2010 IEEE

[Cur14] D. Cure, T.M. Weller, T. Price, F.A. Miranda and F.W. Van Keuls, "Low-Profile Tunable Dipole Antenna Using Barium Strontium Titanate Varactors", IEEE Trans. Antennas Propag., vol.62, No.3, pp. 1185-1193, March 2014

[Ekm09] E. Ekmekci, K. Topalli, T. Akin, and G. Turhan-Sayan, "A tunable multi-band metamaterial design using micro-split SRR structures," Optics Express, vol. 17, no. 18, pp. 16046–16058, 2009.

upna Universidad Pública de Navarra Nafarroako Unibertsitate Publikoa

[Fer10] J. Sanz-Fernández, G. Goussetis, and R. Cheung, "Tunable 2D electromagnetic band-gap (EBG) structures based on micro-electro-mechanical systems (MEMS) for THz frequencies," in Proceedings of the IEEE International Symposium on Antennas and Propagation, pp. 1–4, Toronto, Canada, July 2010.

[Gar01] R. Garg, P. Bhartia, I. Bahl, A. Ittipiboon, "Microstrip Antenna Design Handbook", ARTECH HOUSE, Boston 2001.

[Gil06] I. Gil, J. Bonache, J. García-García, and F. Martín, "Tunable metamaterial transmission lines based on varactor-loaded split-ring resonators," IEEE Transactions on Microwave Theory and Techniques, vol. 54, no. 6, pp. 2665–2674, 2006.

[Gil07] I. Gil, F. Martin, X. Rottenberg, and W. De Raedt, "Tunable stop-band filter at Q-band based on RF-MEMS metamaterials," Electronics Letters, vol. 43, no. 21, pp. 1153–1154, 2007.

[Gil09] M. Gil, C. Damm, A. Giere et al., "Electrically tunable split-ring resonators at microwave frequencies based on barium-strontium-titanate thick films," Electronics Letters, vol. 45, no. 8, pp. 417–418, 2009.

[Gol09] A. B. Golovin and O. D. Lavrentovich, "Electrically reconfigurable optical metamaterial based on colloidal dispersion of metal nanorods in dielectric fluid," Applied Physics Letters, vol. 95, no. 25, Article ID 254104, 2009.

[Han07] T. Hand and S. Cummer, "Characterization of tunable metamaterial elements using MEMS switches,"IEEE Antennas and Wireless Propagation Letters, vol. 6, pp. 401–404, 2007.

[Han08] J. Han, A. Lakhtakia, and C.-W. Qiu, "Terahertz metamaterials with semiconductor split-ring resonators for magnetostatic tunability," Optics Express, vol. 16, no. 19, pp. 14390–14396, 2008.

[Han09] T. H. Hand and S. A. Cummer, "Controllable magnetic metamaterial using digitally addressable split-ring resonators," IEEE Antennas and Wireless Propagation Letters, vol. 8, pp. 262–265, 2009.

[Hig03] J. A. Higgins, H. Xin, A. Sailer, and M. Rosker, "Ka-band waveguide phase shifter using tunable electromagnetic crystal sidewalls," IEEE Transactions on Microwave Theory and Techniques, vol. 51, no. 4, pp. 1281–1288, 2003.

[Hou10] G. Houzet, X. Mélique, D. Lippens, L. Burgnies, G. Velu, and J.-C. Carru, "Microstrip transmission line loaded by split-ring resonators tuned by ferroelectric thin film," Progress In Electromagnetics Research C, vol. 12, pp. 225–236, 2010.

[Hra10] S. Hrabar, I. Krois, and A. Kiricenko, "Towards active dispersionless ENZ metamaterial for cloaking applications," Metamaterials, vol. 4, no. 2-3, pp. 89–97, 2010.

[Jep10] C. Jeppesen, S. Xiao, N. A. Mortensen, and A. Kristensen, "Capacitance tuning of nanoscale split-ring resonators," in Metamaterials V, vol. 7711 of Proceedings of SPIE, pp. 1–6, April 2010.

[Joa08] John D. Joannopoulos, Robert D. Meade, Joshua N. Winn, "Photonic Crystals: Molding the Flow of Light", Princetone University Press, Oxfordshire 2008.

[Kan08] L. Kang, Q. Zhao, H. Zhao, and J. Zhou, "Magnetically tunable negative permeability metamaterial composed by split ring resonators and ferrite rods," Optics Express, vol. 16, no. 12, pp. 8825–8834, 2008.

[Kas09] T. S. Kasirga, Y. N. Ertas, and M. Bayindir, "Microfluidics for reconfigurable electromagnetic metamaterials," Applied Physics Letters, vol. 95, no. 21, Article ID 214102, 3 pages, 2009.

[Kat11] A. R. Katko, A. M. Hawkes, J. P. Barrett, and S. A. Cummer, "RF limiter metamaterial using p-i-n diodes," IEEE Antennas and Wireless Propagation Letters, vol. 10, pp. 1571–1574, 2011.

[Kwo08] D.-H. Kwon and D. H. Werner, "Restoration of antenna parameters in scattering environments using electromagnetic cloaking," Applied Physics Letters, vol. 92, no. 11, Article ID 113507, 3 pages, 2008.

[Kwo10] D.-H. Kwon and D. H. Werner, "Transformation electromagnetics: an overview of the theory and applications," IEEE Antennas and Propagation Magazine, vol. 52, no. 1, pp. 24–46, 2010.

[Lia05] T. Liang, L. Li, J. A. Bossard, D. H. Werner, and T. S. Mayer, "Reconfigurable ultra-thin EBG absorbers using conducting polymers," in Proceedings of the IEEE Antennas and Propagation Society International Symposium, vol. 2, pp. 204–207, July 2005.

[Lia09] J. Liang and H. Y. D. Yang, "Microstrip patch antennas on tunable electromagnetic band-gap substrates," IEEE Transactions on Antennas and Propagation, vol. 57, no. 6, pp. 1612–1617, 2009.

[Lim08] H. Lim, W.-S. Jeong, S.-H. Lim, D.-H. Shin, and N.-H. Myung, "A tunable notch resonator based on varactor-loaded complementary split-ring resonators," in Proceedings of the IEEE International Workshop on Antenna Technology (iWAT '08), pp. 426–429, Chiba, Japan, 2008.

[Liu10] Q. Liu, Y. Cui, D. Gardner, X. Li, S. He, and I. I. Smalyukh, "Self-alignment of plasmonic gold nanorods in reconfigurable anisotropic fluids for tunable bulk metamaterial applications," Nano Letters, vol. 10, no. 4, pp. 1347–1353, 2010.

[Ou11] J. Y. Ou, E. Plum, L. Jiang, and N. I. Zheludev, "Reconfigurable photonic metamaterials," Nano Letters, vol. 11, no. 5, pp. 2142–2144, 2011.

[Men11] F.-Y. Meng, K. Zhang, Q. Wu, and L. Jong-Chul, "Reconfigurable composite right/left-handed magnetic-metamaterial waveguide at sub-wavelength scale," Journal of Applied Physics, vol. 109, no. 7, Article ID 07A309, 3 pages, 2011.

[Mia07] C. Mias and J. H. Yap, "A varactor-tunable high impedance surface with resistive-lumped-element biasing grid," IEEE Transactions on Antennas and Propagation, vol. 55, no. 7, pp. 1955–1962, 2007.

[Mir11] H. Mirzaei and G. V. Eleftheriades, "A compact frequency-reconfigurable metamaterial-inspired antenna," IEEE Antennas and Wireless Propagation Letters, vol. 10, pp. 1154–1157, 2011.

[Mun00] Ben A. Munk, Frequency Selective Surfaces: Theory and Design, 1st ed. New York: John Wiley & Sons, Inc., 2000.

[Ou13] J.-Y. Ou, E. Plum, J. Zhang, and N. I. Zheludev, "An electromechanically reconfigurable plasmonic metamaterial operating in the near-infrared," Nature Nanotechnology, vol. 8, no. 4, pp. 252–255, 2013.

[Ozb07] E. Ozbay, K. Aydin, S. Butun, K. Kolodziejak, and D. Pawlak, "Ferroelectric based tuneable SRR based metamaterial for microwave applications," in Proceedings of the 37th European Microwave Conference (EUMC '07), pp. 497–499, Munich, Germany, October 2007.

[Pad06] W. J. Padilla, A. J. Taylor, C. Highstrete, M. Lee, and R. D. Averitt, "Dynamical electric and magnetic metamaterial response at terahertz frequencies," Physical Review Letters, vol. 96, no. 10, Article ID 107401, 4 pages, 2006.

[Rat07] P. Ratajczak, P. Brachat, and J.-M. Baracco, "Active reflectarray based on high impedance surface," inProceedings of the IEEE Antennas and Propagation Society International Symposium, pp. 5327–5330, Honolulu, Hawaii, USA, June 2007.

upna Universidad Pública de Navarra Nafarroako Unibertsitate Publikoa

[Rem00] T. Remmel, et al., "Barium Strontium Titanate thin film analysis", Advances in X-ray Analysis, Vol. 43, pp. 510, 2000.

[Rey04] O. Reynet and O. Acher, "Voltage controlled metamaterial," Applied Physics Letters, vol. 84, no. 7, pp. 1198–1200, 2004.

[San03] V. Sanchez and E. Paller, "A tunable artificial magnetic conductor using switched capacitance in a concentric overlapping geometry," in Proceedings of the IEEE International Antennas and Propagation Symposium, vol. 2, pp. 439–442, Columbus, Ohio, USA, June 2003.

[She06] Z. Sheng and V. V. Varadan, "Effect of substrate dielectric properties and tunable metamaterials," inProceedings of the IEEE Antennas and Propagation Society International Symposium, pp. 4497–4500, 2006.

[She07] Z. Sheng and V. V. Varadan, "Tuning the effective properties of metamaterials by changing the substrate properties," Journal of Applied Physics, vol. 101, no. 1, Article ID 014909, 7 pages, 2007.

[Shr11] D. Shrekenhamer, S. Rout, A. C. Strikwerda et al., "High speed terahertz modulation from metamaterials with embedded high electron mobility transistors," Optics Express, vol. 19, no. 10, pp. 9968–9975, 2011.

[Sie01] D. Sievenpiper, J. Schaffner, B. Loo et al., "Electronic beam steering using a varactor-tuned impedance surface," in Proceedings of the IEEE Antennas and Propagation Society International Symposium, pp. 174–177, Boston, Mass, USA, July 2001.

[Sie02] D. Sievenpiper and J. Schaffner, "Beam steering microwave reflector based on electrically tunable impedance surface," Electronics Letters, vol. 38, no. 21, pp. 1237–1238, 2002.

[Sie12] P. E. Sieber and D. H. Werner, "A reconfigurable near-infrared circularly polarizing reflector based on phase changing anisotropic metamaterials," in Proceedings of the IEEE Antennas and Propagation Society International Symposium, pp. 1–2, Chicago, Ill, USA, 2012.

[Sie13] P. E. Sieber and D. H. Werner, "Reconfigurable broadband infrared circularly polarizing reflectors based on phase changing birefringent metasurfaces," Optics Express, vol. 21, no. 1, pp. 1087–1100, 2013.

[Spe06] Thomas G. Spence and Douglas H. Werner "A Novel Miniature Broadband/Multiband Antenna Based on an End-Loaded Planar Open-Sleeve Dipole", IEEE Trans. Antennas Propag., vol. 54, pp. 3614-3620, Dec. 2006

[Tao11] H. Tao, A. C. Strikwerda, K. Fan, W. J. Padilla, X. Zhang, and R. D. Averitt, "MEMS based structurally tunable metamaterials at terahertz frequencies," Journal of Infrared, Millimeter, and Terahertz Waves, vol. 32, no. 5, pp. 580–595, 2011.

[Tre10] Ethan J. Tremblay, "Metamaterials: classes, properties and applications", ed. New York : Nova Science Publishers, 2010.

[Tur14] Jeremiah P. Turpin, Jeremy A. Bossard, Kenneth L. Morgan, Douglas H. Wener, and Pingjuan L. Werner, "Reconfigurable and Tunable Metamaterials: A Review of the Theory and Applicattions", International Journal of Antennas and Propagation, Vol. 2014, Article ID 429837, 18 pages, http://dx.doi.org/10.1155/2014/429837

[Ves98] V.G Veselago, "The electrodynamics of substances with simultaneously negative values of ε and μ", Sov. Phys. Usp. 10 509, 1968.

[Wan08] D. Wang, H. Chen, L. Ran, J. Huangfu, J. A. Kong, and B.-I. Wu, "Reconfigurable cloak for multiple operating frequencies," Applied Physics Letters, vol. 93, no. 4, Article ID 043515, 3 pages, 2008.

[Wei08] A. R. Weily, T. S. Bird, and Y. J. Guo, "A reconfigurable high-gain partially reflecting surface antenna,"IEEE Transactions on Antennas and Propagation, vol. 56, no. 11, pp. 3382–3390, 2008.

[Wel11] T. Price, T. Weller, Y. Shen, and X. Gong, "Comparison of barium strontium titanate varactors on magnesium oxide and alumina sub- strates," presented at the IEEE Wireless Microw. Technol. Conf. (WAMICON), Clearwater, Fl, USA, 2011.

[Wer11] D. H. Werner, T. S. Mayer, C. Rivero-Baleine et al., "Adaptive phase change metamaterials for infrared aperture control," in Unconventional Imaging, Wavefront Sensing, and Adaptive Coded Aperture Imaging and Non-Imaging Sensor Systems, vol. 8165 of Proceedings of SPIE, pp. 1–9, August 2011.

[Wiw11] N. Wiwatcharagoses and P. Chahal, "A novel reconfigurable metamaterial unit cell based composite right/left handed microstrip design," in Proceedings of the IEEE International Symposium on Antennas and Propagation, pp. 2954–2957, Spokane, Wash, USA, July 2011.

[Xia09] S. Xiao, U. K. Chettiar, A. V. Kildishev, V. Drachev, I. C. Khoo, and V. M. Shalaev, "Tunable magnetic response of metamaterials," Applied Physics Letters, vol. 95, no. 3, Article ID 033115, 3 pages, 2009.

[Yan08] F. Yang, Y. Rahmat-Samii "Electromagnetic band gap (EBG) structures in Antenna Engineering" The Cambridge RF and Microwave Engineering, 2008, pp. 14–58.

[Zha07] Q. Zhao, L. Kang, B. Du et al., "Electrically tunable negative permeability metamaterials based on nematic liquid crystals," Applied Physics Letters, vol. 90, no. 1, Article ID 011112, 3 pages, 2007.

upna Universidad Pública de Navarra Nafarroako Unibertsitate Publikoa

[Zhu12] W. M. Zhu, A. Q. Liu, T. Bourouina et al., "Microelectromechanical Maltese-cross metamaterial with tunable terahertz anisotropy," Nature Communications, vol. 3, p. 1274, 2012.

[Zhu13] S. Zhu, D. G. Holtby, K. L. Ford, A. Tennant, and R. J. Langley, "Compact low frequency varactor loaded tunable SRR antenna," IEEE Transactions on Antennas and Propagation, vol. 61, no. 4, pp. 2301–2304, 2013.